

Supercritical Technologies for the Valorization of Wine Industry By-Products

Kurabachew Simon Duba



UNIVERSITY OF TRENTO
Department of Civil, Environmental
and Mechanical Engineering

2015

Doctoral thesis in **Environmental Engineering**, 27th cycle

Faculty of Engineering, **University of Trento**

Academic year **2014/2015**

Supervisor: **Dr Luca Fiori, DICAM**



Copyright © 2015 by Kurabachew Simon Duba: This work is made available under the terms of the Creative Commons Attribution-NonCommercial-NoDerivatives 4.0 International Public License, <http://creativecommons.org/licenses/by-nc-nd/4.0/legalcode>

University of Trento

Trento, Italy

March 2015

Dedicated to:

My wife Asefu Endris

&

My son Yahya Kurabachew

“O my Rabb! Increase me in knowledge.”

(Qur'an, 20:114)

Acknowledgements

This PhD thesis is carried out in the University of Trento, Doctoral School of Civil, Environmental and Mechanical Engineering (DICAM) between January 2012 and March 2015. The work will not have been in the current form without the help and support of several people for which I would like to forward my sincere gratitude.

First of all I would like to thank the University of Trento for the 27° cycle doctoral grant to carry out this research through financial support by AGER (project number 2010-2222).

Special thanks go to my supervisor Dr Luca Fiori, for his constant support, guidance, constructive comments and suggestions. I am particularly grateful to him for believing in me during difficult times. Truly, I get exceptional experience by working with him. I want to thank him for being not only a supervisor but also a closest friend. Luca, you are and will always be my role model, thank you for your professionalism.

I also want to acknowledge the contribution made by our collaborators, namely, prof. Graziano Guella of Bio-organic Chemistry Laboratory, Department of Physics, University of Trento, prof. Patrizia Perego and Dr. Alessandro Alberto Casazza of Department of Civil, Chemical and Environmental Engineering, University of Genoa, Dr. Vera Lavelli and Mr. Pedapati Siva Charan Sri Harsh of Department of Food, Environmental and Nutritional Sciences, University of Milan and Dr. Hatem Ben Mohamed of Laboratory of Horticulture, National Agricultural Research Institute of Tunisia for their contribution of the material included in Chapter 2 or/and Chapter 6.

Very special thank go to my wife, Asefu Endris Seid for her love, constant support and above all for being patient with me for over three years; I have no word to express my feelings. Honey, I love you more than you can imagine. I am also grateful for my parents for their constant words of encouragement and love. I wish them long life.

Certainly, I am not sincere if I didn't forward my humble gratitude to the administrative staff at DICAM and Doctorate Office – Science and Technology, I am grateful for all the information and cooperation you gave me when I needed. Finally to the nation of Italy, thank you for your hospitality; I received your message of goodwill, I will carry it with me and I will be your ambassador.

Lastly but not the least, I must thank Allah Subhanahu Wa Ta'ala for every things.

Contents

<i>Acknowledgements</i>	<i>vii</i>
<i>Contents</i>	<i>ix</i>
<i>List of Figures</i>	<i>xiii</i>
<i>List of Tables</i>	<i>xvii</i>
<i>Summary</i>	<i>xix</i>
1. Overview of High Pressure Technologies	1
1.1 Fundamental of Supercritical CO ₂	1
1.2 Some Application of Supercritical CO ₂	2
1.2.1 <i>Extraction</i>	2
1.2.2 <i>Fractionation</i>	3
1.2.3 <i>Particle formation</i>	4
1.2.4 <i>Disinfection</i>	4
1.3 Fundamental of Subcritical Water	5
1.4 Some Application of Subcritical Water	6
1.4.1 <i>Extraction</i>	6
1.4.2 <i>Reaction</i>	7
1.4.3 <i>Chromatography</i>	7
1.5 Research Objective	8
2. Extraction and Characterization of Grape Seed Oil	9
2.1 Introduction	9
2.2 Materials and methods	11
2.2.1 <i>Grape seeds</i>	11
2.2.2 <i>Chemicals</i>	11
2.2.3 <i>Sample preparation</i>	11
2.2.4 <i>Extraction techniques and procedures</i>	11
2.2.5 <i>Qualitative analysis of the crude oil extracts</i>	14

2.2.6	<i>Quantitative analysis of fatty acids (FAs)</i>	14
2.2.7	<i>HPLC analysis of tocol contents</i>	15
2.2.8	<i>Statistical analysis of data</i>	16
2.3	Results and discussion	16
2.3.1	<i>Oil yield</i>	16
2.3.2	<i>Analysis of the crude oil extracts by NMR and MALDI-TOF</i>	17
2.3.3	<i>Quantitative analysis of FA profile</i>	20
2.3.4	<i>Tocopherols and tocotrienols</i>	21
2.4	Conclusions	25
3.	Kinetic Models for Supercritical CO₂ Extraction	27
3.1	Introduction	27
3.2	Extraction kinetics models	28
3.2.1	<i>The Broken and Intact Cell (BIC) model</i>	29
3.2.2	<i>The Shrinking Core (SC) model</i>	30
3.2.3	<i>The combined BIC-SC model</i>	31
3.2.4	<i>Model adjustable parameters</i>	32
3.3	Materials and Methods	33
3.4	Results and Discussion	33
3.5	Conclusions	35
4.	Solubility of Grape Seed Oil in Supercritical CO₂: Experiment and Modeling	37
4.1	Introduction	37
4.2	Experimental	38
4.2.1	<i>Solubility determination</i>	38
4.3	Modeling	39
4.3.1	<i>Density-based models</i>	39
4.3.2	<i>Thermodynamic model</i>	42
4.4	Results and Discussion	43

4.4.1	<i>Solubility data</i>	43
4.4.2	<i>Correlation of Solubility</i>	46
4.5	Conclusions	51
5.	Effect of Process Parameters on the Extraction Kinetics	53
5.1	Introduction	53
5.2	Material and Methods	54
5.2.1	<i>Sample preparation</i>	54
5.2.2	<i>SC-CO₂ extraction equipment and procedure</i>	55
5.3	Mathematical Modeling	56
5.4	Results and Discussion	57
5.4.1	<i>Effect of pressure</i>	58
5.4.2	<i>Effect of temperature</i>	60
5.4.3	<i>Effect of flow rate</i>	61
5.4.4	<i>Effect of particle diameter</i>	64
5.4.5	<i>Effect of bed porosity</i>	65
5.4.6	<i>Effect of extractor diameter to length ratio (D/L)</i>	68
5.4.7	<i>Extractor free volume</i>	69
5.4.8	<i>Effect of grape cultivars</i>	70
5.4.9	<i>Critical evaluation of the key-parameters affecting extraction kinetics</i>	73
5.5	Conclusions	77
6.	Subcritical water Extraction of polyphenols from grape skins and defatted grape seeds	79
6.1	Introduction	79
6.2	Material and Methods	80
6.2.1	<i>Defatting of grape seeds</i>	80
6.2.2	<i>Subcritical water extraction</i>	80
6.2.3	<i>Determination of total polyphenol</i>	82

6.3	Modeling	82
6.4	Statistical analysis	85
6.5	Results and Discussion	85
6.5.1	<i>Total Polyphenol Yields</i>	85
6.5.2	<i>Grape skins SW extraction kinetics</i>	86
6.5.3	<i>Defatted grape seeds SW extraction kinetics</i>	87
6.5.4	<i>Extraction kinetics: modeling results</i>	89
6.6	Conclusions	93
7.	Scale-up and Economic Analysis of Supercritical CO₂ extraction process	95
7.1	Introduction	95
7.2	Scale-up operation	97
7.3	Economic Analysis	98
7.3.1	<i>Fixed capital investment (FCI)</i>	98
7.3.2	<i>Working capital investment (WCI)</i>	99
7.3.3	<i>Feasibility studies of SC-CO₂ extraction process</i>	99
7.3.4	<i>Profitability analysis</i>	101
7.4	Result and discussion	101
7.5	Conclusions	109
8.	Final Remark	111
9.	References	113
10.	Appendix	135
	About the author	135

List of Figures

Figure 1.1	Phase diagram of CO ₂	2
Figure 1.2	Dielectric constant of subcritical water at saturated pressure and organic solvents at room temperature	6
Figure 2.1	P&ID of supercritical CO ₂ extraction equipment	12
Figure 2.2	Soxhlet extractor and rotary evaporator under hood (left) and hydraulic press (right)	13
Figure 2.3	¹ H-NMR spectrum in CDCl ₃ of Moscato seed oil by SC-CO ₂ extraction; capital letters represent the attribution of ¹ H-NMR signals to specific protons of the linolenic acyl chain reported at the top of the figure.	18
Figure 2.4	GC-FID chromatogram representing the fatty acids distribution of Moscato seed oil by SC-CO ₂ extraction; reported peaks were assigned by their EI-MS spectra.	20
Figure 3.1	Extraction kinetics: (a) BIC model; (b) SC model	34
Figure 4.1	Kinetics of extraction of oil from surface of glass beads	44
Figure 4.2	Solubility correlation by Chrastil model and its modifications	46
Figure 4.3	Solubility correlations with second class of density-based models	49
Figure 4.3	Solubility correlations Peng–Robinson Equation of State	51
Figure 5.1	Extractor assembly: the various components of the three extractors. D and L represent, respectively, the extraction basket internal diameter and length: D = 4.07 x 10 ⁻² m; L = 7.75 x 10 ⁻² m (0.1 L basket), 15.5 x 10 ⁻² m (0.2 L basket), 38.3 x 10 ⁻² m (0.5 L basket).	56
Figure 5.2	Extraction curves at different pressures: oil yield <i>versus</i> solvent consumption. The operating conditions are reported in Table 5.1.	58
Figure 5.3	Extraction curves at different temperatures: oil yield <i>versus</i> solvent consumption. The operating conditions are reported in Table 5.2.	61
Figure 5.4	Extraction curves at different solvent flow rates. (a) oil yield <i>versus</i> solvent consumption; (b) oil yield <i>versus</i> time. The operating conditions are reported in Table 5.3.	62

Figure 5.5	Extraction curves at different particle diameters: oil yield <i>versus</i> solvent consumption. The operating conditions are reported in Table 5.4.	64
Figure 5.6	Extraction curves at different particle bed porosity. (a) oil yield <i>versus</i> solvent consumption; (b) oil extracted <i>versus</i> time. The operating conditions are reported in Table 5.5	66
Figure 5.7	Extraction curves at different extractor diameter to length ratios: oil yield <i>versus</i> solvent consumption. The operating conditions are reported in Table 5.6.	68
Figure 5.8	Extraction curves at different extractor free volume: oil yield <i>versus</i> solvent consumption. The operating conditions are reported in Table 5.7.	70
Figure 5.9	Extraction curves at different grape cultivars: oil yield <i>versus</i> extraction time. The operating conditions are reported in Table 5.8.	71
Figure 5.10	Free oil amount <i>versus</i> particle diameter. G_{x_0} : g free oil/g seeds; ϕ_f and ϕ_f^* : cm^3 free oil/ cm^3 seed particle. Filled circles: significant data. Empty circles: questionable data from Table 5.7.	74
Figure 5.11	Comparison between the external mass transfer coefficient by this work ($k_{f\text{Mod}}$) and the external mass transfer coefficient by the correlation proposed by Mongkholkhajornsilp et al. [163] ($k_{f\text{MDDETP}}$). Filled circles: significant data. Empty circles: questionable data from Table 5.7	75
Figure 5.12	$F_M = k_s d_p / D_m$ <i>versus</i> particle diameter. Filled circles: significant data. Empty circles: questionable data from Table 5.7. “Star” symbols: data relevant to Table 5.4.	76
Figure 6.1	P&ID of the extraction equipment	81
Figure 6.2	TP yield ($\text{mg}_{\text{GAE}}/\text{g}$) relevant to SW extraction from grape skins at different temperatures. (a) solvent flow rate equal to 2 mL/min; (b) solvent flow rate equal to 5 mL/min. Experimental data.	87
Figure 6.3	TP yield ($\text{mg}_{\text{GAE}}/\text{g}$) relevant to SW extraction from defatted grape seeds at different temperatures and at a solvent flow rate equal to 2 mL/min. Experimental data.	88
Figure 6.4	TP yield (dimensionless) relevant to SW extraction from grape skins at different temperatures and solvent flow rates. Experimental data and model curves	90

Figure 6.5	TP yield (dimensionless) relevant to SW extraction from defatted grape seeds at different temperatures and at a solvent flow rate equal to 2 mL/min. Experimental data and model curves	92
Figure 7.1	Schematic diagram of multi-unit SC-CO ₂ extraction plant	103
Figure 7.2	Cumulative cash position at minimum retail price	109

List of Tables

Table 2.1	Grape seed oil yield obtained from various cultivars (Cv) by SC-CO ₂ and <i>n</i> -hexane extraction (years 2011-2012).	17
Table 2.2	Lipids compositions of grape seed oils obtained by SC-CO ₂ extraction as established by ¹ H-NMR quantitative analysis, all values represent % molar fractions. Unsaturation index (UI) is defined by UI=(2*DUFA % molar fraction + MUFA % molar fraction)/100.	19
Table 2.3	Fatty acid composition (% of total fatty acids) from FAME GC-FID-MS analysis of the grape seed oil obtained from various cultivars (Cv) by SC-CO ₂ . Data are expressed as mean ± SD. Different letters in the same column indicate significant differences among grape cultivars (LSD, p < 0.05).	23
Table 2.4	Tocopherol and tocotrienol contents (mg/kg) of the grape seed oils obtained from various cultivars (Cv) by SC-CO ₂ , mechanical extraction and <i>n</i> -hexane extraction (harvesting year 2012).	24
Table 3.1	Adjustable parameters for grape seed oil SCO ₂ extraction and deviations from experimental data	35
Table 4.1	Solubility of Grape seed oil in supercritical CO ₂	45
Table 4.2	Models adjustable parameters of Chrastil model and its modifications	47
Table 4.3	Models adjustable parameters of the second class of density-based models	50
Table 4.4	Models adjustable parameters of Peng–Robinson Equation of State	51
Table 5.1	Operating conditions and estimated model adjustable parameters for different pressures (T = 40 °C, ε = 0.41, x ₀ = 0.120).	59
Table 5.2	Operating conditions and estimated model adjustable parameters for different temperatures (P = 500 bar, ε = 0.41, x ₀ = 0.120).	59
Table 5.3	Operating conditions and estimated model adjustable parameters for different flow rates (T = 40 °C, P = 350 bar, y _s = 8.60 mg/g, ε = 0.41, x ₀ = 0.120)	63
Table 5.4	Operating conditions and estimated model adjustable parameters for different particle sizes (T = 50 °C, P = 500 bar, y _s = 13.4 mg/g, ε = 0.41, x ₀ = 0.167)	63

Table 5.5	Operating conditions and estimated model adjustable parameters for different bed porosity. ($T = 50\text{ }^{\circ}\text{C}$, $P = 500\text{ bar}$, $y_s = 13.4\text{ mg/g}$, $x_0 = 0.167$)	67
Table 5.6	Operating conditions and estimated model adjustable parameters for different D/L ($T = 40\text{ }^{\circ}\text{C}$, $P = 350\text{ bar}$, $y_s = 8.60\text{ mg/g}$, $x_0 = 0.147$).	67
Table 5.7	Operating conditions and estimated model adjustable parameters for different extractor free volume ($T = 50\text{ }^{\circ}\text{C}$, $P = 500\text{ bar}$, $y_s = 13.4\text{ mg/g}$, $m_{\text{seeds}} = 100\text{ g}$, $x_0 = 0.167$)	67
Table 5.8	Operating conditions, mass transfer parameters and grinding efficiency (k_s , a_p and G from best fitting), and modeling errors for SC-CO ₂ extractions - cultivar (Cv) 2012.	72
Table 6.1	Extraction yield of TP for Pinot Nero grape skins and defatted seeds	61
Table 6.2	Model adjustable parameters for SW extraction of grape skins and defatted seeds	91
Table 7.1	Operating scenario of the extraction process	103
Table 7.2	Estimated fixed capital investment of the complete SC-CO ₂ extraction plant	105
Table 7.3	Specific enthalpy at position of the supercritical extraction plant at a given condition	107
Table 7.4	Estimated total working capital investment per year	108

Summary

This study aims at the valorization of wine industry by-products; particularly on the extraction and characterization of grape seeds oil using supercritical CO₂ (SC-CO₂) and polyphenols from grape skins and defatted grape seeds using subcritical water (SW) and then, modeling of the kinetics of extractions and process economic analysis. The overall objective of the work is to develop recovery strategies for wine-making wastes in order to reduce their environmental impact and to valorize them in order to provide wine-makers with the possibility of selling by-products at a profitable price. To address the objectives, the work is divided into seven Chapters.

In Chapter 1, some general overview and the fundamental of SC-CO₂ and SW technologies along with emerging areas of applications are presented. Special emphasis is given to the work in the field of valorization of agro-industrial by-products. Then, the Chapter ends by stating the general and specific objectives of the thesis.

The second Chapter is devoted to the characterization of grape seeds oil. To make the result more holistic, grape seeds from six grape cultivars were extracted using SC-CO₂ in two subsequent harvesting years and the resulting oils were characterized. Comparative extractions were also performed by utilizing conventional solvent extraction using *n*-hexane and by mechanical press. The results testify the potentiality of grape seed oil as a source of unsaturated fatty acids and tocopherols. Moreover, they offer a clear picture of the similarities and differences among oils from different grape cultivars and obtained through different extraction techniques.

The third Chapter is dedicated to compare the effectiveness of the models used to evaluate the kinetic of SC-CO₂ extraction curves. Particularly, three models, the broken and intact cells (BIC), the shrinking core (SC), and the bridge (combined BIC-SC) models are critically analyzed. The objective of the Chapter is to objectively choose the best model that can be used in the subsequent Chapters.

In order to model the kinetics of SC-CO₂ extraction, one of the very important parameters is the solute solubility. But solubility data (especially of grape seed oil) is very scarce in the literature. The bulk majority of the scientific works estimate the value of solubility of solute in SC-CO₂ from theoretical models. So, the fourth Chapter is devoted to experimental determination of solubility of grape seed oil in SC-CO₂ over a range of

pressure and temperature of practical importance and the data were modeled by different models to compare their effectiveness.

The fifth Chapter is aimed to study the effect of the main process variables affecting the SC-CO₂ extraction of oil from grape seeds, both experimentally and through modeling. The dependency of the extraction kinetics on the variables more tested in the literature (pressure, temperature, particle size and solvent flow rate) was confirmed, and original trends were obtained for the less investigated variables, such as the bed porosity (ε), the extractor diameter to length ratio (D/L), the extractor free volume and the type of cultivars.

In the sixth Chapter the attention is moved to the valorization of grape skins and defatted grape seeds by using SW. The results show that, both skins and defatted seeds contain significant concentration of polyphenols and SW is a potential green solvent for extracting valuable polyphenols from wine-making by-products. The extraction kinetics was also simulated by a simple model available in the literature.

In the seventh and last Chapter, a preliminary economic feasibility study was investigated for the establishment of SC-CO₂ extraction plant for the extraction of grape seeds oil. The result shows that, a SC-CO₂ extraction plant is technically viable and economically feasible for the extraction of grape seed oil with estimated rate of return on investment at 8.5% and payback period of 5 year at current minimum retail selling price of grape seed oil in the market. The project has an attractive socio-economic and environmental benefit and generates substantial revenue for the local government in the form of tax and will allow wine-makers to sell wet grape marc at a price of up to US\$ 10/ton.

1. Overview of High Pressure Technologies

In this Chapter, the definition, principle and areas of applications of high pressure technologies with particular emphasis on the two emerging green solvents; supercritical CO₂ (SC-CO₂) and subcritical water (SW) are presented. Special attention is given to the most recent works and an effort is made to show how these technologies are particularly being used in the valorization of food by-products.

1.1 Fundamental of Supercritical CO₂

Supercritical fluid is a fluid above its critical pressure and temperature. The concept is better explained through phase diagram. Figure 1.1 shows the phase diagram of CO₂ which is the plot of temperature on abscissa *versus* pressure on ordinate. The data used for plotting the diagram is taken from [1]. At triple point all the three phases (i.e. solid, liquid and gas) co-exist and the system is said to be in thermodynamic equilibrium. For CO₂ the triple point occurs at -56.56 °C and 5.18 bar. At pressure and temperature above the sublimation and melting line the fluid is solid, between the melting and saturation line the fluid is liquid whereas below sublimation and saturation line it is gas. Across the sublimation, saturation and melting line, a change in pressure at constant temperature or a change in temperature at constant pressure will result in change in fluid phase. But there exists a point called 'critical point' along the saturation line after which the fluid is neither a liquid nor a gas and is termed as supercritical fluid. For CO₂ the critical point is at temperature of 30.97 °C and 73.77 bar. Above the critical point the fluid has gas-like viscosity and diffusivity, and liquid-like density and solvating power [2,3]. Owing to these peculiar characteristics, in the past few decades there has been an increase in research interest in the field of supercritical fluids.

SC-CO₂ is particularly receiving a central attention as a future industrial solvent especially in the field of food and pharmaceutical industries, mainly because CO₂ has moderately low critical point, non-toxic, non-flammable, non-polluting, cheap substance

and no solvent traces remain in the product as it can be removed automatically from the product by simple depressurization. Moreover, the thermodynamic properties of CO₂ can easily be adjusted by changing the operating conditions. The drawback of the use of SC-CO₂ technology is the greater costs of initial investment linked to high pressure technology compared to conventional processes. However, the operating costs are usually lower due to zero/minimum post processing of products. Therefore, the total costs are believed to be comparable to conventional techniques if the process is carried out at optimum operating conditions and in a sufficient volume [4,5] especially when dealing with large volume of materials [6].

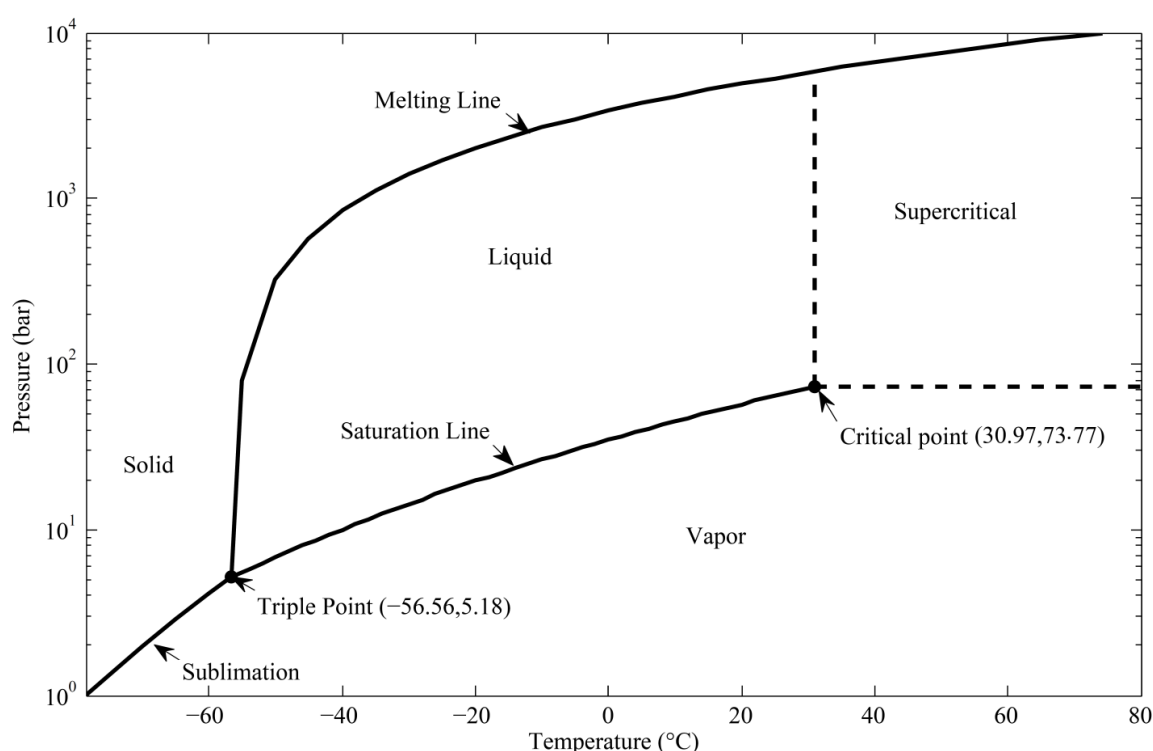


Figure 1.1: Phase diagram of CO₂ (Data from [1])

1.2 Some Application of Supercritical CO₂

Some of the applications of SC-CO₂ technology include, extraction, fractionation, particle formation, disinfection, drying and cleaning, chemical reaction, refrigeration systems and power cycles, polymer processing and many more [2]. Few examples are discussed as follow.

1.2.1 Extraction

Perhaps, SC-CO₂ extraction of compounds from natural sources is the single most

studied and widely applied technique among the field of high pressure CO₂ technologies. Certainly there are thousands of scientific papers published in the past two to three decades with hundreds of patents filed [7,8]. Indeed, SC-CO₂ has clear advantages over traditional extraction techniques and is a promising alternative that can achieve comparable product yield with respect to the conventional organic solvent extraction and with quality better or similar to that of mechanical pressing. There are several review papers available in the literature [7,9–11] which compiled the recent advances in the field. The magnitude of the works clearly indicates the mounting interest in the application of SC-CO₂ in a wide range of domain, mainly extraction. Recent survey by J. King [12] indicates, currently there are more than 150 SC-CO₂ extraction plants with a total extraction volume of more than 500 L exist throughout the world and many of these production plants are generally dedicated to the extraction of natural products, leading to the recovery of high-added value products. The work by de Melo et al.[11] reported that in span of 13 years (i.e. between 2000 and 2013), more than 300 plant species have been extracted and studied using SC-CO₂ of which 28% seeds, 17% leaves, 10% fruits, 7% roots, 5% flowers, 2% barks and the remaining others (processed parts, mixtures etc.). Significant number of researches is also done regarding SC-CO₂ application for the extraction of grape seed oil [13–16].

1.2.2 Fractionation

Fractionation (especially of oil and essential oils) is another commonly used application of SC-CO₂. The conventional fractionation technologies including steam, vacuum and molecular distillation have reported to have a major drawbacks like for example the processes are carried out at high temperature which may degrade heat sensitive compounds, loss of volatile fraction, contamination of the product by residual solvent or simply too costly. SC-CO₂ fractionation has emerged as a potential alternative. In SC-CO₂, the fractionation is achieved through three distinctive approaches [17]. The first approach is to fractionate while extracting, this can be achieved either by collecting the extracts in to different vessel with time (the more soluble solute collected first) or through manipulation of physical properties of SC-CO₂ while extracting (by changing pressure and/or temperature during the extraction starting from lower to higher) and collecting the product at certain time intervals. One example of the this approach is the work done by Zaidul et al. [18] in which SC-CO₂ is used for extraction and fractionation of palm kernel oil in to four different fractions. The second approach is through the use of

series of separators and depressurizing the outlet stream step by step to precipitate the product at different grade. Example of the second type of fractionation include the work of Reverchon and Dalla Porta [19] which used single step extraction and double step fractionation for rose oil. The third and the final approach is the use of fractionation column through which the oil and SC-CO₂ flow in a countercurrent direction to collect the high volatile substance at the top and the less volatile substance at the bottom the column. Two recent practical application of the this approach includes the work by Fiori et al. [20] on fractionation of omega-3 lipids from fish by-products and the work by Brunner and Machado [21] on the fractionation of fatty acids from palm fatty acid distillates in countercurrent packed columns.

1.2.3 Particle formation

SC-CO₂ recently emerged as a solvent in the field of micro and nanoparticles formation which has widespread application in the field of pharmaceutical, nutraceutical, cosmetic, specialty chemistry industries [22]. Conventionally, micro and nanoparticles are produced through crushing, spray drying, spray chilling and spray cooling, extrusion coating, fluidized bed coating, centrifugal extrusion, rotational suspension separation, air micronization, sublimation, and recrystallization from solution [23]. However, all of these techniques have inherent limitations. For example some particle are unstable under conventional milling, the particle size distribution is not uniform, contamination may occur during post-processing [24]. The use of SC-CO₂ enables the production of ultra-fine powders with desired properties and allows precise control of particle size and morphology. Besides, CO₂ can easily be separated from crystalline products [25]. There are different techniques by which particle can be formed in SC-CO₂ including, rapid expansion of supercritical solutions, gas anti-solvent processes, supercritical anti-solvent process, particles from gas-saturated solutions, and others [22,24,26–28]. For detail discussions, advantage and disadvantage of each methods, readers can refer to Fahim et al. [27].

1.2.4 Disinfection

Recently SC-CO₂ is receiving wide spread attention also in the field of microbial inactivation particularly in the area of food preservation. A review of historical background, effects of SC-CO₂ on microorganisms and SC-CO₂ sterilization processes and equipment was recently presented by Perrut [29]. Traditionally, food preservation is made through thermal processing like pasteurization, sterilization, drying, freezing, UV radiation,

fermentation or addition of preservatives etc. [30]. These techniques are associated with some disadvantages, including the denaturation of heat sensitive nutrients and change in sensorial properties food, so food industries are looking for a technology which guarantee the smallest possible deterioration during preservation [31]. SC-CO₂ is effective against bacteria, viruses and insects at different stages of development [32] but the mechanism of microbial inactivation is yet to be fully understood and currently, the topic is the subject of active research. An interesting review on the hypothesis of the mechanisms microbial inactivation and effect of process parameter on inactivation efficiency is presented by Garcia-Gonzalez et al.[33]. Some examples of recent practical application of SC-CO₂ as a disinfection technology includes: the microbial inactivation of fresh-cut carrot and coconut [30,34], paprika (red pepper) [35], liquid whole egg [36] and medical device [37] just to mention few.

1.3 Fundamental of Subcritical Water

SW also called pressured hot water or superheated water is a water at temperatures between its boiling and critical point while the pressure is kept high in order to maintain a liquid state [38–42]. Under subcritical conditions, the intermolecular hydrogen bonds of water break down and the dielectric constant of water decreases [43]. The dielectric constant is a measure of polarity of water [40,41]. At standard pressure and temperature, water is a polar compound with dielectric constant of 80, but as temperature increases the value decreases and water acts like non polar compounds [41,44]. For example, at temperature between 250-300 °C the dielectric constant of water is comparable to that of organic solvent like methanol, ethanol or acetone at room temperature as shown in Figure 1.2 (the data are taken from [45] &[44]). A similar graph of dielectric constant of water as a function of temperature at saturated pressure are presented by Carr et al [41] and Herrero et al [40]. Water under subcritical condition has high diffusivity, low viscosity and surface tension which improve the mass transfer kinetics and solutes solubility [40,46]. Besides water is environmentally friendly, non-flammable, non-toxic and low cost solvent [47]. The fact that the polarity can be tuned by changing temperature makes water useful for wide range of applications [41,48,49].

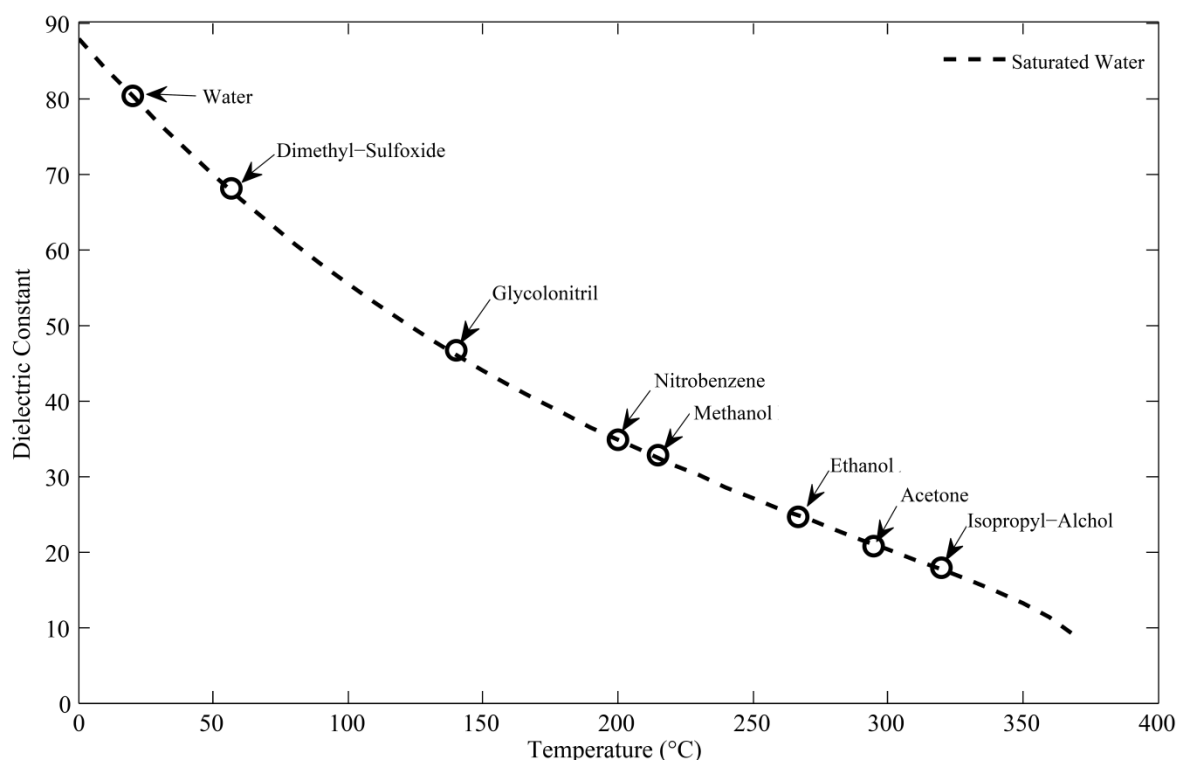


Figure 1.2: Dielectric constant of subcritical water at saturated pressure and organic solvents at room temperature (Data from [45] & [44])

1.4 Some Application of Subcritical Water

SW is receiving widespread industrial application as a green solvent/reagent especially in the field of extraction, reaction and chromatography.

1.4.1 Extraction

Traditionally, the extraction of natural products (specifically polyphenols) are made using organic solvents [50]. However, these techniques require long extraction times and result in low yields of extract [43]. To overcome these limitations, considerable research effort has been done in the extraction of plant constituents using non-conventional techniques like ultrasonic-assisted and microwave-assisted extraction [51–53]. Even though these techniques allow improving the extraction yield and reducing the extraction time, they still use conventional solvents (ethanol, methanol, etc.) and the urge for searching for an environmentally friendly solvent remains challenging. Recently,

subcritical water has been used as an alternative technique for the extraction of both polar and non-polar compounds [41,54–56]. Some example of research work in the recent past particularly concerned with the valorization of agro-industrial by-products using subcritical water includes the extraction of bioactive compounds from citrus peel [39,49,57], onion skins [47], grape marc [58–61], blackberry residues [48], potato peel [43,62], sugar beet pulp [63], mango leaves [64], olive leaves [38,65], coffee silver-skins [66], apple pomace [57,67] and many more.

1.4.2 Reaction

In addition to the characteristics discussed in Section 1.3, the ionization product of SW is several orders of magnitude higher than that of water at ambient condition, thus providing a source of hydronium and hydroxide ions, which can act as catalytically active species in a wide range of chemical reactions from bond formation to break up bonds [68]. Same of the widely reported SW mediated reaction includes the degradation, hydrolysis and synthesis reactions. The degradation reaction is particularly avoided in most application of SW system but it is predominantly important when dealing with environment remediation in the removal of toxic contaminants like pesticides, dyes, and high explosives chemicals [69–71]. In what concern hydrolysis reaction, SW is applied in the conversion of for example agricultural residues which are rich in cellulose, hemicellulose and lignocellulose material to second generation bioethanol [72,73]. Substantial amount of literatures are also available in the synthesis of aromatic compounds using SW in the presence of oxygen. For example alkyl aromatic compounds were oxidized to aldehydes, ketones and acids by molecular oxygen mediated by transition metal catalysts in SW [74]. An interesting review of a wide range of reactions including alkylation, condensation, coupling, cyclization, decomposition, elimination, isomerization etc. under SW mediated condition is presented by Simsek Kus [68].

1.4.3 Chromatography

SW is recently being used as an eluent in a reversed-phase liquid chromatography as an alternative to the conventional technique which uses a non-polar stationary phase and a polar mobile phase [75,76]. Using SW as a mobile phase not only lower operation cost and is environment friendly, but also reduce the wavelength of detection which enables the detection of the compounds with weak chromophores [77]. Several researches applied SW

to separate wide range of compounds. An interesting review is presented by Yang [78] on the potential use of SW as a green solvent in liquid chromatography by highlighting on advantages, limitations and technical features of separating polar, moderately polar, and even some nonpolar solutes using this technology. The main challenge in the use of SW in the field of chromatography is the thermal stability of the stationary phase as most of the packing materials currently available in the market are designed for low temperature application [79,80].

1.5 Research Objective

The research project (Valorvitis) is funded by AGER (project number 2010-2222) on valorization of wine industry by-products for the production of high-added value compounds. The research was conducted by five Italian partner universities, namely Università Cattolica del Sacro Cuore (UCSC), Università degli Studi di Milano (UNIMI), Università degli Studi di Torino (UNITO), Università degli Studi di Trento (UNITN), and Università di Scienze Gastronomiche (UNISG). The overall objective of the project is the development of complete recovery strategies for wine-making wastes in order to reduce their environmental impact and to valorize them in order to provide wine-makers with the possibility of selling by-products at a profitable price.

Within the frame work of general objective, this PhD thesis specifically concerned with and targeted:

- ❖ To extract and characterize oil from seeds of different grape cultivars and model the kinetics of supercritical CO₂ extraction
- ❖ To extract polyphenols from skins and defatted grape seeds using subcritical water and model extraction kinetics and
- ❖ Scale-up and economic analysis of supercritical CO₂ extraction process.

To address the objectives, the work is divided into six sections (Chapter 2 to 7). An effort is made to make all the sections to stand alone with occasional brief reference to the proceeding Chapters where needed. Therefore, the readers need not have to read the whole document to understand the concept addressed in a particular Chapter. Nevertheless, to drive the maximum possible benefit and to appreciate the work, the readers are strongly advice to go through the text in a prescribed order.

2. Extraction and Characterization of Grape Seed Oil

In this Chapter, the focus is on the extraction and characterization of grape seed oil. Seeds from six grape cultivars were extracted in two subsequent harvesting years, and the resulting oils were characterized for the relative amount of: lipid classes, lipid acyl chains, tocopherols and tocotrienols. Comparative extractions were performed by utilizing *n*-hexane as solvent and by mechanical press. The results reported in this study testify the potentiality of grape seed oil as a source of unsaturated fatty acids and tocols. Moreover, they offer a clear picture of the similarities and differences among oils from different grape cultivars and obtained through different extraction techniques.

2.1 Introduction

The management of agricultural waste has become a major problem for the food industries due to their excess production and limited exploitation. Winemaking is one of the most important agricultural activities that contribute substantially to national economy in many countries. Grape marc, the by-product of winemaking, has been found to be a source of nutritionally valuable fractions that could have further applications in the food and nutraceutical industries [81,82].

Traditionally seed oils are extracted either by organic solvent or mechanical techniques. Organic solvent extraction gives better extraction yield, but the technique requires solvent recovery through distillation which may degrade thermally labile compounds; moreover, the presence of traces of residual solvent in the final product makes

* Part of the present Chapter has been published as: Luca Fiori, Vera Lavelli, Kurabachew Simon Duba, Pedapati Siva Charan Sri Harsha, Hatem Ben Mohamed, Graziano Guella, *Supercritical CO₂ extraction of oil from seeds of six grape cultivars: Modeling of mass transfer kinetics and evaluation of lipid profiles and tocol contents*, *J. of Supercritical Fluids* 94 (2014) 71–80

the process less attractive from health and environmental point of views. In mechanical extraction, even though the product quality is superior (after proper filtration), the technique provides relatively lower yield. Supercritical CO₂ (SC-CO₂) extraction technology represents an alternative that can achieve comparable oil yield with respect to the traditional liquid solvent technique. The economic viability of grape seed oil extraction is linked to the quality of the oil [83], which can be utilized not only by the food industry, but also by the cosmetic industry [13].

It is widely reported that, grape seed oil is a good source of unsaturated fatty acids, tocopherols and tocotrienols [84]. SC-CO₂, covering the principles of green technology has been proposed to extract tocopherols and tocotrienols from various by-products and unconventional sources for their use as nutraceuticals [85,86]. In fact, both tocopherols and tocotrienols possess vitamin E activity, with numerous functions i.e., antioxidant, anti-inflammatory, antithrombotic effects and protection against damage caused by various pollutants [87]. γ -Tocopherol seems to be more potent than α -tocopherol in increasing superoxide dismutase (SOD) activity. Although both α -tocopherol and γ -tocopherol increase nitric oxide production by modulating nitric oxide synthase (NOS) activity, only γ -tocopherol increases NOS protein expression [87]. Tocotrienols have been shown to possess distinctive roles. In particular, γ -tocotrienol seems to suppress the production of 3-hydroxy-3-methylglutaryl-coenzyme A reductase (HMG CoA) [87]. Interestingly, Choi and Lee [88] have shown that tocotrienol-rich fractions from grape seeds have higher *in vitro* anti-proliferative activity against various cancer cell lines with respect to α -tocopherol.

This knowledge enlightens the properties of grape seed oil and endorses its recovery from winemaking by-products. Hence, with reference to a specific winemaking area, the most important grape cultivars in terms of wine-making potential need to be characterized for their oil content and quality. Moreover, taking into consideration the possible variation due to climate on grape quality, characterization needs to be extended over different production years.

In order to make the result holistic, in this study grape seeds oil from six model grape cultivars in Northern Italy were extracted by SC-CO₂, and assessed for: a) oil yield; b) oil composition (fatty acid profile, triacylglycerols, diacylglycerols, phytosterols, oxidized lipids); c) tocopherol and tocotrienol contents over two years of production. Conventional organic solvent, *n*-hexane extraction was used as a reference for calculating oil yield, while mechanical extraction was used as a reference extraction for assessing oil

quality (fatty acid and tocol contents).

2.2 Materials and methods

2.2.1 Grape seeds

Grape marc samples of Barbera (BA), Chardonnay (CH), Moscato (MO), Muller Thurgau (MT), Nebbiolo (NE) and Pinot Noir (PI) were obtained by winemakers in Northern Italy, for the harvesting years of 2011 and 2012. At the winery, stalks were separated from the seeds and skins. The mixture of seeds and skins was taken to the laboratory and stored at -20 °C before drying. The samples were dried at 55 °C for 48 h, and then the skins and seeds were separated by means of vibrating sieves and further cleaned manually. Finally, the seeds were stored in dark under vacuum at ambient temperature.

2.2.2 Chemicals

CO₂ (4.0 type, purity greater than 99.99 %) used as a supercritical solvent was purchased from Messer (Padova, Italy). *n*-Hexane for the atmospheric pressure extraction was purchased from Sigma Aldrich (Milano, Italy). R-tocopherol isomers and R-tocotrienol isomers were obtained from VWR International PBI (Milano, Italy). All other reagents are purchased from Sigma Aldrich (Milano, Italy).

2.2.3 Sample preparation

Dried grape seeds were milled by a grinder (Sunbeam Osterizer blender, Boca Raton, USA) just before extraction. To avoid overheating, the sample was flaked for 10 s, then grinding was halted and the sample was shaken for another 10 s, and the milling process was continued.

2.2.4 Extraction techniques and procedures

2.2.4.1 Supercritical extraction

The supercritical extraction equipment (Proras, Rome, Italy) and procedure were previously described [13]. The screen capture of the control flow sheet when the equipment is under operation is also presented in Figure 2.1. Referring to the P&ID and the extraction vessel and cylindrical extraction basket assembly presented in [13], the system was improved by adding a mini Cori-Flow digital mass flow meter (Bronkhorst,

Ruurlo, The Netherlands) placed on the liquid CO₂ line upstream the CO₂ pump (not shown in the Figure 2.1); the CO₂ consumption was totalized and recorded during the experiments by this additional flow meter. The system was operated in the down-flow mode, i.e. with the SC-CO₂ flowing downwards through the substrate to be extracted. Another improvement is represented by the utilization of a tailor made spacer which allowed to place the extraction basket close to the exit of the extraction vessel, which assures meaningful measurement of the extraction kinetics (Refer to Chapter 5, Figure 5.1 for great detail). The extraction basket utilized in this study had an internal volume of 0.1 L and, for each test, batches of about 65 g of grape seeds were placed in the basket and utilized for the extraction. Pressure and temperature were kept constant during the different tests with accuracy of ±10 bar and ±1 °C respectively. For work in this Chapter, the tests were performed at a pressure of 500 bar and a temperature of 50 °C. Solvent flow rate was fixed at about 8 g/min. After extractions, the particle size distribution of the exhausted grape seeds was evaluated by utilizing sieves having different mesh sizes placed in a vibrating device (Automatic Sieve Shaker D406 control, Auckland, New Zealand). The resulted oil was stored under ambient temperature in a tightly closed dark glass vials sealed with Parafilm before used for further analysis.

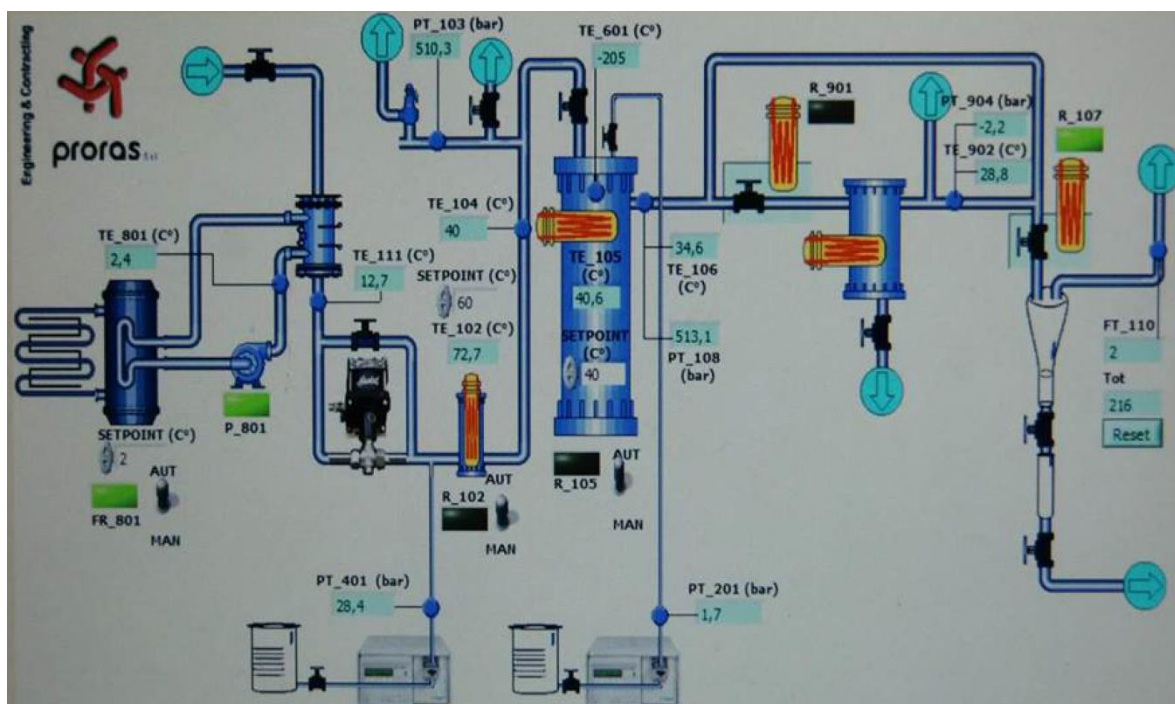


Figure 2.1: P&ID of supercritical CO₂ extraction equipment.

2.2.4.2 Soxhlet extraction

Soxhlet extraction was performed in a SER 148/3 (Velp Scientifica, Usmate, Italy) solvent extractor (Figure 2.2 left), which works according to the Randall technique with three samples in parallel. Batches of 10 g of milled grape seeds were placed in each extraction thimble and the relevant extraction cup was filled with 60 mL of *n*-hexane. The Randall technique foresees the sample inside the thimble to be immersed in the boiling solvent (in the present case at 69 °C, the boiling temperature of *n*-hexane at atmospheric pressure). The immersion step was followed by a washing step, where the extraction was completed according to the standard Soxhlet technique. The immersion and the washing steps lasted for one and three hours, respectively. Solvent recovery was made in rotary evaporator (Heidolph, Schwabach, Germany) at a reduced pressure of 335 mbar, bath water temperature of 40 °C and rotation speed of 30 rpm.



Figure 2.2: Soxhlet extractor and rotary evaporator under hood (left) and hydraulic press (right).

2.2.4.3 Mechanical extraction

The mechanical extraction was performed by means of a hydraulic press machine (Galdabini, PMA/10, Cardano al Campo, Italy) equipped with a stainless steel punch and a stainless steel high strength specimen holder specially built for this purpose in the workshop of the University of Trento (Figure 2.2 right). The ground seeds were placed in

the holder and the press machine applied a force to the punch growing up to a maximum value of 100 kN (loads is controlled by PC). Oil surfaced from the edges of the punch was collected for analysis.

2.2.5 *Qualitative analysis of the crude oil extracts*

The qualitative analysis of the crude oils was carried out by both Nuclear Magnetic Resonance (NMR) and Matrix Assisted Laser Desorption Ionization-Time of Flight- Mass Spectrometry (MALDI-TOF-MS) techniques. ^1H -NMR spectra were recorded on a Bruker-Avance 400MHz NMR spectrometer (Bruker Inc., Bremen, Germany) - operating at 400.13 MHz for ^1H -NMR and at 100.61 MHz for ^{13}C -NMR - by using a 5 mm BBI probe with 90° proton pulse length of 9 μs (transmission power of 0 db) with a delay time between acquisitions of 30 s. All spectra were taken at 25 $^\circ\text{C}$ in CDCl_3 (700 μL , 50-100 mM solution) on the crude grape seed oils. The chemical shift scales (δ) were calibrated on the residual signal of CDCl_3 at δ_{H} 7.26 ppm. MALDI-TOF measurements were performed on Bruker Daltonics Ultraflex MALDI-TOF mass spectrometer (Bruker Daltonics, Bremen, Germany) equipped with a 337-nm nitrogen laser and with a reflectron. The acceleration voltage was set at 20 kV. For desorption of the components, a nitrogen laser beam ($\lambda=337$ nm) was focused on the template. The laser power level was adjusted to obtain high signal-to-noise ratios, while ensuring minimal fragmentation of the parent ions. All measurements were carried out in the delayed extraction mode, allowing the determination of monoisotopic mass values (m/z ; mass-to-charge ratio). After crystallization at ambient conditions, positive ion spectra were acquired in the reflectron mode, giving mainly sodiated adducts ($[\text{M}+\text{Na}]^+$). Samples were directly applied onto the stainless-steel spectrometer plate as 1 μL droplets, followed by the addition of 1 μL of 2,5-dihydroxybenzoic acid (DHB) (0.5 M in methanol). Every mass spectrum represents the average of about 100 single laser shoots.

2.2.6 *Quantitative analysis of fatty acids (FAs)*

The quantitative determination of the relative amount of FAs in every extract was carried following two steps: 1) conversion of crude oil lipids into fatty acid methyl esters (FAMEs); 2) analysis of the FAMEs through Gas Chromatography-Flame Ionization Detector-Mass Spectrometer (GC-FID-MS) technique.

2.2.6.1 Conversion of crude oil lipids into FAMES

The transesterification was carried in basic media on 200 μ L of crude oil, at room temperature, by adding 5mL of a 0.5 M solution of KOH in methanol for 3 h avoiding any contamination with water and was monitored using TLC (*n*-hexane/ethyl acetate 93:7 v/v). After neutralization of the basic solution with sulphuric acid and in vacuum evaporation of the organic solvents (Rotovapor, Heidolph, Schwabach, Germany), FAMES were isolated by flash chromatography on Silica gel with *n*-hexane/ethyl acetate gradient elution (first fractions), whilst oxidized lipids and phytosterols eluted later and were not further analyzed.

2.2.6.2 GC analysis of FAMES

A Thermo-Finnigan Trace GC Ultra (Thermoquest, Rodano, Italy), equipped with a flame ionization detector (FID) and a Thermo-Finnigan Trace DSQ quadrupole mass spectrometer, was used to carry out the GC-MS analysis of FAMES. The chromatographic column used was a DB-WAX 30 m x 0.250 mm x 0.50 μ m. The temperatures of the injector and detector were kept constant at 250 °C and 280 °C, respectively. The flow rate of the carrier gas (He) was 1.4 mL/min. The source and the transfer line were kept at 300 °C. The detector gain was set at 1.0×10^5 (multiplier voltage: 1326 V). For every chromatographic run, 1.0 μ L of sample solution was injected. The oven program started with an initial temperature of 50 °C held for 1 min, followed by a linear ramp from 50 to 200 °C at 25 °C/min and from 200 to 230 °C at 3 °C/min. The final temperature of 230 °C was held for 19 min. The source filament and the electron multiplier were switched off during the initial 5 min to avoid the detection of the solvent front. Mass spectra were recorded both with 70 eV Electron Impact ion (EI) and Chemical Ionization (CI) ion sources. The mass range scanned was from *m/z* 50 to *m/z* 500 at 500 amu/s. Data were collected and processed with Xcalibur (version 1.4).

FAMES were identified by comparing their retention times with those of a reference solution run at identical GC conditions and by matching the MS spectra with the MS-library implemented in the GC apparatus. GC analysis was performed in duplicate and results were expressed as the percentage of total fatty acids (mean FID area ratio).

2.2.7 HPLC analysis of tocol contents

Grape seed oil was diluted with *n*-hexane to a final concentration of 10 mg/mL and directly analyzed for tocol content by High Performance Liquid Chromatography in

duplicate. The HPLC equipment consisted of a model 600 HPLC pump (Waters, Vimodrone, Italy) coupled with a model X-20 fluorimetric detector (Shimadzu, Milan, Italy) operated by Empower software (Waters, Vimodrone, Italy). A sample volume of 50 μL was injected. Chromatographic separation of the compounds was achieved with the normal phase method of Panfili et al. [89]. In brief, a 250 mm x 4.6 mm i.d., 5 μm particle size, Kromasil Phenomenex Si column (Torrance, CA) was used. The mobile phase was *n*-hexane/ethyl acetate/acetic acid (97.3:1.8:0.9 v/v/v) at a flow rate of 1.6 mL/min. Fluorimetric detection was performed at an excitation wavelength of 290 nm and an emission wavelength of 330 nm.

2.2.8 Statistical analysis of data

Experimental data were analyzed by both one-way and two-way ANOVA with the least significant difference (LSD) as a multiple range test using Statgraphics 5.1 (STCC Inc.; Rockville, MD). Results are reported as average of at least two duplicates \pm SD.

2.3 Results and discussion

2.3.1 Oil yield

Oil yield values are reported in Table 2.1. SC-CO₂ extractions were performed at least twice and *n*-hexane extractions were repeated at least three times for each cultivar and harvesting year. The Sauter mean diameter (Smd) of the milled particles used for extraction was lower than 0.5 mm in all the cases.

The oil yields ranged from a minimum value of 10.1% (MT, SC-CO₂, 2012) to a maximum value of 16.6% (CH, *n*-hexane, 2011). A wide range of oil content in grape seeds is reported in the literature. Fernandes et al. [90] reported oil yields of 3.95-12.4% for ten grape cultivars, Passos et al. [91] found oil yields of 11.5% and 16.5% without and with enzymatic treatment before SC-CO₂ extraction, respectively. Da Porto et al. [92] reported 14% oil yields using Soxhlet and ultrasound-assisted extraction. Actually, the oil yield depends on several factors, from the type of seed pretreatment and extraction technique to the type of solvent and operating conditions applied. The variety of cultivars and the environmental factors during grape ripening (harvesting year) also play a significant role. As shown by two-way ANOVA, the cultivar effect on oil yield (f-ratio = 49 in 2011 and 85 in 2012) was greater than the extraction technology applied, i.e., SC-CO₂ or *n*-hexane (f-ratio = 9 in 2011 and 14 in 2012). The yields obtained with *n*-hexane were significantly

different ($p < 0.05$) from those obtained with SC-CO₂ for CH and NE in 2011 and MO, NE and MT in 2012. The effect of harvesting year on yield of SC-CO₂ extraction process was statistically significant for CH and MT (ANOVA results not shown). Agostini et al. [93] also observed that oil yield varies in different harvesting years.

Table 2.1: Grape seed oil yield obtained from various cultivars (Cv) by SC-CO₂ and *n*-hexane extraction (years 2011-2012).

Cv	2011		2012		x_0
	SC-CO ₂	<i>n</i> -hexane	SC-CO ₂	<i>n</i> -hexane	
BA	11.0 ^{a,x} ± 0.6	11.1 ^{a,x} ± 0.5	10.9 ^{b,x} ± 0.6	11.0 ^{a,x} ± 1.3	13.0
CH	15.0 ^{c,x} ± 0.4	16.6 ^{d,y} ± 0.3	13.8 ^{d,x} ± 0.6	14.2 ^{c,x} ± 0.4	14.7
MO	13.8 ^{b,x} ± 0.3	13.8 ^{b,x} ± 0.1	12.6 ^{c,x} ± 1.3	14.7 ^{c,y} ± 1.5	16.0
NE	14.0 ^{b,x} ± 0.5	15.1 ^{c,y} ± 0.5	10.9 ^{ab,x} ± 1.4	12.6 ^{b,x} ± 0.7	13.3
PI	14.0 ^{b,x} ± 0.4	14.1 ^{b,x} ± 0.5	15.5 ^{e,x} ± 0.5	15.5 ^{c,x} ± 0.5	16.7
MT	13.6 ^{b,x} ± 0.2	14.1 ^{b,x} ± 0.6	10.1 ^{a,x} ± 0.5	11.3 ^{ab,y} ± 0.5	12.0

Data in Table 2.1 are expressed as mean ± SD. Two-way ANOVA was performed considering Cv and extraction process as factors. Different letters in the same column indicate significant differences among Cv (LSD, $p < 0.05$). With reference to same Cv and harvesting year, different letters in the same row (x-y) indicate significant differences between extraction processes (LSD, $p < 0.05$).

Table 2.1 also reports the maximum value for the observed oil yield for the harvesting year 2012, i.e. x_0 , considering all the tests performed, both by SC-CO₂ and by *n*-hexane extractions. The values of x_0 were utilized as reference values for grape seed oil content when modeling the extraction kinetics curves (for detail see Chapter 5).

2.3.2 Analysis of the crude oil extracts by NMR and MALDI-TOF

The crude oil samples obtained by SC-CO₂ extraction were first analyzed by NMR measurements whereby detailed information about their overall chemical composition can be easily obtained (Figure 2.3 and Table 2.2). ¹H-NMR spectra showed that these extracts were largely dominated by triacylglycerols (TAGs, ~98%), but minor amounts of 1,2 diacylglycerols (1-2% of 1,2 DAGs) and oxidized lipids (0.1-0.3% as hydroperoxy-octadienoic) were also detected. The presence of DAGs was established by the ¹H-doublet signal at δ_H 3.72 ppm attributable to proton at sn-2 position whilst oxidized lipids showed the characteristic olefinic protons of the conjugated diene system

at δ_H 6.56, 5.98 and 5.76 ppm.

The presence of unsaturated ω -3 lipids is near or below the NMR detection limit ($\leq 0.5\%$) as confirmed by the presence in the 1H -NMR spectrum of a weak triplet at δ_H 0.969, a structural feature for homo-allylic Me group in unsaturated ω -3 fatty chains. Finally, the presence of phytosterols (mainly β -sitosterol) was established to represent only a minor contribution (0.2-0.5%) to the overall composition of these oil extracts. No significant differences were noticed in the relative amounts of these minor metabolites (DAGs, oxidized lipids and phytosterols) with respect to major TAGs components in the different samples

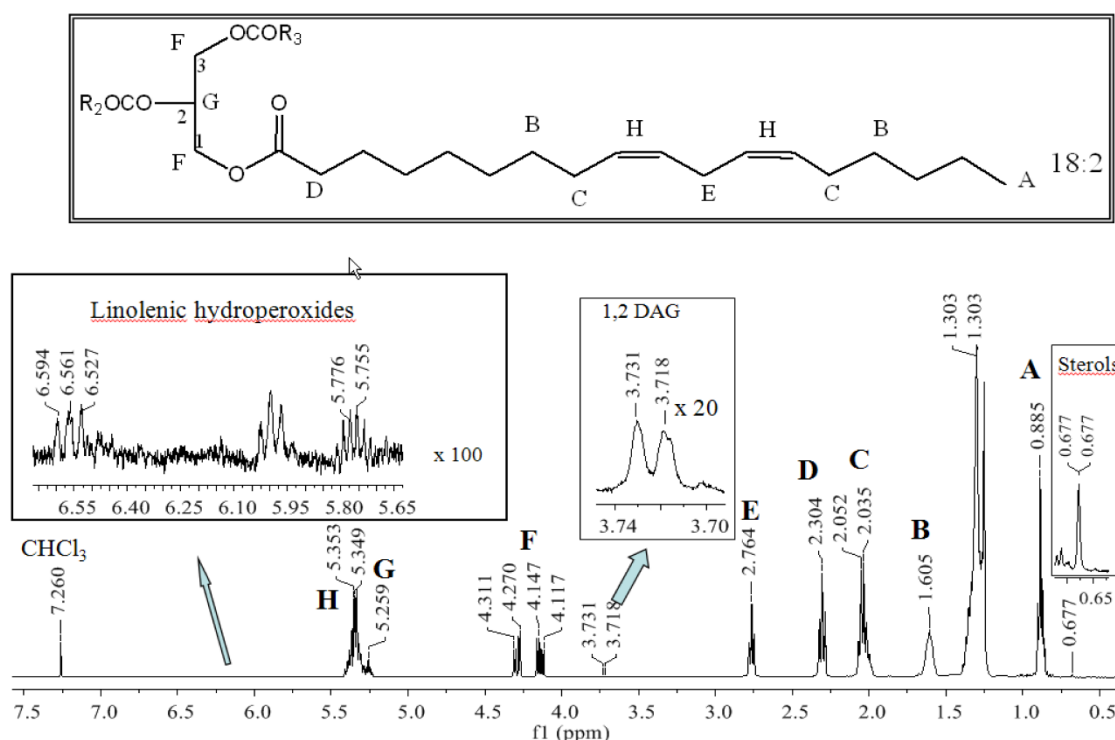


Figure 2.3: 1H -NMR spectrum in $CDCl_3$ of Moscato seed oil by $SC-CO_2$ extraction; capital letters represent the attribution of 1H -NMR signals to specific protons of the linolenic acyl chain reported at the top of the figure.

The integration of the 1H -NMR signals attributable to lipids with different number of unsaturations allowed to establish the quantitative distribution among saturated (SFA), mono-unsaturated (MUFA) and di-unsaturated (DUFA) acyl chains on the glycerol backbone. Thus, the ratio of the peak area of the bis-allylic protons (2H at δ_H 2.76 ppm) to the area of protons in α position to the carbonyl groups (2H at δ_H 2.30) allowed to establish the relative molar fraction of DUFA (mainly 18:2, linoleic acid, L). On the other hand, the ratio of the peak area of the allylic protons (4H at δ_H 2.04) to the area of protons

in α position to the carbonyl groups (2H at δ_{H} 2.30) leads to the relative molar ratio of MUFA (mainly 18:1, oleic acid, O), thus leaving the relative molar abundance of all the saturated chains (SFA) as the difference between total FA and all the unsaturated MUFA+DUFA.

Significant differences among cultivars were found for the relative amount of DUFA which ranged from the lowest limit of CH (70.3%) to the highest of MT (74.9%); it is worth noting that the changes in the relative amount of MUFA follow an opposite trend with CH (19.0%) as the highest and MT (16.4%) as the lowest. Somehow, these opposite trends compensate the overall unsaturation index (UI) of these oils whose change results in a narrow range of values (1.58-1.66, 5% of variation).

Table 2.2: Lipids composition of grape seed oils obtained by SC-CO₂ extraction as established by ¹H-NMR quantitative analysis, all values represent % molar fractions. Unsaturation index (UI) is defined by $UI = (2 * DUFA \% \text{ molar fraction} + MUFA \% \text{ molar fraction}) / 100$.

Cv	TAG ^a	1,2 DAG	Sterols ^c	Hydroperox ^d	SFA ^e	MUFA ^f	DUFA ^g	UI ^h
BA	98.4	1.10	0.40	0.10	12.8	15.2	72.0	1.59
CH	98.3	1.20	0.30	0.20	10.7	19.0	70.3	1.60
MO	98.2	1.10	0.50	0.20	10.2	18.8	71.0	1.61
NE	98.1	1.40	0.20	0.30	11.6	14.3	74.1	1.62
PI	97.8	1.70	0.20	0.30	12.3	17.1	70.6	1.58
MT	97.3	2.10	0.40	0.20	8.7	16.4	74.9	1.66

^{a)} SD \pm 0.5; ^{b)} SD \pm 0.03; ^{c)} SD \pm 0.02; ^{d)} SD \pm 0.03; ^{e)} SD \pm 0.2; ^{f)} SD \pm 0.1; ^{g)} SD \pm 0.1; ^{h)} SD \pm 0.02

These results are in very satisfactory agreement (see Table 2.3) with those obtained by GG-FID-MS analysis and discussed in the following section. As a further support, MALDI-TOF mass spectral data were consistent with NMR data above discussed. In fact, most of the major TAGs contained the linoleic (18:2) acyl chain. A total of 7 TAGs were identified among which trilinolein (LLL) was the most abundant detected as Na⁺ adduct at m/z 901.8. Among the others, triolein (OOO) and palmitoyl-diolein (POO) did not contain any linoleic chains.

The major TAGs found were: PLL (16:0,18:2,18:2) detected at m/z 877.8, POL (16:0,18:1,18:2) at m/z 879.8, POO (16:0,18:1,18:1) at m/z 881.8, LLL (18:2,18:2,18:2) at m/z 901.8, OLL (18:1,18:2,18:2) at m/z 903.8, OOL (18:1,18:1,18:2) at m/z 905.8 and finally OOO (18:1,18:1,18:1) at m/z 907.8.

2.3.3 Quantitative analysis of FA profile

Since NMR is not able to resolve lipids with different carbon lengths and MALDI-TOF is not a quantitative technique, a complete analysis of the acyl chains diversity was carried out on FAMES obtained by alkaline trans-esterification followed by Silica gel flash chromatography. The last step implied that only FAMES deriving from TAGs and DAGs (~ 98% of the overall oil content) were analyzed since oxidized linoleic acid (deriving from hydrolysis of oxidized TAGs) and phytosterols had higher polarity on Silica column and were not present in chromatographic fractions containing the FAMES themselves. Figure 2.4 reports a chromatogram where the retention time of the various assigned peaks is evidenced.

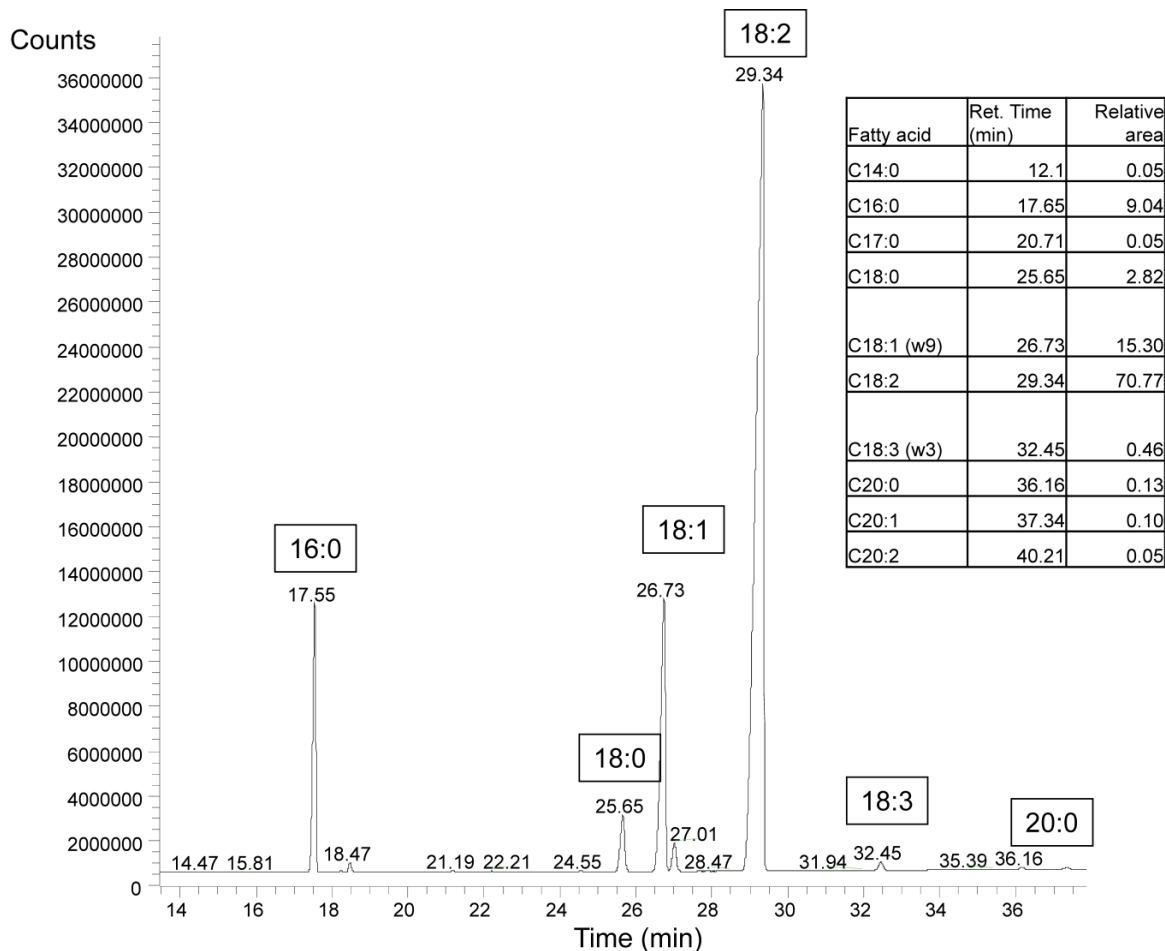


Figure 2.4: GC-FID chromatogram representing the fatty acids distribution of Moscato seed oil by SC-CO₂ extraction; reported peaks were assigned by their EI-MS spectra.

The major fatty acids found in grape seed oils were linoleic acid (C18:2 ω₆, 70.4–74.3%), oleic acid (C18:1 ω₉, 13.6–16.8%), palmitic acid (C16:0, 6.53–8.89%), and

stearic acid (C18:0, 2.84–4.16%) (Table 2.3). The amounts of these major fatty acids were in the intervals of values indicated for grape seed oil in the *Codex standard*, which however are much wider than those observed in this study. Other fatty acids detected in grape seed oils were myristic acid (C14:0), heptadecanoic acid (C17:0), linolenic acid (C18:3 ω 3), arachidic acid (C20:0), eicosenoic acid (C20:1 ω 9), eicosadienoic acid (C20:2 ω 6). In the analysis, only minor FAs were not identified, as supported by data in Table 2.3 which shows that about 99% of the total peak area was accounted for by the assigned FA species. The fatty acid contents of grape seed oils extracted by SC-CO₂ did not vary significantly ($p < 0.05$) with respect to those of oils extracted by mechanical pressure.

2.3.4 Tocopherols and tocotrienols

The total tocol contents of the six grape seed oils extracted by SC-CO₂ ranged between 355 (MO) and 559 (NE) mg/kg in 2012. According to the *Codex Alimentarius*, the level of tocopherols and tocotrienols in crude grape seed oil is in the range of 240–410 mg/kg. Based on this standard, NE and BA oils had higher total tocol contents, while the other varieties were in a similar range (Table 2.4). It is worth noting that Crews et al. [84] reported a wider range for tocol contents in grape seed oils extracted with *n*-hexane (63–1208 mg/kg) following a survey of winemaking sites in France, Italy and Spain, which are the major world grape producers. However, there is scarce information on tocol contents of oils extracted by SC-CO₂. Beveridge et al. [94] observed higher tocol contents in grape seed oils extracted by SC-CO₂ from Barbera (701 mg/kg) and Pinot noir (606 mg/kg) than those observed in the current study.

These differences could be due to different geographical origin and maturity stage of the aforementioned varieties and on different handling of seeds after collection. In fact, in the study by Beveridge et al. [94], grape pomace was freeze-dried and butylated hydroxytoluene was added to the oils to prevent oxidation, whereas in this study a cost-effective drying (air-drying) was selected with no addition of additives. Beveridge et al. [94] also found that most of the oils extracted by SC-CO₂ had similar tocol contents with respect to those extracted by *n*-hexane, but for some cultivars SC-CO₂ extraction was more efficient. Mechanical extraction was not considered. In this study, it was observed that in comparison with *n*-hexane extraction, SC-CO₂ extraction lead to production of oils with higher or similar tocol contents. It is to remark that all oils extracted by SC-CO₂ had

similar tocol contents as those obtained by mechanical extraction that is considered as a process with minimal impact on oil quality [84].

Regarding tocol composition of the oils, the major tocol compounds, i.e., α -tocotrienol, γ -tocotrienol, α -tocopherol and γ -tocopherol were quantified, whereas the δ - β -isomers were below the limit of detection for all the oils (2 mg/kg). γ -tocotrienol was found to be the prevalent tocol for all the varieties characterized. Considering γ -tocotrienol as a promising antioxidant compound for prevention of both cardiovascular disease and cancer [87], grape seed oils could have applications in the nutraceutical, food and cosmetic industry.

In general, the harvesting year had no effect on total tocol content of the oils. For the PI oil only, the tocol content was significantly lower in 2011 (by 10%) than in 2012 ($p < 0.05$). Hence, similar tocol contents could be forecasted in the future harvesting years.

Table 2.3: Fatty acid composition (% of total fatty acids) from FAME GC-FID-MS analysis of the grape seed oil obtained from various cultivars (Cv) by SC-CO₂. Data are expressed as mean \pm SD. Different letters in the same column indicate significant differences among grape cultivars (LSD, $p < 0.05$).

Cv	Fatty acid									
	C14:0	C16:0	C17:0	C18:0	C18:1 (ω -9)	C18:2 (ω -6)	C18:3 (ω -3)	C20:0	C20:1 (ω -9)	C20:2 (ω -6)
BA	0.073 ^d \pm 0.004	6.66 ^a \pm 0.15	0.047 ^a \pm 0.003	4.04 ^c \pm 0.02	16.0 ^c \pm 0.1	71.7 ^b \pm 0.1	0.47 ^d \pm 0.01	0.14 ^b \pm 0.01	0.13 ^c \pm 0.01	0.035 ^a \pm 0.004
CH	0.064 ^{cd} \pm 0.001	7.62 ^b \pm 0.02	0.055 ^b \pm 0.004	3.55 ^b \pm 0.01	16.8 ^f \pm 0.1	70.4 ^a \pm 0.1	0.36 ^a \pm 0.01	0.15 ^b \pm 0.01	0.15 ^d \pm 0.01	0.033 ^a \pm 0.001
MO	0.051 ^b \pm 0.003	8.89 ^c \pm 0.21	0.049 ^a \pm 0.001	2.84 ^a \pm 0.02	15.3 ^c \pm 0.1	71.0 ^a \pm 0.3	0.46 ^d \pm 0.01	0.14 ^b \pm 0.01	0.11 ^a \pm 0.01	0.041 ^a \pm 0.010
NE	0.061 ^c \pm 0.010	6.53 ^a \pm 0.39	0.061 ^c \pm 0.001	4.16 ^d \pm 0.11	13.6 ^a \pm 0.2	74.3 ^d \pm 0.5	0.43 ^c \pm 0.01	0.18 ^c \pm 0.01	0.15 ^d \pm 0.01	0.038 ^a \pm 0.002
PI	0.058 ^{bc} \pm 0.000	7.47 ^b \pm 0.06	0.060 ^c \pm 0.003	3.56 ^b \pm 0.01	15.6 ^d \pm 0.1	71.8 ^b \pm 0.1	0.38 ^b \pm 0.01	0.13 ^{ab} \pm 0.01	0.14 ^d \pm 0.01	0.046 ^a \pm 0.010
MT	0.041 ^a \pm 0.001	6.82 ^a \pm 0.16	0.051 ^{ab} \pm 0.001	3.64 ^b \pm 0.01	14.8 ^b \pm 0.1	73.2 ^c \pm 0.2	0.43 ^c \pm 0.01	0.12 ^a \pm 0.01	0.12 ^b \pm 0.01	0.045 ^a \pm 0.006

Table 2.4: Tocopherol and tocotrienol contents (mg/kg) of the grape seed oils obtained from various cultivars (Cv) by SC-CO₂, mechanical extraction and n-hexane extraction (harvesting year 2012).

Cv	Tocol											
	α- Tocopherol			α- Tocotrienol			γ- Tocopherol			γ- Tocotrienol		
	SC-CO ₂	n-hexane	mechanical	SC-CO ₂	n-hexane	mechanical	SC-CO ₂	n-hexane	mechanical	SC-CO ₂	n-hexane	mechanical
BA	196 ^{c,y} ± 6	106 ^{c,x} ± 3	199 ^{d,y} ± 12	97 ^{a,x} ± 42	68 ^{b,x} ± 3	62 ^{ab,x} ± 8	55 ^{c,y} ± 2	62 ^{c,y} ± 4	30 ^{c,x} ± 2	151 ^{b,y} ± 3	106 ^{b,x} ± 10	190 ^{b,z} ± 11
CH	68 ^{a,y} ± 6	39 ^{a,x} ± 3	73 ^{b,y} ± 4	122 ^{a,y} ± 11	88 ^{bc,x} ± 7	131 ^{c,y} ± 1	21 ^{a,y} ± 1	11 ^{ab,x} ± 1	24 ^{b,y} ± 1	170 ^{bc,y} ± 9	131 ^{bc,x} ± 13	172 ^{b,y} ± 7
MO	131 ^{b,y} ± 14	63 ^{b,x} ± 2	127 ^{c,y} ± 8	81 ^{a,y} ± 13	26 ^{a,x} ± 1	67 ^{a,y} ± 5	33 ^{b,y} ± 6	20 ^{a,x} ± 1	48 ^{d,z} ± 2	110 ^{a,y} ± 21	52 ^{a,x} ± 3	87 ^{a,xy} ± 3
NE	157 ^{b,y} ± 21	114 ^{c,x} ± 9	115 ^{c,x} ± 5	170 ^{b,y} ± 5	124 ^{d,x} ± 11	167 ^{d,y} ± 21	53 ^{c,x} ± 4	51 ^{c,x} ± 15	53 ^{d,x} ± 2	179 ^{c,x} ± 4	154 ^{cd,x} ± 9	185 ^{b,x} ± 17
PI	79 ^{a,x} ± 9	94 ^{c,x} ± 21	61 ^{ab,x} ± 15	82 ^{a,x} ± 7	93 ^{c,x} ± 20	75 ^{ab,x} ± 19	23 ^{a,x} ± 4	25 ^{b,x} ± 7	24 ^{b,x} ± 2	253 ^{e,x} ± 2	224 ^{e,x} ± 40	279 ^{e,x} ± 74
MT	51 ^{a,x} ± 2	27 ^{a,x} ± 2	41 ^{a,x} ± 2	98 ^{a,x} ± 20	105 ^{cd,x} ± 7	103 ^{bc,x} ± 8	18 ^{a,x} ± 2	14 ^{ab,x} ± 1	17 ^{a,x} ± 1	212 ^{d,x} ± 4	187 ^{e,x} ± 10	198 ^{b,x} ± 22

Data are expressed as mean ± SD. Two-way ANOVA was performed considering Cv and extraction process as factors. Different letters in the same column indicate significant differences among Cv (LSD, p < 0.05). Different letters in the same row (x-y) indicate significant differences among the extraction processes (LSD, p < 0.05).

2.4 Conclusions

Supercritical CO₂ (SC-CO₂) extraction was studied as a green technology to recover grape seed oils from winemaking by-products. Oil yields from SC-CO₂ extraction resulted in the range 10.9 – 15.0%, with a remarkable dependence on grape cultivar and, for some cultivars, on harvesting years. The oils extracted by SC-CO₂ had similar quality, in terms of fatty acid and tocol contents, as those obtained by mechanical extraction. The strong agreement of the quantitative results obtained by ¹H-NMR measurements carried out on the raw oil extracts with those obtained by classical GC-FID-MS techniques carried out on their FAME derivatives suggests that NMR can represent a robust, fast and reliable alternative to the latter. It is worth noticing that from simple NMR analysis it is possible to gain useful information not only on the dominant chemical species (TAGs), but also on minor interesting metabolites often present in natural oil extracts such as DAGs, sterols and oxidized lipids. Finally, the level of tocopherols and tocotrienols found in grape seed oils in two harvesting years supports their potential applications in food, nutraceutical and cosmetic industries.

3. Kinetic Models for Supercritical CO₂ Extraction

In this Chapter, the models used to evaluate the supercritical CO₂ (SC-CO₂) extraction kinetic curves are compared and discussed. Particularly, three models, the broken and intact cells (BIC), the shrinking core (SC), and the bridge (combined BIC-SC) models are critically analyzed. The models not only allowed fitting satisfactorily the experimental data, but also resembling the real physical structure of the vegetable matrix and the actual elementary steps (mass transfer phenomena) which are expected to occur at the micro-scale level. The main objective of this Chapter is to objectively choose the best model that can be used in the subsequent Chapters. The analysis also provides an insight of interest for the audience concerned with modeling the supercritical extraction process.

3.1 Introduction

The extraction process involves a solid-SC-CO₂ operation where mechanically pretreated solid materials are kept in vertical cylindrical column with CO₂ flowing down the bed. The operation consists of static and dynamic extraction periods. During static period there is no product collection and is usually equal to the time required to reach the extraction conditions. The dynamic phase is from the time the products are start to be collected to the end of extraction process. At the start of dynamic extraction period there is typically a time delay in kinetics curve which corresponds to the time required for the fluid to flow between the expansions valves to the product collection tank. It is worthwhile to

* Part of the present Chapter has been published as: Kurabachew Simon Duba, Luca Fiori, *Supercritical Fluid Extraction of Vegetable Oils: Different Approach to Modeling the Mass Transfer Kinetics*, *Chemical Engineering Transactions*, Volume 43,2015. In press

mention that, the amount of solute collected at this stage is less than the actual value which is extracted because of surface wetting property of solute once the carrier phase (CO₂) is expanded; this is especially useful if lab scale model parameters are used for scale up purpose.

In general, the evaluation of overall extraction curves through kinetic models has a paramount importance in establishing the optimum operating conditions, determining parameters used for scale-up and process design, and ensuring technical and economic viability of SC-CO₂ extraction processes at industrial scale [95–97].

3.2 Extraction kinetics models

In the literature there are several kinetic models developed for the SC-CO₂ extraction. These models can be broadly classified into two general categories. The first category accounts for the empirical models and for the models describing the mass transfer resorting to analogies with other physical systems and transfer phenomena. Among them, it is worth citing the Crank [98] hot ball diffusion model (HBD), the Naik et al. [99] empirical model, the Tan and Liou [100] desorption model, and the Martinez et al. [101] logistic model. In the second category, models where the solute mass flux is defined by the concentration gradient as driving force can be clustered. Under this category, the Veress [102] diffusion layer theory model, the Sovová [4] broken and intact cell (BIC) model, the Goto et al. [103] shrinking core (SC) model, and the Fiori et al. [104] bridge model (combined BIC-SC model) can be classified.

Substantial efforts have been made in the literature to compare the relative performances of the various models. For example, Bernardo-gil et al. [105] applied empirical, HBD model, and BIC models to the SC-CO₂ extraction of olive husk oil. Campos et al. [106] applied desorption, logistic, single plate, HBD, and BIC models to the SC-CO₂ extraction of marigold (*Calendula officinalis*) oleoresin. Machmudah et al. [96] applied BIC and SC models to the SC-CO₂ extraction of nutmeg oil. Domingues et al. [107] applied desorption, logistic, single plate and HBD models to the SC-CO₂ extraction of *Eucalyptus globulus* bark.

There is no holistic agreement in the research community regarding the model which performs the best under all the experimental conditions. The fact that the models are applied to different solid substrates with different initial extractable substances under

various operating conditions hinders the comparisons across the literatures. During the derivation of kinetic models, the type of simplifying assumptions made and the governing principles on which the mechanism of extraction is based on make one type of model to best fit to a specific extraction situation than the others. However, it must be stressed that the best fitting alone should not be considered the only objective of the extraction kinetics models, which should not be only merely capable to provide a simple input output mapping. The models should describe the underlining physical phenomena occurring during extraction and, in addition, they should be reasonably simple.

In this work the attention is on the Sovovà [4] BIC model, the Goto et al. [103] SC model and the Fiori et al. [104] bridge (combined BIC-SC) model. These models have been selected considering that they attempt to describe the extraction kinetics mechanism accounting for the morphological structure of the substrates, the vegetable seeds. The author also compared almost all (eight) models (with Goto and Hirose [108] version instead of Goto et al. [103] SC model) but chose not to include in this thesis to focus on only the second categories of the model discussed above (interested readers can find the detail discussion in Duba and Fiori [109]).

The models have been compared in terms of effectiveness in predicting experimental data and in terms of the calculated (through optimization) parameters: internal and external mass transfer coefficients and percentage of easily extractable oil. To this regards, the common selected parameter was the effective diffusivity (D_{eff}) which governs the extraction from the inside of the seed particles. The experimental data for this study were taken from a previous work Fiori [13].

3.2.1 The Broken and Intact Cell (BIC) model

The Sovovà [4] BIC model assumes that as a result of mechanical milling pretreatment some cells in the solid matrix are broken and the remaining cells in the particle core are intact. The oil in the broken cells (referred as “free oil”) is exposed to the particle surface, i.e. to the SC-CO₂, and can be easily extracted. Under this condition the rate of extraction depends in particular on the oil solubility in the supercritical fluid, while the oil in the intact cells (referred as “tied oil”) is much more difficult to extract as a result of high mass transfer resistances. Under steady state plug flow conditions with homogenous particle size distribution, the analytical solution for the extraction yield is given by Šťastová et al. [110] as:

$$\frac{E}{Nx_0} = \begin{cases} \psi[1 - e^{-Z}] & \text{for } \psi \leq \frac{G}{Z} \\ \psi - \frac{G}{Z} e^{[Z(h_k-1)]} & \text{for } \frac{G}{Z} \leq \psi \leq \psi_k \\ \left\{ 1 - \frac{1}{Y} \ln \left[1 + [e^Y - 1] e^{[Y(\frac{G}{Z} - \psi)]} \right] (1 - G) \right\} & \text{for } \psi \geq \psi_k \end{cases} \quad (3.1)$$

$$\text{Where, } \psi = \frac{tQy_s}{Nx_0}, \quad Y = \frac{Nk_s a_p x_0}{Q(1-\varepsilon)y_s}, \quad Z = \frac{Nk_f a_p \rho_f}{Q(1-\varepsilon)\rho_s}, \quad \psi_k = \frac{G}{Z} + \frac{1}{Y} \ln\{1 - G[1 - e^Y]\}, \quad h_k =$$

$$\frac{1}{Y} \ln \left[1 + \frac{\left\{ e^{[Y(\psi - \frac{G}{Z})] - 1} \right\}}{G} \right]$$

E is the amount of oil extracted, N is the initial mass of the solid used for extraction, x_0 is the initial oil concentration in the solid, t is extraction time, Q is solvent mass flow rate, ε is bed void fraction, a_p is particle specific interfacial area, ρ_f is solvent density, ρ_s is solid density, k_f is external mass transfer coefficient, k_s is internal mass transfer coefficient, y_s is oil solubility in the solvent.

Moreover, other dimensionless parameters appear in the above set of equations: ψ is dimensionless time; Z and Y are parameters, respectively, for the first and second extraction period; ψ_k is ψ at the boundary between first and second extraction period; finally h_k is the extractor coordinate dividing the extractor in two regions, the former, close to the solvent entrance, where free oil has been completely extracted, the latter where free oil is still being extracted. For a detailed description of the model, the reader can refer to [110]. Interestingly, the model utilized here practically coincides with ‘‘Type A’’ model, as later defined (and proved) by Sovová [111].

3.2.2 The Shrinking Core (SC) model

The SC model accounts for an irreversible desorption of oil from the solid followed by diffusion in the porous solid through the pores as proposed by Goto et al. [103]. It is assumed that there is a moving boundary between the extracted and non-extracted parts. The core of inner region shrinks inward with the progress of the extraction leaving behind an irreversibly exhausted solid matrix. Solute in the core diffuses to the surface of the particle through a network of pore without refilling the space already exhausted. The internal mass transfer from inner core to the pore is much greater than the convective transport through the pores. The general mass balance equations in dimensionless form are given by Eq.s (3.2) and (3.3) which can be solved numerically under proper initial and

boundary conditions [103]:

$$\frac{\partial \chi}{\partial \theta} + \alpha \frac{\partial \chi}{\partial z} = \frac{\alpha}{p_e} \frac{\partial^2 \chi}{\partial z^2} - \frac{(1-\varepsilon)}{\varepsilon} \frac{3B_i(\chi-1)}{1-B_i(1-1/\xi_c)} \quad (3.2)$$

$$\frac{\partial \xi_c}{\partial \theta} = \frac{bB_i(\chi-1)}{[1-B_i(1-1/\xi_c)]\xi_c^2} \quad (3.3)$$

The dimensionless groups are defined as $\chi = \frac{y}{y_s}$, $\alpha = \frac{uR^2}{LD_{eff}}$, $B_i = \frac{k_f R}{D_{eff}}$, $\theta = \frac{tD_{eff}}{R^2}$, $P_e =$

$$\frac{uL}{D_{ax}}, b = \frac{y_s}{x_0}, \xi_c = \frac{r_c}{R}$$

Where y is the solute concentration in the bulk fluid phase, u is solvent flow rate, R is radius of the particle, L is length of extractor, D_{eff} is effective diffusivity, D_{ax} is axial dispersion, r_c is the un-extracted core radius, z is axial coordinate and the others variables are as defined in Section 3.2.1. In this work, the so called quasi-steady state solution was applied [103].

$$E = \frac{ab\varepsilon}{1-\varepsilon} \int_0^\theta \chi d\theta \quad (3.4)$$

3.2.3 The combined BIC-SC model

The BIC-SC model was proposed by Fiori et al. [104] and is a model somehow between the broken and intact cell and the shrinking core models. In this model it was assumed that the milled seed particles contain M concentric shells of oil bearing cells of diameter d_c . The cells on the surface of the particles are broken as a result of the mechanical pretreatment like in the BIC model. The oil in the broken cells is exposed to the surface and can be easily extracted while the oil in the inner concentric shells is irreversibly depleted starting from the external layer towards the internal core resembling the SC model. The general mass balance over the extractor is given by:

$$\frac{\partial y}{\partial t} + u \frac{\partial y}{\partial z} - D_{ax} \frac{\partial^2 y}{\partial z^2} = \frac{1}{\varepsilon} K a_p (y_s - y) \quad (3.5)$$

Where K is overall mass transfer coefficient and other variable as defined in Section 3.2.1 and 3.2.2.

In order to model the internal mass transfer resistance, three cases were proposed, namely, discrete, semi continuous and continuous. In the case of discrete model (the case which was considered in this work), it was assumed that the mass transfer resistance of

the j^{th} shell is equal to the sum of the external mass transfer resistance plus the resistance of each shell up to the j^{th} concentric shell, i.e.

$$\frac{1}{k_j} = \frac{1}{k_f} + \frac{1}{k_c} \sum_{n=1}^{j-1} \left[\frac{M}{M-n} \right]^2 \quad \text{for } j=1 \dots M \quad (3.6)$$

Where k_j is overall mass transfer coefficient up to j^{th} shell, k_c is the single layer inner shell mass transfer coefficient (equal for each concentric layer), and M is the number of entire spherical shells. The exhaustion degree of the particle ϕ is given by:

$$\phi_j = 1 - \left[\frac{M-j}{M} \right]^3 \quad (3.7)$$

$$K = K_j \quad \text{for } \phi_{j-1} \leq \phi \leq \phi_j \quad (3.9)$$

3.2.4 Model adjustable parameters

The adjustable parameters of each model are as follow: For BIC model, the grinding efficiency (G), the external ($k_f a_p$) and internal mass transfer coefficient ($k_s a_p$), for SC model, the effective diffusivity (D_{eff}) and the external mass transfer coefficient (k_f) and for BIC-SC model the inner shell mass transfer coefficient (k_c). Thus, BIC, SC and BIC-SC models have, respectively, three, two and one adjustable parameters.

All the three models were compared by taking the effective diffusivity as common parameter. For BIC and BIC-SC models the effective diffusivity was calculated, respectively, as follows:

$$D_{eff} = \frac{3d_p k_s}{2} \quad (3.9)$$

$$D_{eff} = k_c d_c \quad (3.10)$$

Furthermore, the external mass transfer coefficient $k_f a_p$ between the BIC and SC models were compared. For obtaining $k_f a_p$ for the SC model, the SC model output k_f was multiplied by a_p which was calculated according to:

$$a_p = (1 - \varepsilon) \frac{6}{d_p} \quad (3.11)$$

Finally, the fraction of free oil was compared for BIC and BIC-SC models. In BIC model the grinding efficiency G is one adjustable parameter through which the fraction of free oil can be calculated as Gx_o . For BIC-SC model the fraction of free oil was

calculated according to the Eqn. (3.12) which was originally proposed by Reverchon and Marrone [112] and later modified by Fiori and Costa [113]:

$$\varphi_f = 3\omega \frac{d_c}{d_p} \quad (3.12)$$

Where, φ_f is the fraction of the particle volume filled by the free oil, d_p is diameter of the particle and ω is a free oil parameter ($0 < \omega < 1$) which was optimized to be 0.472 for grape seed according to what was called the double shell hypothesis [113]. In Table 3.1, the parameter G and $f = \varphi_f/x_0$ were compared.

3.3 Materials and Methods

The experimental kinetic data used in this Chapter was taken from the literature [13] which used the same equipment to extract grape seeds oil. In particular, data obtained with different seed particle diameters were utilized here. The experimental data were fit to the models by minimizing mean squares error using MATLAB^R 7.10 with nonlinear optimization lsqcurvefit function for BIC model, and ode45 followed by fminsearch optimization algorithm for SC model. Previously, the BIC-SC model was simulated in FORTRAN environment [104].

The goodness of the model fitting was evaluated and quantified calculating, for each experimental run, the percent average absolute relative deviation (AARD (%)), given by Eq. (3.13), and the root mean square error (RMSE), calculated according to Eq. (3.14).

$$AARD(\%) = \frac{1}{n} \sum_{i=1}^n \left| \frac{\gamma_{\text{exp}} - \gamma_{\text{model}}}{\gamma_{\text{exp}}} \right|_i 100 \quad (3.13)$$

$$RMSE = \sqrt{\sum_{i=1}^n \frac{(\gamma_{\text{exp}} - \gamma_{\text{model}})^2}{n}} \quad (3.14)$$

Where n represents the number of available experimental data, and γ_{exp} and γ_{model} are, respectively, the experimental extraction yield and the extraction yield predicted by the model – yield expressed as mass of extracted oil per mass of seeds.

3.4 Results and Discussion

Grape seeds contains 8-16% of oil [114]. Actually, the oil content varies according

to cultivar and other environmental factors as discussed in Chapter 2. In this Chapter, 12% was chosen to represent the initial oil content in the seeds, i.e. the maximum value obtained from the experiment according to [13]. Figure 3.1 shows the kinetics of extraction modeled by BIC and SC models. The models adjustable parameters and the RMSE between experimental data and model output are presented in Table 3.1 for the different seed particle size.

The effective diffusivity (D_{eff}), the parameter which is made deliberately common among the models, is in close agreement for all the three models. The average values of D_{eff} of 4.13×10^{-12} , 2.69×10^{-12} and 1.09×10^{-12} m²/sec were obtained respectively for BIC, SC and BIC-SC models. Theoretically, D_{eff} should not depend on the milled particle size, but the output reported in Table 3.1 seems to contradict this.

The SC model seems to predict higher D_{eff} values when the particle size is large, while the BIC-SC model shows an opposite trend; the BIC model does not show any particular trend though it predicted relatively higher values of D_{eff} at small particles sizes like the BIC-SC model.

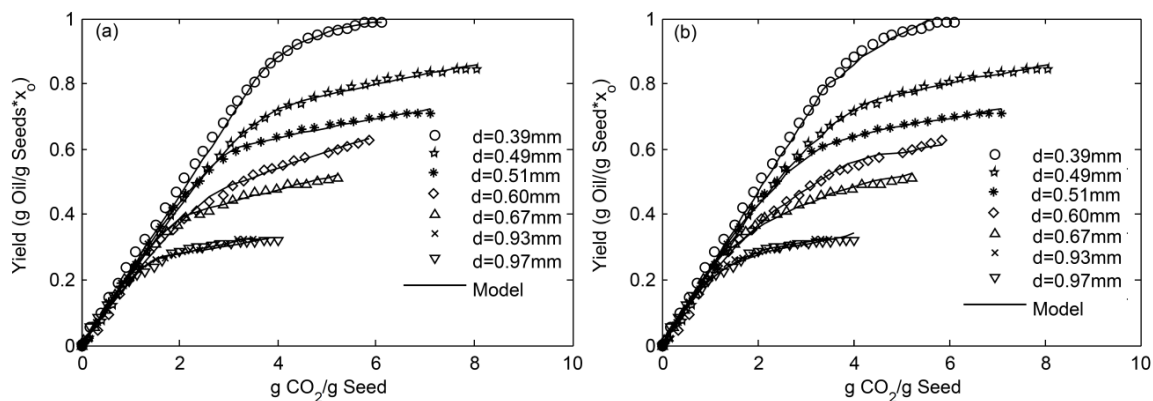


Figure 3.1: Extraction kinetics: (a) BIC model; (b) SC model

The maximum deviations from average values are observed at small particle size for BIC and BIC-SC models and at the two extremes for SC model. To find an explanation to the model output obtained at the extreme values of the particle diameter, it is worth considering that, when the ground seed particle size is very large, substantial amount of the outer surface of the particle is covered by the hard woody structure of the outer surface of the seed: this can influence the extraction kinetics. Conversely, when the particles are very small, the model outputs are influenced to a large extent by the value assumed for the oil content (12% in the present case). Moreover, at low particle size, the bed is more prone to

compaction, so the void fraction may change during the course of the extraction [115] which creates delay in extracted solute flow and/or even channeling. Furthermore, if there is any correlation between particle size and D_{eff} , particle size distribution should be accounted for [116]. Finally, the possibility of solute-solid interactions (not taken into account in any of these models) can influence the extraction kinetics.

As far as the free oil fraction is concerned, the values of G (BIC model) and f (BIC-SC model) are quite similar for the various particle diameters. Unsurprisingly, the smaller was the particle, the larger the free oil. Consistent values of $k_f a_p$ were obtained for BIC and SC models. A minimum deviation in terms of mean square error was observed for the BIC model followed by the SC model. In general, for all the models a remarkable good agreement between experimental data and model predictions was achieved.

Table 3.1: Adjustable parameters for grape seed oil SCO_2 extraction and deviations from experimental data

Models	P (bar) / T (°C)	550 / 40							
BIC	d (mm)	0.39	0.49	0.51	0.60	0.67	0.93	0.97	Average
	$k_f a \cdot 10^2$ (min^{-1})	34.9	3.38	4.88	2.52	3.68	2.98	2.53	2.20
	$k_s a \cdot 10^3$ (min^{-1})	13.5	2.46	1.40	1.72	0.93	0.44	0.59	2.20
	G	0.45	0.66	0.56	0.42	0.36	0.25	0.26	0.42
	D_{eff} (m^2/sec) $\cdot 10^{12}$	14.8	4.31	2.62	4.40	2.90	2.49	4.06	4.13
	RMSE $\cdot 10^2$	1.00	0.20	0.13	0.25	0.14	0.043	0.28	0.35
SC	$k_f a \cdot 10^2$ (min^{-1})	2.68	4.00	3.73	3.42	1.21	3.08	3.10	3.34
	D_{eff} (m^2/sec) $\cdot 10^{12}$	0.63	1.29	1.41	2.44	1.59	7.66	8.77	2.69
	MSE $\cdot 10^2$	1.93	0.43	0.59	0.37	0.91	0.17	0.33	0.81
BIC-SC	k_c (m/s) $\cdot 10^8$	12.7	6.98	4.75	4.87	3.13	3.09	2.56	5.44
	D_{eff} (m^2/sec) $\cdot 10^{12}$	2.54	1.40	0.95	0.97	0.63	0.62	0.51	1.09
	RMSE $\cdot 10^2$	0.80	1.56	1.66	0.74	0.60	0.34	0.80	0.98
	f	0.61	0.48	0.46	0.39	0.35	0.25	0.24	0.40

3.5 Conclusions

Supercritical CO_2 (SC- CO_2) extraction of seed oil was modeled by using different models: particularly, BIC, SC, and BIC-SC. The deviation between model predictions and experimental data was quantified using mean square error RMSE. Remarkably, good agreement between all the three models and experimental data was achieved. The values of model adjustable parameters were consistent among the various models. The BIC model allowed for the minimum RMSE followed by SC and BIC-SC model. These results reflect

the number of adjustable parameters of the different models: 3, 2 and 1 for BIC, SC and BIC-SC respectively. All the three models, which account for the morphological structure of the seeds, represent significant tools for addressing process scale-up. The BIC model is chosen to be used in the subsequent Chapters to model the kinetic of extraction. Besides the three adjustable parameters, in order to use effectively the BIC model, the solute solubility data is required.

4. Solubility of Grape Seed Oil in Supercritical CO₂: Experiment and Modeling

In this Chapter, an effort is made to determine the solubility of grape seed oil over a range of pressure and temperature of practical importance using dynamic technique and then, the experimental data are modeled by eight density-based models and a thermodynamic model based on Peng-Robinson equation of state with Van der Waals' mixing rule. The predictive capability of the thermodynamic model is comparable to that of density-based models. The experimental data generated in this Chapter will be used to model the kinetics of extraction in Chapter 5.

4.1 Introduction

The effective design and scale-up supercritical fluids equipment/process requires the knowledge of fluid phase equilibria. Thus, determination of solute solubility in supercritical phase is the first step in the development and evaluation of any supercritical processes and establishing the optimal operating conditions [117–120].

Experimental determination of solubility generally takes two approaches in the literatures, i.e. static and dynamic techniques. During static method the components are placed in a fixed volume vessel which is stirred mechanically or by recirculating the vapor phase until equilibrium is established. While in the dynamic technique a continuous apparatus is used to contact the two phases and the composition of the stream leaving the vessel is determined after expansion and separation of oil from CO₂ [117,121].

Significant research work were published in the past two decades dedicated to the determination of solubility of diverse organic compounds in SC-CO₂ such as drugs

* Part of the present Chapter is ready to be submitted for publication as: Kurabachew Simon Duba, Luca Fiori, Solubility of grape seed oil in supercritical CO₂: Experiment and Modeling, to *The Journal of Chemical Thermodynamics*.

[119,122,123], seeds oil [124–126], pollutants [127], dyes [128–130], food colorants [131] and many more. However, the reported solubility data are extremely divergent and inconclusive.

In this work, the dynamic method was used to determine the solubility of grape seed oil in SC-CO₂ in the range of pressure and temperature of practical importance i.e. for pressure between 20 MPa and 50 MPa and temperature between 313 K and 343 K. It is worth to highlight that, only a limited number of literatures report are available which deals with the solubility of grape seeds oil and those available are in restricted range of pressure and temperature. The bulk majority of the scientific literatures determined solute solubility in SC-CO₂ through theoretical models. Therefore, testing the predictive power of the commonly used solubility models in the literatures under the same condition has a vital importance. In this regard, the experimental data were modeled using eight density-based models and a thermodynamic model based on Peng-Robinson equation of state with classical Van der Waals mixing rule. The models are compared and discussed in terms of their effectiveness in predicting the experimental data.

4.2 Experimental

4.2.1 Solubility determination

The solubility (y_s) of grape seed oil at different temperatures and pressures was determined by thoroughly blended 5 gram of oil and 145 gram of 1.05 mm diameter glass beads in an extractor of 0.1 L volume and re-extracted by SC-CO₂ in the procedure describe in Chapter 2. The mass of oil use in the experiment was selected in such a way that no oil flow down the column by gravity which may result in a misleading result as proposed by Sovovà et al. [117]. According to the dynamic method for measuring the solubility in supercritical solvent [132], the initial slope of the extraction curve was used to calculate the solubility at the given pressure and temperature. The range of flow rate required to saturate the solvent was first established by conducting a repeated experiment at the same pressure and temperature by varying the flow rate. The initial slopes on the plot of mass of oil per mass of solid *versus* mass of CO₂ consumption per mass of solid were taken as solubility for a given pressure and temperature. The oil solubility values were obtained utilizing oil from Moscato cultivar, but the values are representative for all other grape cultivars, as grape seed oil composition is extremely similar for the different

cultivars (See Chapter 2 for detail of composition of grape seed oil) [114].

4.3 Modeling

Modeling of solubility of solute in SC-CO₂ generally follows two approaches i.e. a density-based correlations and a thermodynamic models using equation of states. The experimental data were fit to the models using MATLAB R2014a by nonlinear optimization function *lsqcurvefit*. The deviation between the models prediction and experimental data were quantified using percent average absolute relative deviation and root mean square error according to eqn. (3.12) and (3.13) presented in Chapter 3.

4.3.1 Density-based models

In the scientific literatures there are at least three broad categories of density-based models; the first group includes those models that are based on the law of mass action. Notable example of this group are the Chrastil [133] model and its modifications which foresees a linear relationship between the logarithm of solubility and logarithm of solvent density. Some of the important modifications comprises the model by Adachi and Lu [134], del Valle and Aguilera [135] and Sparks et al [136]. The second categories are those models that are based on theory of infinite dilution; this group of models assumes an equi-fugacity condition between the solute in the solid and the supercritical phase. They include the model by Kumar and Johnston [137], Bartle et al [138] and Mendez-Santiago and Teja [139]. The third groups of density-based models are purely empirical in nature which correlates the solubility with pressure and temperature in a simple polynomial fashion. A important example of this last class is Yu et al model [140] which also have several modification.

The model developed by Chrastil [133] is derived based on associates law. It is assumed that, at equilibrium one molecule of the solute A will associate with k molecule of the solvent B to form a solute solvent complex. The final expression of the solubility in supercritical phase is given by Eqn. (4.1). On the derivation of the equation can be seen in the original work of Chrastil [133].

$$\ln S = \Delta H/RT + k \ln(\rho) + \ln[M_A + kM_B] - k \ln(M_B) + q \quad (4.1)$$

Where, S is the solubility in ($\text{g}\cdot\text{L}^{-1}$), ΔH is the total heat of reaction ($\Delta H = \Delta H_{\text{solv}} + \Delta H_{\text{vap}}$) the sum of heat of solvation and heat of vaporization in ($\text{kJ}\cdot\text{mol}^{-1}$)

¹), M_A and M_B are the molecular weights of the solute in ($\text{g}\cdot\text{mol}^{-1}$), k is the associates constant and the solvent, R is the universal gas constant in ($\text{J}\cdot\text{mol}^{-1}\cdot\text{K}^{-1}$), T is system temperature in (K), ρ is solvent density in ($\text{g}\cdot\text{L}^{-1}$), and q is a constant. Eqn. (4.1) can be rewritten as:

$$\ln S = k \ln(\rho) + \alpha/T + \beta \quad (4.2)$$

Where $\alpha = \Delta H/R$ and $\beta = \ln[M_A + kM_B] - k \ln(M_B) + q$

Since it was first introduced, Chrastil [133] model underwent several empirical modifications including by Adachi and Lu, del Valle and Aguilera and Sparks and co-workers.

Adachi and Lu [134] applied Chrastil model to over 37 different solute in supercritical CO₂ and ethylene. They argue that, in the application of Chrastil model, the density of the solvent plays a vital role, therefore, the association constant, k must be a function of density. They proposed empirical modification which correlate k and ρ as given by Eqn. (4.3). This correlation adds two more additional adjustable parameters to the Chrastil model.

$$k = \epsilon_0 + \rho\epsilon_1 + \rho^2\epsilon_2 \quad (4.3)$$

Where ϵ_0 , ϵ_1 and ϵ_2 are constant parameters which are determined by fitting the model to experimental data.

According to del Valle and Aguilera [135] the major drawback of Chrastil model is its applicability over restricted temperature range. Hence, an empirical modification was introduced to compensate for the variation of ΔH_{vap} with temperature. Consequently, Chrastil model was modified as given in Eqn. (4.4) by adding one more temperature dependent parameter γ .

$$\ln S = k \ln(\rho) + \alpha/T + \gamma/T^2 + \beta \quad (4.4)$$

Sparks et al [136] applied six density-based models to six solute-supercritical system and ascertained that, the Adachi-Lu and del Valle–Aguilera modification are indeed improved the performance of Chrastil model. But there exist a case where one is better than the other and vice versa. Therefore, Sparks et al. [136] proposed a further modification by incorporating both the Adachi-Lu and del Valle–Aguilera modification in single equation. They recommend that, the third term in the association constant correlation according to Adachi-Lu modification can be left out without compromising

the performance of the resulting equation. Therefore, Sparks et al. [136] model can be used with five or six adjustable parameters.

The Kumar and Johnston model [137] was developed under the assumption that, the solute is incompressible and at equilibrium, the chemical potential of the solute in solid and supercritical phase are the same. Consequently Eqn. (4.5) was developed to correlate solubility and density. Further simplification of Eqn. (4.5) was also proposed under the condition where the ratio of partial molar volume of the component to its isothermal compressibility is independent of the solvent density which is valid in the range of $0.5 < \rho_r < 2.0$ as detailed in [137].

$$\ln y_2 = -C_1 + \ln \left[\frac{p_2^{sub}}{\rho_c RT} \right] + \frac{p v_2^s}{RT} + \left[\frac{\tilde{v}_2}{\kappa_T RT} \right]_{\rho_r=1} \ln \rho_r \quad (4.5)$$

Where, y_2 is the mole fraction of solute in the supercritical phase, p_2^{sub} is the saturation vapor pressure, v_2^s is the molar volume of solute, κ_T is isothermal compressibility, \tilde{v}_2 is the partial molar volume of the solute in supercritical phase, ρ_r is the reduced density, ρ_c is the critical density and C_1 is constant. Eqn. (4.5) can be rewritten as:

$$\ln y_2 = A + \frac{B}{T} + C \ln \rho_r \quad (4.6)$$

$$\text{Where } A = \ln \left[\frac{p_2^{sub}}{\rho_c RT} \right] - C_1, B = \frac{p v_2^s}{R} \text{ and } C = \left[\frac{\tilde{v}_2}{\kappa_T RT} \right]_{\rho_r=1}$$

The Bartle et al [138] proposed a Kumar and Johnston [137] type model using the concept of enhancement factor, which is the ratio of actual solubility to ideal solubility. A reference pressure and density were also introduced in their work as show in Eqn. (4.7):

$$\ln \left[y_2 \frac{P}{P_{ref}} \right] = A + \frac{B}{T} + C [\rho - \rho_{ref}] \quad (4.7)$$

Where, ρ_{ref} is the reference density (take as $700 \text{ kg} \cdot \text{m}^{-3}$) and P_{ref} is the reference pressure (taken as 0.1 MPa). However, note that, A, B and C in the Bartle et al. model are not the same as the Kumar and Johnston model.

Mendez-Santiago and Teja [139] develop yet another Kumar and Johnston [137] type model using the concept of infinite dilution. The model is semi-empirical in nature and foresees a linear relationship between the logarithm of enhancement factor and density. The model has three adjustable parameters as shown in Eqn. (4.8).

$$T \ln[y_2 P] = A + BT + C\rho \quad (4.8)$$

Yu et al. [140] argue that the solubility of solute in supercritical CO₂ follow a curvilinear behavior with pressure at a constant temperature and with temperature at a constant pressure and with the interaction of these two physical property. Thus, a second order polynomial correlation with both temperature and pressure was proposed as shown in Eqn. (4.9):

$$y_2 = 1 - (A + BP + CP^2 + DT + ET^2 + FPTy_2) \quad (4.9)$$

Yu et al. model latter modified by Gordillo et al. [141] and Jouyban et al.[142]. The final form of the modified version are the same as the original Yu et al. [140] proposal with reduction in one or two parameter and therefore they are not discussed in this work.

4.3.2 Thermodynamic model

The widely accepted thermodynamic method for determination of solute solubility in supercritical phase is the Peng-Robinson equation of state with classical Van der Waals mixing rule [123,124,126,130,143]. The technique was development based on iso-fugacity condition between supercritical and solid phase under the general assumption that the solute is pure, incompressible and have low vapor pressure [124,130]. For binary system, the final expression of solubility in supercritical phase is given by equation shown in Eqn. (4.10) [144]:

$$y_2 = \frac{p_2^{\text{sub}}}{P\phi_2^{\text{SCF}}} \exp\left(\frac{v_2^{\text{s}}(P-P_2^{\text{sub}})}{RT}\right) \quad (4.10)$$

Where, ϕ_2^{SCF} is the fugacity coefficient of solute in supercritical CO₂ phase and the other variables are as defined in the Section 4.3.1. The fugacity coefficient is determined from Peng-Robinson equation of state [145] with Van der Waals mixing rule and the binary interaction coefficients (k_{ij} and l_{ij}) in Van der Waals mixing are used as an adjustable parameter to fit the model in to experimental data in this work. The physical properties used in this work are taken from Yu et al. [140] by approximating the triglycerides of oil with triolein. The vapor pressure at different temperature are estimated by Wagner vapor pressure equation [146].

4.4 Results and Discussion

4.4.1 Solubility data

During the determination of solute solubility with dynamic method, one of the main challenges is to make sure that the solvent leaving the extractor is indeed saturated. The technique frequently used in the literature to guarantee solvent saturation is to conduct repeated experiment under the same operating condition by varying the solvent flow rate. Under saturation condition, the initial slope of the extraction kinetics curve i.e. the plot of mass of solute extracted *versus* mass of solvent consumption must overlap. Figure 4.1 shows the kinetics of extraction of oil from surface of glass beads at pressure of 50 MPa and temperature of 323 K. As can be seen, the extraction curves overlaps in the tested flow rate range of 6-9 g/min indicating the solvent is certainly saturated. But when using ground seed matrix, the range of flow rate is much lower than the value reported for glass beads. For instance, Duba & Fiori [147] (Chapter 5) reported a similar value of solubility as reported in Table 4.1 when using ground matrix at 313 K and 35 MPa only at low flow rate of 4.71 g/min and at higher flow rate (7-10 g/min) the solvent was not saturated.

The majority of the research work dealing with the determination of the solubility of vegetable oil in SC-CO₂ uses directly ground seed matrix instead of glass beads to observed solvent saturation. The main advantage of using glass beads over the ground matrix are, it eliminates any error incurred from internal mass transfer resistance when using ground matrix while preserving the packed bed structure of the extractor. However, care must be taken and glass beads should only be used with caution when determining the solubility. Sovovà et al. [117] found out that the maximum amount of oil to be added on the surface of glass beads was 0.5 gram when using an extractor volume of 8 cm³. When the amount of oil feed to the extractor was greater than the recommended value, it was observed that part of the oil flow down the extractor by gravity and result in misleading value of solubility [117].

The extractor used in this work was more than ten time (100 cm³) the volume of the extractor employed by Sovovà et al. [117]. Consequently, the mass of oil used was ten times the proposed amount. In fact, before the start of the experiment in this work, a thoroughly mixed oil and glass beads in the extractor was allowed to stand for an hour on a white paper to check any natural down flow. In a previous work by Firoi [13], the

solubility value reported for grape seed oil were slightly higher than the value reported in this work, even though the values fall within the general range of vegetable oil solubility in SC-CO₂ as stated in del Valle et al. [125]. The authors believed that the main reason for that was the way the CO₂ flow was quantified. In the original equipment configuration detailed in Fiori [13], the system allows to measure the CO₂ flow only after the expansion and separation of the product. Which means the CO₂ flow meter F1 as indicated on the P&ID of the extraction equipment in Figure 1 of Fiori [13] is on the CO₂ outlet line. However, during the extraction operation, though it is certain that the majority of the CO₂ passes through F1, there is still a probability that some of the expanded CO₂ may leave the system through product recovery line which makes the measured CO₂ flow rate slightly less than the actual value and hence apparently higher solubility.

To offset this problem, a modification discussed in Chapter 2 was introduced and the total CO₂ consumption was measured in the incoming stream instead of the vent line in the current work.

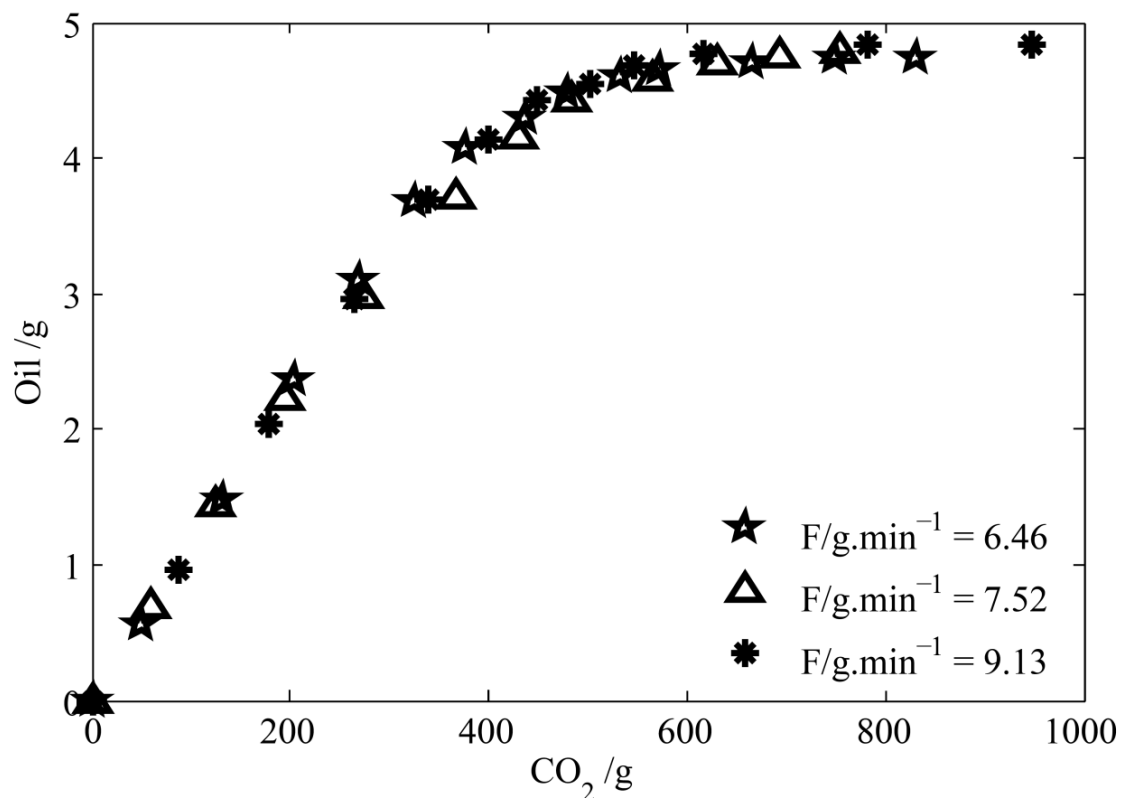


Figure 4.1: Kinetics of extraction of oil from surface of glass beads

Table 4.1, shows the experimental values of solubility of grape seed oil over the range of pressure and temperatures. Each data point represents an average of at least three consecutive points on the linear part of the extraction kinetics curve. As can be seen, with an increase in pressure at constant temperature the solubility increase in line with an increase in solvent density as expected. On the other hand, the effect of temperature is different for low and high pressure because of two competing factors i.e. the solute vapor pressure and solvent density [148]. At low pressure, increasing temperature has a negative effect on the solubility indicating the density effect dominate the vapor pressure effect while at high pressure increases in temperature enhances solute solubility as the result of revers phenomenon. Table 4.1, also shows the range of vegetable oil solubility computed according the so-called ‘General model’ proposed by del Valle et al. [125].

Table 4.1: Solubility of Grape seed oil in supercritical CO₂

T/K	P/MPa	ρ /(kg·m ⁻³)	S/(g·kg ⁻¹)	General model S/(g·kg ⁻¹)
313	20	839.81	4.20±0.05	2.17-5.07
	35	934.81	8.60±0.09	6.23-14.53
	40	956.07	10.40±0.16	7.59-17.71
	50	991.30	13.00±0.30	10.15-23.68
323	20	784.29	3.53±0.44	1.60-3.72
	35	899.23	9.50±0.27	6.59-15.39
	40	923.32	11.06±0.10	8.49-19.81
	50	962.45	13.40±0.21	12.27-28.64
333	20	723.68	3.12±0.05	1.05-2.45
	35	862.94	10.00±0.13	6.62-15.45
	40	890.14	12.00±0.23	9.06-21.15
	50	933.50	14.60±0.12	14.27-33.29
343	20	659.05	2.91±0.30	0.64-1.450
	35	826.10	10.60±0.25	6.34-14.79
	40	856.70	12.70±0.63	9.27-21.63
	50	904.54	16.10±0.82	15.99-37.32

The general structure of ‘General model’ model is the same as that of Sparks et al. [136] model except that the model parameters are optimized for a wide range of vegetable oil. del Valle et al. [125] claimed that, the model is capable of predicting

vegetable oil solubility within the range of $\pm 40\%$ for combination of temperature and pressure of practical importance. As can be seen, the reported experimental solubility data are within the range of predicted value of the general model except for 20 MPa at temperature of 333 K and 343 K. According to the del Valle et al. [125], the proposed model does not apply for low solubility ($\leq 1 \text{ g}\cdot\text{dm}^{-3}$) unless the system pressure is $> 21 \text{ MPa}$ or very high solubility ($> 100 \text{ g}\cdot\text{dm}^{-3}$) or when pressure is $> 80 \text{ MPa}$.

4.4.2 Correlation of Solubility

The solubility correlation by Chrastil model and its modifications are shown in Figure 4.2. The models adjustable parameters along with the deviation from experimental data are presented in Table 4.2.

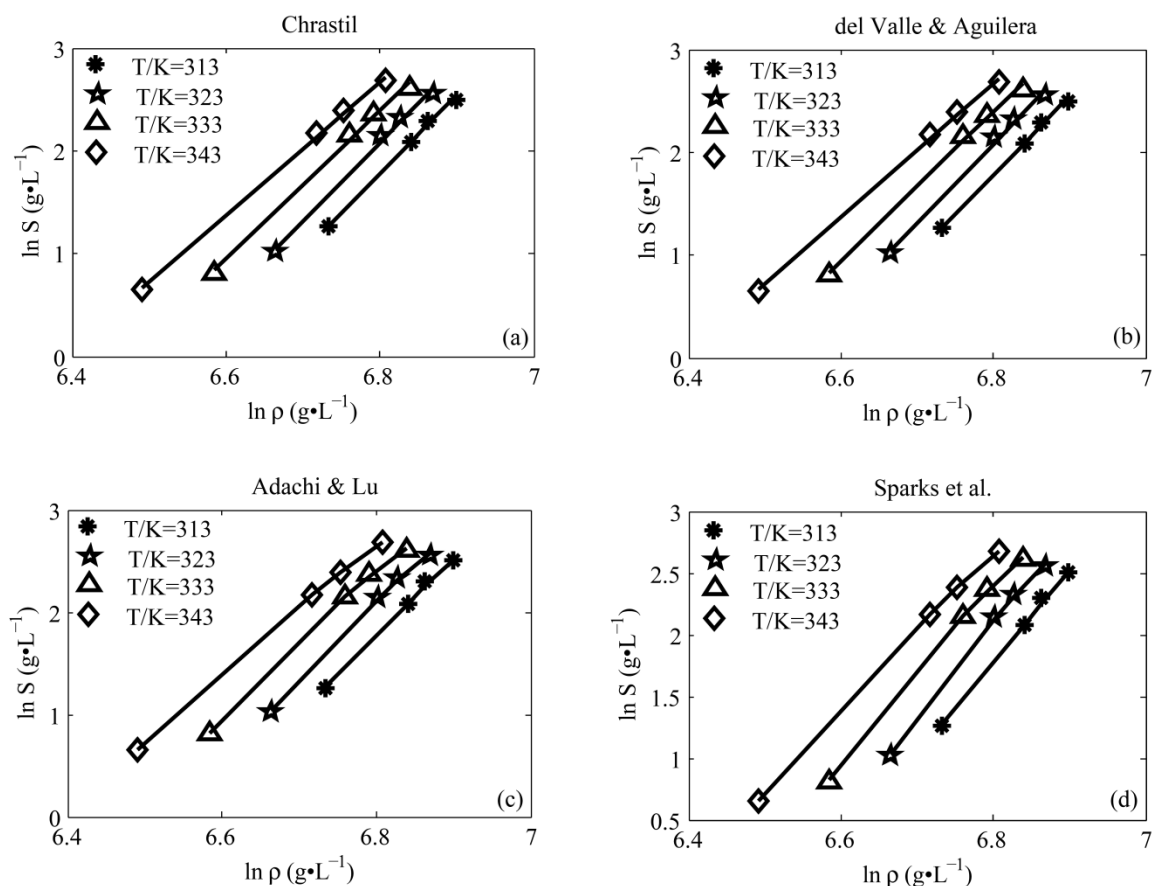


Figure 4.2: Solubility correlation by Chrastil model and its modifications

As discussed in Section 4.3.1, the del Valle and Aguilera, Adachi and Lu and Sparks modifications have one, two and three more adjustable parameters than the original Chrastil model respectively. As can be seen in Table 4.2, the model adjustable

parameters, k , α and β of the Chrastil model and del Valle and Aguilera modification are quite similar. Surprisingly the additional parameter introduced to offset the effect of temperature by del Valle and Aguilera modification takes a constant value of 0.2 for all temperatures. Note also that as a result of very small value of γ , the term γ/T^2 become insignificant relative to the magnitude of $\ln S$, which makes the del Valle and Aguilera and Chrastil model to respond in the same way to the experimental data. Therefore, under the range of temperature and pressure of this study, the del Valle and Aguilera modification have the same or little improvement over the Chrastil model.

Table 4.2: Models adjustable parameters of Chrastil model and its modifications

Model	T/K	k	α	β	γ	ϵ_0	ϵ_1	ϵ_2	RMSE $\cdot 10^{-2}$	AARD /%
Chrastil	313	7.62	0.040	-50.02					5.19	0.51
	323	7.68	0.044	-50.17					8.63	0.99
	333	7.22	0.059	-46.72					8.97	1.03
	343	6.49	0.078	-41.48					6.14	0.69
del Valle & Aguilera	313	7.62	0.040	-50.02	0.20				5.19	0.51
	323	7.68	0.044	-50.18	0.20				8.63	0.99
	333	7.22	0.059	-46.72	0.20				8.86	0.96
	343	6.49	0.079	-41.48	0.20				6.14	0.69
Adachi & Lu	313		0.499	0.14		-1.385	0.0024	0.00	4.44	0.35
	323		0.499	-0.05		-2.385	0.0049	0.00	3.60	0.41
	333		0.499	-0.03		-2.252	0.0049	0.00	2.23	0.23
	343		0.499	0.10		-1.719	0.0039	0.00	0.64	0.07
Sparks et al.	313		0.499	0.14	0.50	-1.379	0.0024	0.00	4.44	0.35
	323		0.499	-0.04	0.50	-2.385	0.0049	0.00	3.60	0.41
	333		0.499	-0.03	0.50	-2.252	0.0049	0.00	2.23	0.23
	343		0.499	0.10	0.50	-1.719	0.0039	0.00	0.64	0.07

The Adachi and Lu modification was proposed to introduce the dependence of association constant, k on solvent density. It can be observed from the trend of adjustable parameters in Table 4.2 that the coefficients of density square in the proposed correlation are constant (zero) with temperature. Sparks et al. [136] hinted that a linear relationship between k and ρ suffice and therefore the coefficient, ϵ_2 can be set to zero without

compromising the performance of the model and hence the number of adjustable parameters can be reduced. Furthermore, the modification made the coefficient of temperature in the Chrastil model constant. This argument is also true for the Sparks et al. modification which responds to the experimental data in exactly the same way as Adachi & Lu modification.

The Sparks et al. modification included both the modification of del Valle & Aguilera and Adachi & Lu as discussed in Section 4.3.1 which makes the model behaves in the same way as the combination of both predecessors. The parameter γ is constant like in the del Valle & Aguilera (but with different value) while α is constant as in the Adachi & Lu model. Unlike del Valle and Aguilera modification, the use of Adachi & Lu and Sparks et al. modification result in a completely different values of adjustable parameters like α and β in Chrastil model models. Therefore, it is impossible to compute the parameter of Chrastil model like association constant from Adachi & Lu model parameter. Consequently, it is difficult to assign any physical meaning to Adachi & Lu and Sparks et al parameters indicating the modification result in different empirical model. Both the Adachi & Lu and Sparks et al modifications has improved the root mean square error and percent average absolute relative deviation than both the original Chrastil and the del Valle & Aguilera model at expense of more number of adjustable parameters.

The solubility correlations with second class of density-based models are shown in Figure 4.3. This category includes the Kumar & Johnston, Bartle et al. and Mendez-Santiago and Teja models as discussed in Section 4.3.1. All the three models have exactly the same number of adjustable parameters (each of them three), but they differ from one another based on the way the relation between solubility and density are defined. For instance the difference between Mendez-Santiago & Teja and Bartle et al. model is on the way the variation of solubility with temperature is defined. The Bartle et al. model introduced the concept of reference pressure (0.1 MPa) and density (700 kg. m⁻³) to reduce the error which may incurred as a result of the variation of parameters with density. Both of these two models have the same form as that of Kumar & Johnston model; see Eqn. (4.6-4.8). But it must be noted that the physical significance of the coefficients are rather different in all the three models. As shown in Table 4.3, Bartle et al. and Mendez-Santiago & Teja models react to the experimental data in exactly similar

fashion with the same value of RMSE and AARD, while Kumar & Johnston model gives relatively lower value of AARD. Note also that, only in the case of Kumar & Johnston model the relationship between logarithms of solute solubility is correlated to logarithm of solvent density.

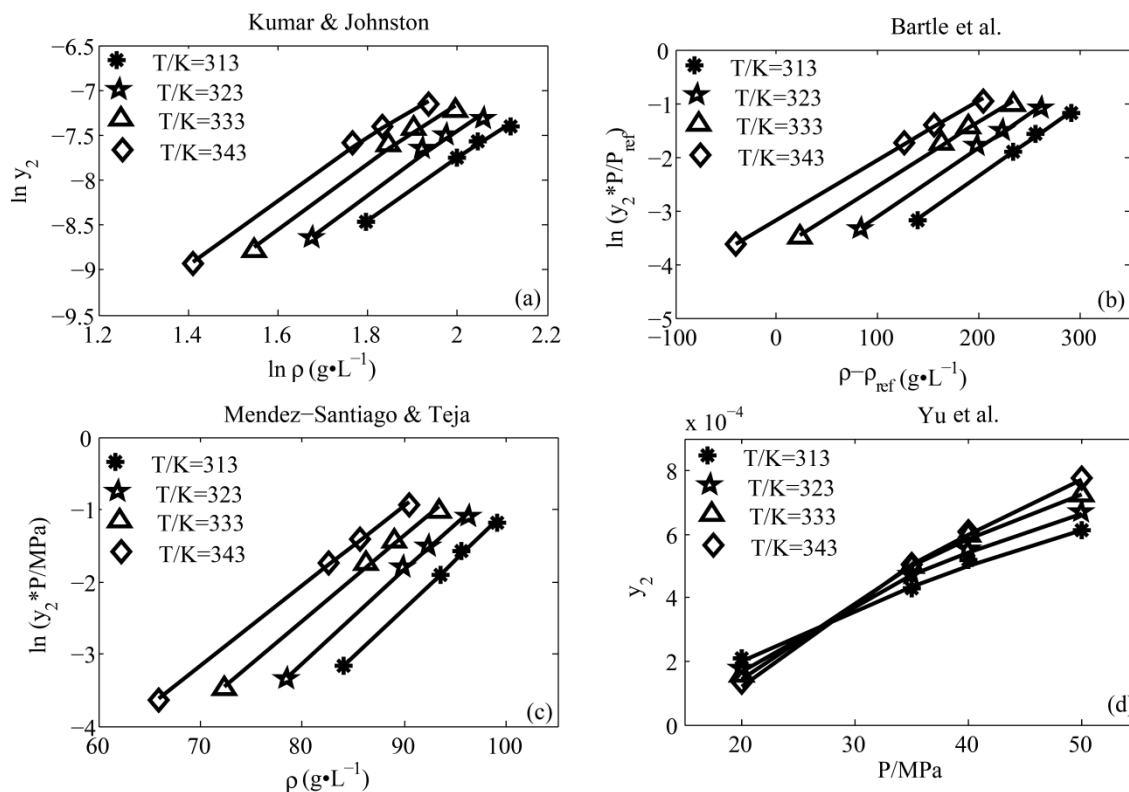


Figure 4.3: Solubility correlations with second class of density-based models

The Yu et al. empirical model is based on the curvilinear relation between solubility and solvent physical properties (temperature and pressure) with second order polynomial. The model fit the experimental data relatively better than the other density-based models as shown in Table 4.3. The major drawback of Yu et al. model is the large number of adjustable parameters besides the lack of any physical significance of the fitting parameters. As can be seen in Table 4.3 the coefficient of P^2 is zero in this study. A zero value for adjustable parameter was also observed by Yu et al. [140] when dealing with the solubility of rapeseed oil in supercritical CO_2 but in their case not for the coefficient of P^2 but rather for PT . Indicating a zero value for certain circumstance does not necessarily mean the number of model adjustable parameter can be reduced.

Table 4.3: Models adjustable parameters of the second class of density-based models

Model	T/K	A	B	C	D	E	F	RMSE .10 ⁻²	AARD /%
Kumar & Johnston	313	-12.31	-7.27	6.61				5.20	0.16
	323	-12.08	0.162	6.68				8.60	0.31
	333	-11.47	0.165	6.22				8.99	0.33
	343	-10.90	7.26	5.69				6.61	0.24
Bartle et al.	313	-5.02	0.18	0.013				5.63	0.96
	323	-4.37	-9.81	0.013				8.64	1.68
	333	-3.76	10.19	0.012				8.63	1.85
	343	-3.14	-9.81	0.011				6.25	1.35
MST	313	-9.81	-14.30	4.16				5.63	0.96
	323	10.12	-13.40	4.14				8.64	1.68
	333	0.16	-12.06	3.96				8.63	1.85
	343	-7.53	-10.89	3.79				6.25	1.35
Yu et al.	313	0.20	-0.91	0.00	0.0029	0.199	-0.0006	2.28	0.96
	323	0.20	-0.88	0.00	0.0027	0.199	-0.0006	1.28	0.38
	333	0.20	-0.86	0.00	0.0026	0.199	-0.0006	1.81	0.52
	343	0.20	-0.87	0.00	0.0025	0.199	-0.0006	1.42	0.39

The prediction of solubility with Peng–Robinson Equation of State (PR-EOS) with Van der Waals mixing rule is presented in Figure 4.4. Interestingly the predictive power of PR-EOS evaluated in terms of RMSE and AARD is comparable to that of density-based models as shown in Table 4.4. In this case, the fitting parameters are the binary interaction coefficients k_{ij} and l_{ij} in Mukhopadhyay [144]. The values of both adjustable parameters are relatively constant with temperature (0.243 ± 0.016 for k_{ij} and 0.138 ± 0.006 for l_{ij}) which makes it possible to determine the solubility only from physical properties of solute and solvent. But the fact that the physical properties data are only approximately known for most of the solute of practical importance is the major drawback of this technique.

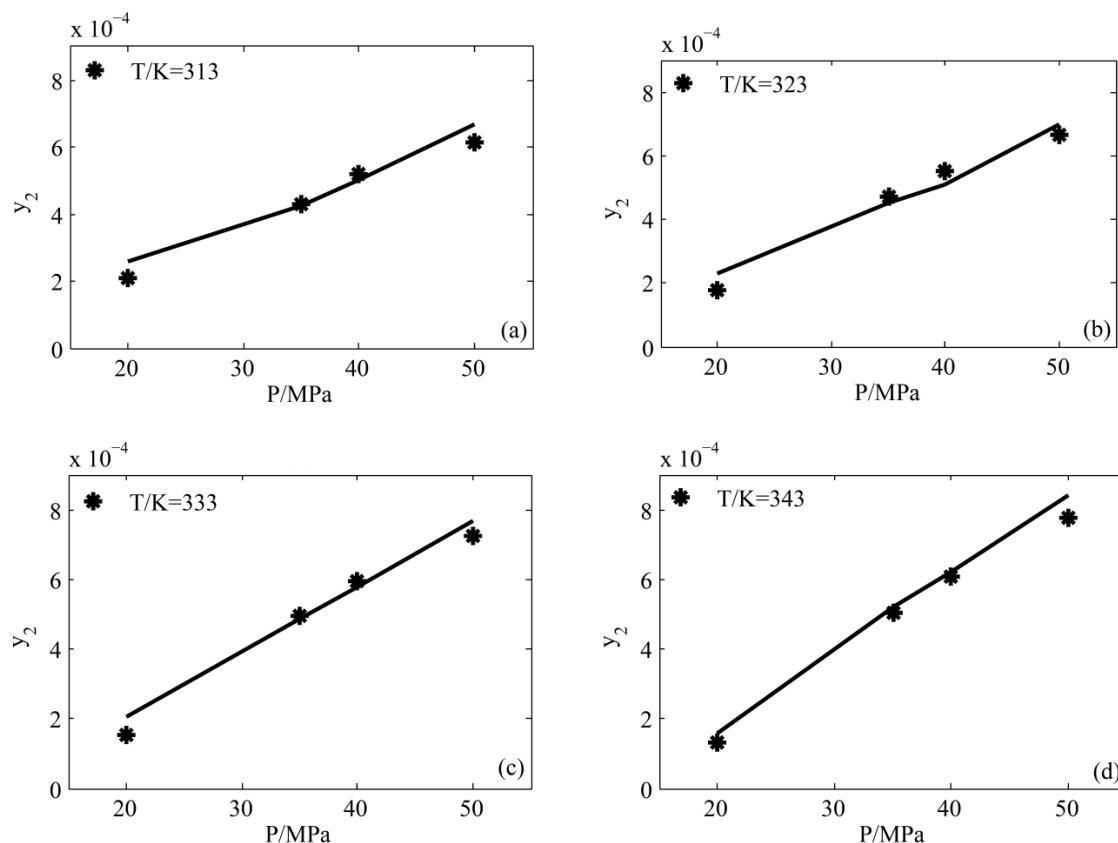


Figure 4.4: Solubility correlations Peng–Robinson Equation of State

Table 4.4: Models adjustable parameters of Peng–Robinson Equation of State

Model	T/K	k_{ij}	l_{ij}	MSE. 10^{-2}	AARD /%
PR-	313	0.2407	0.1389	7.84	2.07
EOS	323	0.2248	0.1312	7.84	2.85
	333	0.2423	0.1356	7.14	1.88
	343	0.2647	0.1464	7.75	2.29

4.5 Conclusions

The solubility of grape seed oil is determined for the temperature, $T = (313, 323, 333, 343)$ K and pressure $P = (20, 35, 40, 50)$ MPa. The result show that, the solubility increases with increase in pressure at constant temperature while the effect of temperature is different for low and high pressure. At low pressure (20 MPa) the solubility decreases with increase in temperature, but at high pressure (≥ 350 MPa) it increases with increase in temperature as a result of the relative importance of the vapor pressure and solvent density. The experimental data are modeled by eight density-based models which are

widely used in the literatures namely the Chrastil, del Valle and Aguilera, Adachi and Lu, Sparks et al., Kumar & Johnston, Bartle et al., Mendez-Santiago and Teja and Yu et al. models along with a thermodynamic model using Peng–Robinson equation of state. The result shows that, all the models can predict the solubility of oil in supercritical CO₂ to a reasonable degree. However, it must be emphasized that, best fitting alone should not be taken for guaranteed. A good model should sufficiently describe the underlining physical phenomenon, reasonably simple and contain less adjustable parameters. To this regard the model by Chrastil and/or del Valle and Aguilera, Kumar & Johnston and Peng–Robinson equation of state can effectively be used to predict the solubility of oil in supercritical CO₂.

5. Effect of Process Parameters on the Extraction Kinetics

In this Chapter, the effect of the main process variables affecting the supercritical CO₂ (SC-CO₂) extraction of oil from grape seeds was investigated, both experimentally and through modeling. The dependency of the extraction kinetics on the variables more tested in the literature (pressure, temperature, particle size and solvent flow rate) was confirmed, and original trends were obtained for the less investigated variables, such as the bed porosity (ϵ), extractor diameter to length ratio (D/L), extractor free volume and type of cultivars. The extraction kinetics did not depend on ϵ for $0.23 \leq \epsilon \leq 0.41$, while a further decrease in ϵ lowered the extraction rate, likely due to the occurrence of channeling. The effect of a variable D/L ratio was studied letting constant the ratio of substrate mass to CO₂ mass flow rate: the lower was D/L, the lower the specific CO₂ consumption. Through modeling, the values of internal and external mass transfer parameters were calculated and critically discussed on the base of well-known literature correlations.

5.1 Introduction

Supercritical CO₂ (SC-CO₂) extraction technology represents an alternative that can achieve comparable oil yield with respect to the traditional liquid solvent technique with all the advantages discussed in Chapter 1. The drawbacks are the greater costs of investment linked to the supercritical technology. However, the operating costs are usually lower due to minimum/zero post extraction processing. Therefore, the total costs are comparable to conventional systems, if the process is carried out at optimum

* Part of the present Chapter has been published as: Kurabachew Simon Duba, Luca Fiori. *Supercritical CO₂ Extraction of Grape Seed Oil: Effect of Process Parameters on Extraction Kinetics*. *J. of Supercritical Fluids* 98 (2015) 33–43.

operating conditions and in a sufficient extractor volume [4,5] considering that the capital amortization sharply decreases when capacity increases [6]. In a design and feasibility study, the volume of exhausted grape marc produced in a specific geographical region was considered and a SC-CO₂ plant with two extractors in series operating in the counter-current mode was sized accordingly, to simulate the extraction process under varying operational conditions. Energy inputs, investment and processing costs were then estimated and the proposed industrial application was found economically interesting [83]. Encouraging results concerning the scale-up of the SC-CO₂ process for grape seed oil extraction were also obtained by Prado et al. [16]. Scale-up operation and economic feasibility study of SC-CO₂ extraction plant is discussed in great detail in Chapter 7.

Comprehensive reviews appeared recently in the literature concerning the SC-CO₂ extraction technology and its perspective [11]. As a matter of fact, the SC-CO₂ extraction process from solid substrates is performed in the semi-continuous mode. The substrate, in the form of a bed of particles, is stationary - contained in one or a series of extraction vessels - while the CO₂ flows through it till the solid is exhausted [83]. Designing such a kind of process requires, among other things, selecting: the value of the process variables (pressure, temperature, CO₂ flow rate); to which extent the particles to be extracted have to be milled, i.e. the particle size; the extractor diameter to length ratio (D/L); the compaction degree of the bed of the milled particles – it is better to compact the bed, or just to completely fill the extractor, or to leave some empty space in the extractor?

This work analyses the effect of the above variables on the extraction rate of oil from grape seeds. Even though information on the effect of some operating conditions (pressure, temperature, solvent flow rate and particle size) on the seed oil extraction kinetics and yield is abundant [149–152], evidence of the effect of parameters like D/L, bed porosity, bed free volume and type of cultivars is rather limited or completely missing in the literature.

5.2 Material and Methods

5.2.1 Sample preparation

Four representative grape cultivars, i.e. Muller Thurgau (MT), Pinot Noir (PI), Chardonnay (CH) and Moscato (MO), were selected at random in this work to study the

effect of process conditions on extraction kinetics while the effect of the type of cultivars are presented for six grape varieties including Barbera (BA) and Nebbiolo (NE).

The oil yield for each cultivar was previously measured, as well as the oil composition in (see Chapter 2) [114]. In particular, accounting for the great compositional similarities among the oils from different grape cultivars, but to evaluate the effect of operating conditions, it is worth using grape seeds from different cultivars to achieve holistic results which can be considered representative of any kind of grape seed oil. MT was used for evaluating the effect of pressure, temperature and solvent flow rate (Sections 5.4.1-5.4.3), PI was used to determine the effect of the particle size, bed porosity and extractor free volume (Sections 5.4.4, 5.4.5 and 5.4.7), and CH was used to study the effect of D/L (Section 5.4.6). MO was used to determine the grape seed oil solubility in SC-CO₂ (Chapter 4) and all the cultivars were used to study the effect of grape variety (Section 5.4.8).

5.2.2 SC-CO₂ extraction equipment and procedure

When analyzing the effect of pressure, temperature, solvent flow rate, particle diameter and bed porosity, the 0.1 L extractor basket was used. Pressure, temperature and CO₂ flow rate were kept constant during the extraction process. The extraction operation was stopped when no more oil was extracted. After extractions, the particle size distribution of the exhausted grape seeds was evaluated by the method detailed in Chapter 2. The measure of the particle size distribution allowed to calculate the Sauter mean diameter of the milled particle population, which was assumed as the reference value representative of the particle diameter, d_p [116].

When analyzing the effect of D/L and extractor free volume, three different extractor baskets were utilized, filled with appropriate mass of milled grape seeds. The baskets consisted of hollow cylinders closed on both ends by metal frits. The frit at the top was intended to uniformly distribute the solvent, while that at the bottom acted as structural support for the solids and as filter medium. Figure 5.1 reports the geometry of the extraction vessel (autoclave) and basket assembly. The baskets had different internal volume, namely 0.1, 0.2 and 0.5 L. They had the same diameter, but different lengths (Figure 5.1). When using the 0.1 and 0.2 L baskets, tailor made spacers were used consisting of stainless steel solid cylinders with a center hole to pipe (down-flow) the CO₂ to the baskets. The utilization of the spacers allowed to avoid the presence of empty

spaces inside the autoclave. The assembly was completed by a cap with a circular seal: the basket, the (eventual) spacer and the cap were screwed together and inserted into the autoclave (Figure 5.1). The circular Teflon™ seal prevented from CO₂ leakage

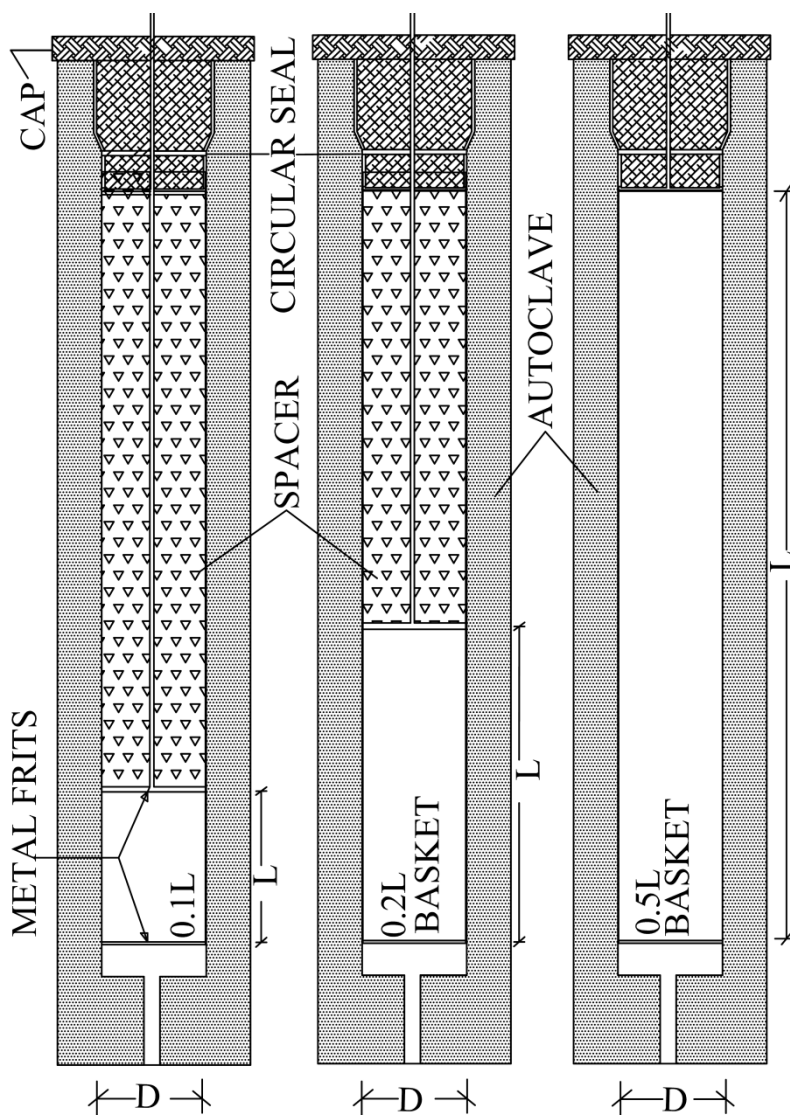


Figure 5.1: Extractor assembly: the various components of the three extractors. D and L represent, respectively, the extraction basket internal diameter and length: $D = 4.07 \times 10^{-2}$ m; $L = 7.75 \times 10^{-2}$ m (0.1 L basket), 15.5×10^{-2} m (0.2 L basket), 38.3×10^{-2} m (0.5 L basket).

5.3 Mathematical Modeling

Modeling of SC-CO₂ extraction of seed oil represents a challenge in the literature. A large variety of models have been developed [9,85,153,154] some of which were

utilized for grape seed oil [14,104,116]. Numerous kinetics models for SC-CO₂ extraction were proposed in the literature to evaluate the extraction course. Among them, it is worth mentioning the broken and intact cell (BIC) model by Sovová [4,97], the shrinking core (SC) model by Goto et al. [103], the combined BIC-SC model by Fiori et al. [104,155] (see Chapter 3 for detailed discussion). The models are mostly based on differential mass balances on solid and fluid phases and differ from one another either by the simplifying assumptions or the proposed mechanism of extraction. In almost all the models, the mass balance equations are derived under general assumptions, such as: isothermal and isobaric system, solvent free of solute at the extractor inlet, mono pseudo-compound solute, constant bed porosity and constant physical properties in the extractor, uniform distribution of solute in the solid and negligible axial dispersion.

In this work the model proposed by Sovová [4] was applied, with the approximate analytical solution given by Šťastová et al. [110]. For details on the model, the reader can refer to the original manuscripts [4,110]; the model equations and variables reported in Chapter 3.

The main parameters of the model are the following: the initial oil concentration in the solid, x_0 ; the oil solubility in the solvent, y_s ; the bed void fraction, ε ; the particle specific interfacial area, a_0 ; the external mass transfer coefficient, k_f ; the internal mass transfer coefficient, k_s ; the so-called grinding efficiency, G [110]. The value of x_0 and y_s are input to the model: the former was previously calculated for the various cultivars in Chapter 2 and the latter in Chapter 4. The value of ε can be easily calculated considering the mass and the density of seeds charged (1103 kg/m³ [8]), and the extractor basket volume. The other variables represent the adjustable parameters of the model. When utilizing the model in best fitting experimental extraction curves, the optimization routine provides the optimum value of the adjustable parameters. In particular, for each experimental extraction curve, the values of $k_f a_0$, $k_s a_0$ and G are obtained.

5.4 Results and Discussion

The results of experimental tests and modeling are reported in the present section. From Section 5.4.1 to 5.4.8, the effect of each single process variable is analyzed separately, first referring to the experimental outcomes, then to the output from model best fitting. Section 5.4.9 presents as a whole the best fitted values of the models

parameter, and analyzes them resorting to correlations largely utilized in the literature.

5.4.1 Effect of pressure

The effect of SC-CO₂ pressure on kinetics of extraction is well established, rather solid and there is a consensus in the research community that increasing operating pressure has a positive effect on the extraction rate. The reason is that an increase in pressure (at constant temperature) makes the density of SC-CO₂ increase, which enhances its solvent power and, ultimately, the extraction rate increase if all the other parameters are kept constant. Nevertheless, the economic feasibility of working at elevated pressure has to be evaluated on a case-by-case basis, as any increase in pressure is associated with an increase in energy consumption. In the case of oil from seeds, working at high pressure seems economically convenient [83].

In this work the pressure was varied in the range 200-500 bar, at a constant temperature of 40 °C, with CO₂ flow rate at 8.46±0.12 g CO₂/min, particle diameter of 0.41±0.05 mm and constant bed porosity of 0.41. The extraction kinetics is shown in Figure 5.2, where the extraction yield is reported *versus* CO₂ consumption. Table 5.1 reports the characteristic values of each experimental trial: the value of operating variables and model adjustable parameters with associated deviation from experimental data represented in terms of RMSE and AARD.

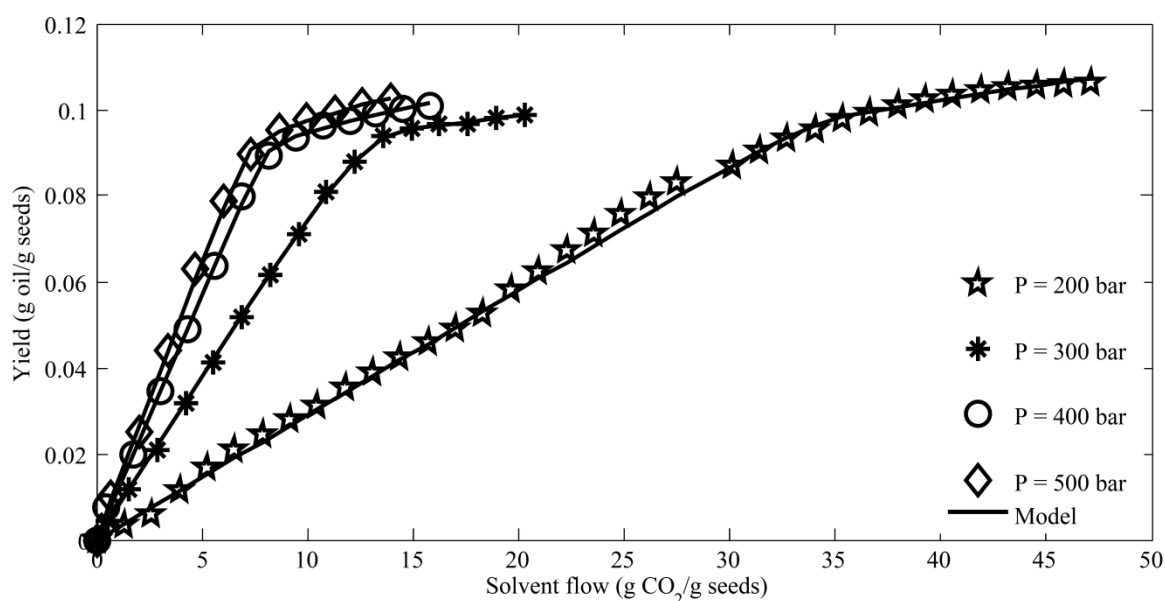


Figure 5.2: Extraction curves at different pressures: oil yield versus solvent consumption. The operating conditions are reported in Table 5.1.

Table 5.1: Operating conditions and estimated model adjustable parameters for different pressures ($T = 40\text{ }^{\circ}\text{C}$, $\varepsilon = 0.41$, $x_0 = 0.120$).

P (bar)	y_s (mg/g)	d_p (mm)	F (g/min)	G	$k_f a_0$ (s ⁻¹)x10 ²	$k_s a_0$ (s ⁻¹)x10 ⁵	$RMSE$ x10 ²	$AARD$ (%)
200	4.20	0.39	8.51	0.71	1.255	3.49	0.871	3.24
300	7.60	0.41	8.43	0.76	0.980	3.45	0.467	1.77
400	10.4	0.48	8.32	0.72	0.829	7.18	0.352	3.31
500	13.0	0.37	8.59	0.72	0.661	9.70	0.375	2.08

Table 5.2: Operating conditions and estimated model adjustable parameters for different temperatures ($P = 500$ bar, $\varepsilon = 0.41$, $x_0 = 0.120$).

T (°C)	y_s (mg/g)	d_p (mm)	F (g/min)	G	$k_f a_0$ (s ⁻¹)x10 ²	$k_s a_0$ (s ⁻¹)x10 ⁵	$RMSE$ x10 ²	$AARD$ (%)
35	12.8	0.41	8.28	0.70	0.302	6.44	0.444	1.88
40	13.0	0.37	8.59	0.72	0.661	9.70	0.375	2.08
50	13.4	0.32	8.70	0.77	0.506	6.19	0.292	1.29

The trend is that expected. Keeping constant the mass of solid in the extractor (namely 65 g), the time necessary to complete the linear section of extraction curve reduced from 270 to 55 min when the pressure increased from 200 to 500 bar. The increase in extraction rate reflected the increase in oil solubility (y_s), as shown in Table 5.1. Similar values of the adjustable parameters (G , $k_f a_0$ and $k_s a_0$) were obtained in the whole range of pressure investigated. More precisely, increasing the pressure made $k_f a_0$ slightly to decrease and $k_s a_0$ slightly to increase. The behavior of $k_f a_0$ reported in Table 5.1 is consistent with the dependence of k_f on Schmidt and Reynolds numbers [156] (see Section 5.4.9 for details).

The small variation in the values of $k_s a_0$ in Table 5.1 can be due, to some extent, to the slightly different value of the particle diameter of the different trials. The internal mass transfer coefficient is inversely proportional to the particle diameter: Tables 5.1 confirms this trend with one exception, at P=400 bar. Comparable results and similar trends of the model parameters were reported for the SC-CO₂ extraction of apricot kernel oil by Özkal et al. [151].

5.4.2 Effect of temperature

The effect of SC-CO₂ temperature on the extraction kinetics is rather conflicting as a result of what is known as “crossover phenomena”. When temperature increases, the density of SC-CO₂ decreases, but the solute solubility can still increase as a result of enhanced solute vapor pressure. The plots of solubility *versus* pressure at constant but different temperatures cross each other twice and these intersections are referred as lower and upper crossover pressure points [157]. At pressures between these two points, solubility decreases with increase in temperature because the solvent density effect overcomes the vapor pressure effect. Whereas above the upper or below the lower crossover point the vapor pressure effect is more pronounced than the density effect, so the solubility increases with an increase in temperature [157–159].

In this work, the effect of temperature was studied at a pressure of 500 bar, which is above the upper crossover point. The other extraction conditions were as follows: flow rate of 8.52 ± 0.2 g CO₂/min, particle size of 0.37 ± 0.04 mm, temperatures of 35, 40 and 50 °C. Figure 5.3 shows the extraction kinetics and Table 5.2 reports the characteristic value of the various parameters of each experimental test. The extraction rate slightly increased with an increase in temperature, and so did the solubility. The difference in value of the

final asymptotic oil yields is very likely not related to temperature, but it is rather due to the slight difference in particle diameter, which is also manifested in the value of the grinding efficiency G . Refer to Section 5.4.4 for an in deep discussion about the dependence of the extraction kinetics on the particle size. In this case both $k_f a_0$ and $k_s a_0$ present similar values for all the tests and no specific trend can be identified.

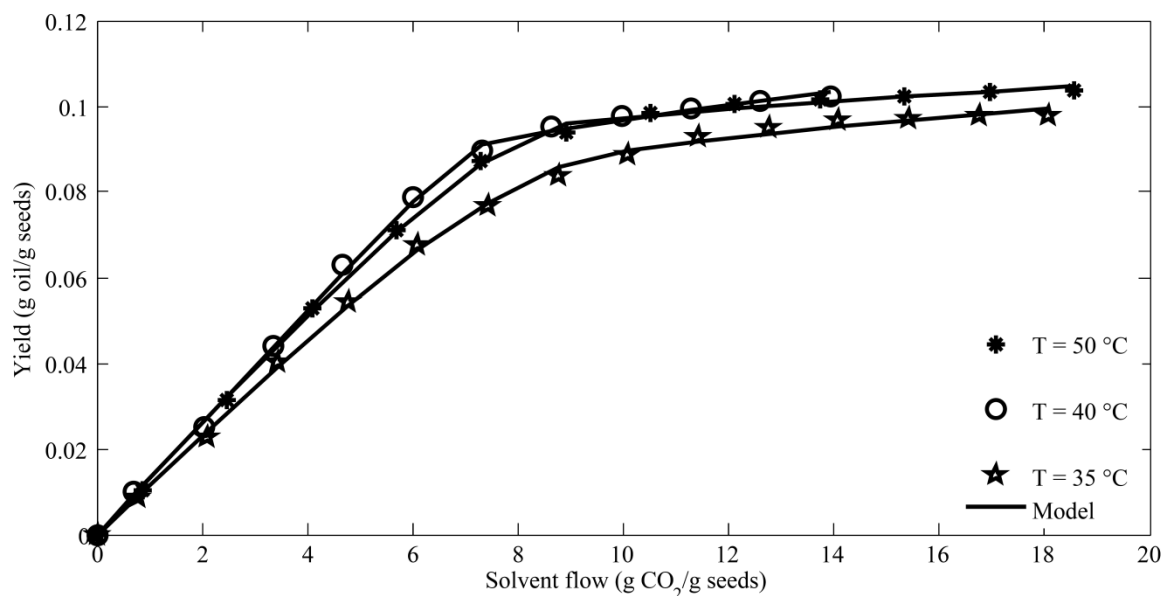


Figure 5.3: Extraction curves at different temperatures: oil yield versus solvent consumption. The operating conditions are reported in Table 5.2.

5.4.3 Effect of flow rate

The effect of flow rate was studied at four different conditions, namely 4.71, 7.45, 8.43 and 10.22 g CO₂/min. The other extraction conditions were as follows: pressure of 350 bar, temperature of 40 °C, particle size of 0.42±0.01 mm. The experiments were designed with the following approach. At first, the test at the highest flow rate (10.22 g CO₂/min) was performed, and in the subsequent tests the flow was reduced till a flow rate value (4.71 g CO₂/min) at which the slope of the extraction curve coincided with the solubility determined using glass beads ($y_s=8.60$ mg/g at 350 bar and 40 °C).

Figure 5.4a reports the oil yield *versus* CO₂ consumption and Figure 5.4b reports the oil yield *versus* time. The higher was the flow rate, the higher the extraction rate (Figure 5.4b), in line with an increase in both the external and internal mass transfer parameters (Table 5.3). While the increase in $k_f a_0$ at increasing flow rate was expected, the increase in $k_s a_0$ at increasing flow rate is difficult to explain, as the particle diameters were very similar for the various tests and k_s should not depend on flow rate on a

theoretical basis. Anyway, such kind of anomalous dependence was already previously found in the literature [151,160]. Thus, the higher was the flow rate, the lower the extraction time. But, conversely, the specific consumption of the solvent increased at increasing SC-CO₂ flow rate (Figure 5.4a). Ultimately, for commercial applications the solvent flow rate has to be optimized in terms of extraction time and solvent volume used per operation.

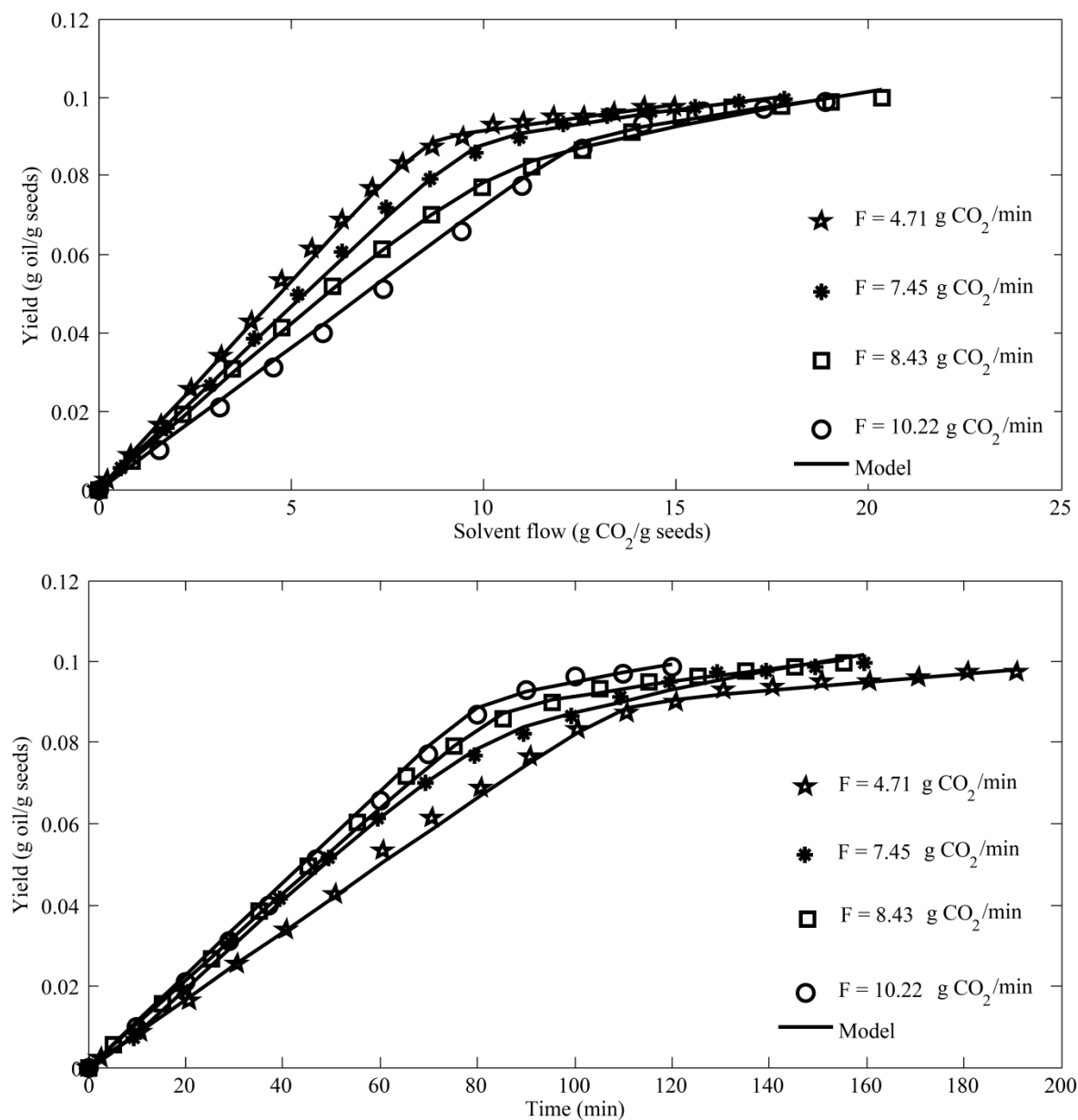


Figure 5.4: Extraction curves at different solvent flow rates. (a) oil yield versus solvent consumption; (b) oil yield versus time. The operating conditions are reported in Table 5.3.

Table 5.3: Operating conditions and estimated model adjustable parameters for different flow rates $(T = 40\text{ }^\circ\text{C}, P = 350\text{ bar}, y_s = 8.60\text{ mg/g}, \varepsilon = 0.41, x_0 = 0.120)$

$F(\text{g/min})$	$d_p(\text{mm})$	G	$k_f a_0(\text{s}^{-1}) \times 10^2$	$k_s a_0(\text{s}^{-1}) \times 10^5$	$RMSE \times 10^2$	$AARD$ (%)
4.71	0.42	0.52	0.384	2.30	0.497	1.95
7.45	0.43	0.62	0.698	5.04	0.407	1.51
8.43	0.41	0.57	1.002	8.87	0.476	1.87
10.22	0.43	0.78	1.270	9.73	0.573	3.93

Table 5.4: Operating conditions and estimated model adjustable parameters for different particle sizes $(T = 50\text{ }^\circ\text{C}, P = 500\text{ bar}, y_s = 13.4\text{ mg/g}, \varepsilon = 0.41, x_0 = 0.167)$

$d_p(\text{mm})$	$F(\text{g/min})$	G	$k_f a_0(\text{s}^{-1}) \times 10^2$	$k_s a_0(\text{s}^{-1}) \times 10^5$	$RMSE \times 10^2$	$AARD$ (%)
0.41	7.34	0.81	0.326	4.98	0.490	1.49
0.45	7.19	0.67	0.427	2.44	1.140	4.78
0.59	7.46	0.55	0.242	2.56	0.993	3.92
0.75	7.31	0.39	0.611	1.98	0.483	2.80

5.4.4 Effect of particle diameter

Figure 5.5 shows the extraction kinetic curves for four different particle diameters, namely: 0.41, 0.45, 0.59 and 0.75 mm. The other extraction conditions were as follows: flow rate of 7.33 ± 0.10 g CO₂/min, pressure of 500 bar, temperature of 50 °C. Figure 5.5 testifies that the asymptotic oil yield decreased with the increase in particle size. Fine particles are easier to extract because they have large surface area per unit volume, contain a high percentage of “free oil” and require less distance for the “tied oil” to reach the surface, which reduces the internal mass transfer resistance [4]. The results reported in Table 5.4 are fully consistent with the above statements: $k_s a_o$ and the grinding efficiency G gradually decrease with the increase in particle size. Figure 5.5 clearly shows that the initial slope of the extraction curves overlap, which can also be verified from the values of the external mass transfer parameter ($k_f a_o$) of Table 5.4: the values are in the same order of magnitude without any specific trend.

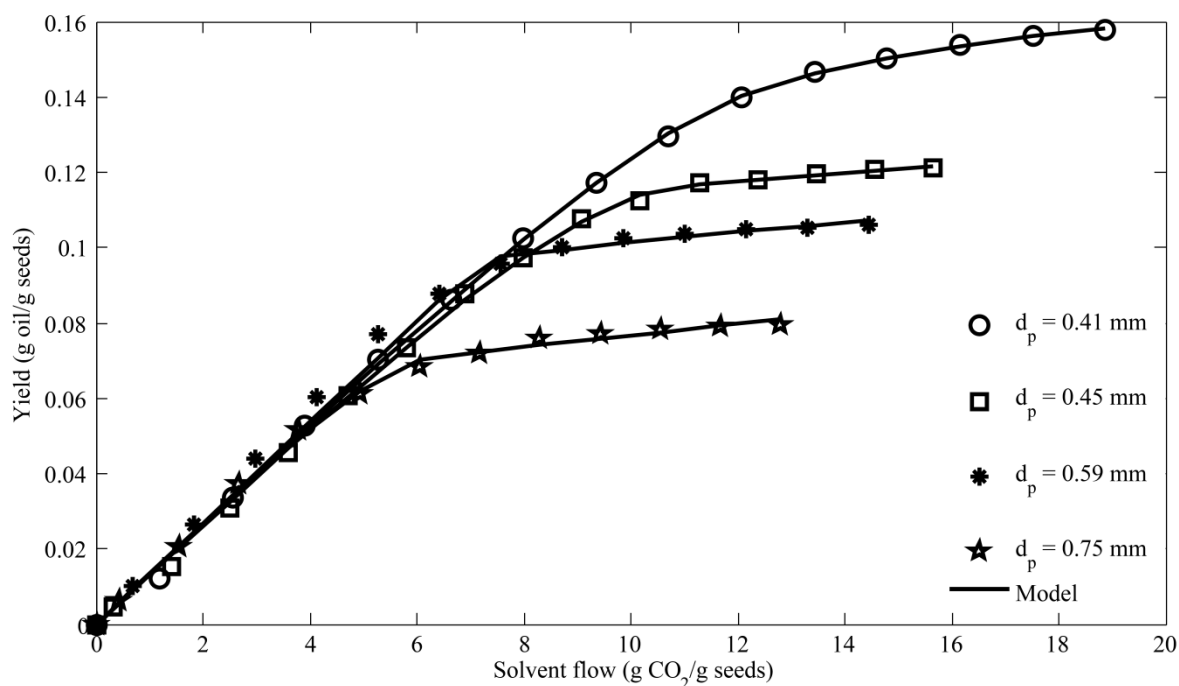


Figure 5.5: Extraction curves at different particle diameters: oil yield versus solvent consumption. The operating conditions are reported in Table 5.4.

5.4.5 Effect of bed porosity

The effect of the bed porosity (or, equivalently, bed void fraction) on the extraction kinetics was evaluated with bed void fraction in the range 10-41%. The other extraction conditions were as follows: pressure of 500 bar, temperature of 50 °C, flow rate of 8.60 ± 0.23 g CO₂/min, particle diameter of 0.44 ± 0.04 mm. In all the cases the extractor basket was full, but compacted to a different degree. In the case of $\varepsilon=0.41$, the bed of particles was not compacted at all. Consequently, each test was characterized by a different amount of substrate charged into the extractor basket.

The extraction kinetic curves are presented in Figure 5.6a (oil yield *versus* CO₂ consumption) and Figure 5.6b (oil extracted *versus* time). The choice of reporting in the y-axis of Figure 5.6b the oil (instead than the oil yield) allows for a correct quantification of the oil extraction rate. It is remarkable that, in the initial stage of the process, the extraction rate did not depend on the bed porosity when this parameter was in range 0.23-0.41 (Figure 5.6b). A further decrease of the bed porosity to 0.10 had a negative effect on the extraction rate, which was probably due to flow inhomogeneity (channeling) due to the high compaction degree. Another potential cause is the reduced residence time of the solvent into the extractor at the reduced bed porosity: the CO₂ residence time decreased from about 270 s at $\varepsilon=0.41$ to about 70 s at $\varepsilon=0.10$.

The values of the external and internal mass transfer parameters are quite similar for bed porosity in the range 0.23-0.41 (Table 5.5). Conversely, the value of both parameters drops down at bed porosity equal to 0.10. Vice-versa, the value of the grinding efficiency G is very large for $\varepsilon=0.10$. This was rather unexpected considering that G should reflect the particle diameter, which is quite similar for all the tests this Section refers to. A possible explanation could be that the best fitting procedure has to cope with an extraction initial slope (too) much lower than the oil solubility. The only way the model can fit such a curve (low initial slope) is to assume a very low value for the external mass transfer parameter ($k_f a_0$). In the following extraction stage, the model compensates by a large value of G . If this was the case, the goodness of the value of the adjustable parameters reported in Table 5.5 for $\varepsilon=0.10$ would go beyond their physical meaning, and therefore these values should be considered with caution.

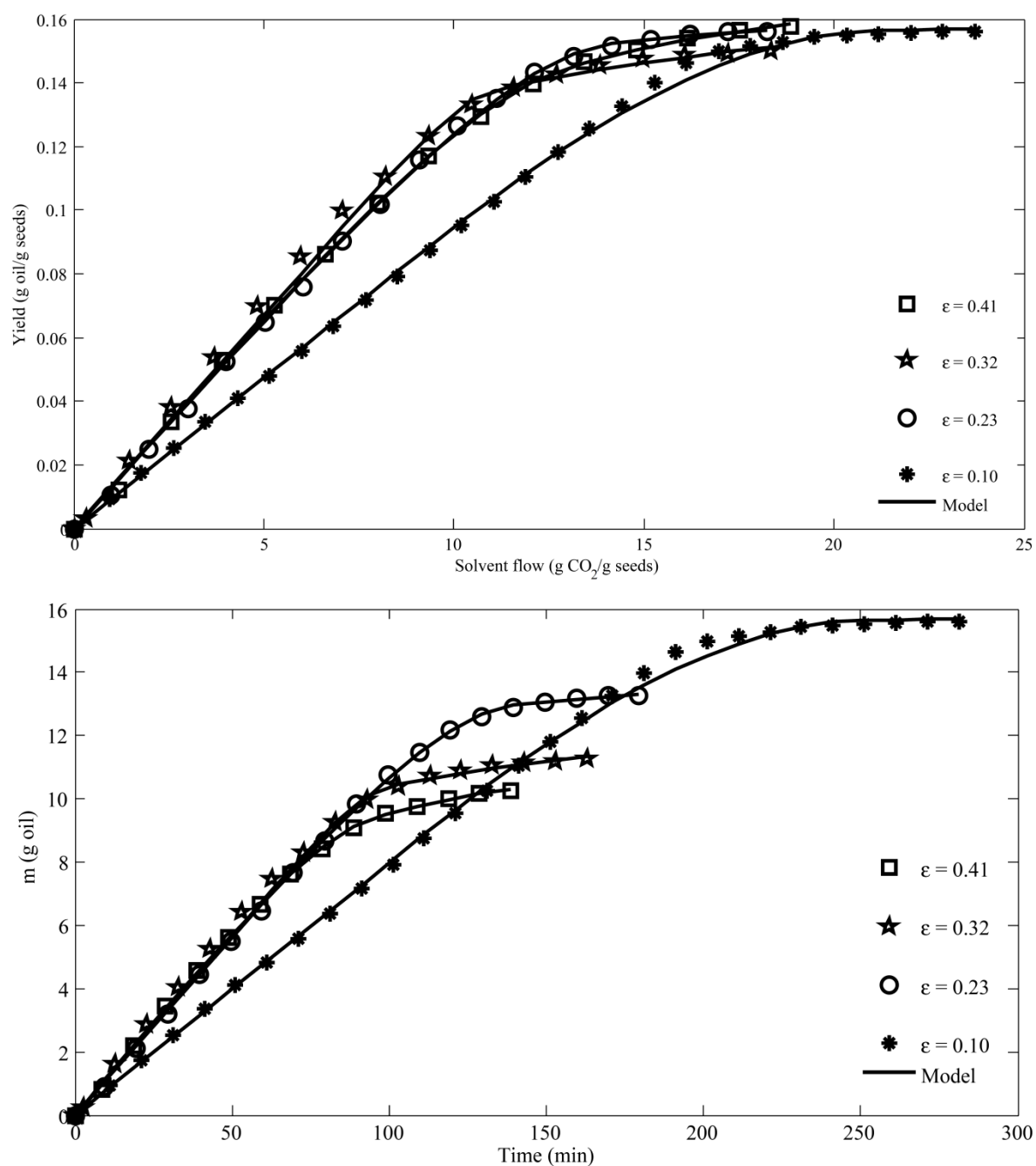


Figure 5.6: Extraction curves at different particle bed porosity. (a) oil yield versus solvent consumption; (b) oil extracted versus time. The operating conditions are reported in Table 5.5.

Table 5.5: Operating conditions and estimated model adjustable parameters for different bed porosity. $(T = 50\text{ }^\circ\text{C}, P = 500\text{ bar}, y_s = 13.4\text{ mg/g}, x_0 = 0.167)$

ε	$d_p(\text{mm})$	$F(\text{g/min})$	G	$k_f a_0(\text{s}^{-1}) \times 10^2$	$k_s a_0(\text{s}^{-1}) \times 10^5$	$RMSE \times 10^2$	$AARD$ (%)
0.41	0.38	8.84	0.81	0.633	9.63	0.417	2.31
0.32	0.47	8.38	0.72	0.487	11.4	1.129	5.39
0.23	0.43	8.63	0.86	0.549	10.8	0.451	2.02
0.10	0.47	8.43	0.93	0.177	2.33	0.974	1.44

Table 5.6: Operating conditions and estimated model adjustable parameters for different D/L $(T = 40\text{ }^\circ\text{C}, P = 350\text{ bar}, y_s = 8.60\text{ mg/g}, x_0 = 0.147)$

D/L	$d_p(\text{mm})$	$F(\text{g/min})$	G	$k_f a_0(\text{s}^{-1}) \times 10^2$	$k_s a_0(\text{s}^{-1}) \times 10^5$	$RMSE \times 10^2$	$AARD$ (%)
0.53	0.47	6.11	0.66	0.679	3.03	0.998	2.97
0.26	0.40	12.97	0.68	0.871	2.47	0.748	6.13
0.11	0.38	32.78	0.75	1.009	4.95	0.594	3.16

Table 5.7: Operating conditions and estimated model adjustable parameters for different extractor free volume $(T = 50\text{ }^\circ\text{C}, P = 500\text{ bar}, y_s = 13.4\text{ mg/g}, m_{seeds} = 100\text{ g}, x_0 = 0.167)$

V (%)	$d_p(\text{mm})$	$F(\text{g/min})$	G	$k_f a_0(\text{s}^{-1}) \times 10^2$	$k_s a_0(\text{s}^{-1}) \times 10^5$	$RMSE \times 10^2$	$AARD$ (%)
10	0.47	8.43	0.93	0.177	2.33	0.974	1.44
55	0.44	8.87	0.69	0.466	8.37	0.489	1.21
82	0.44	8.35	0.62	0.243	3.52	1.244	2.85

5.4.6 Effect of extractor diameter to length ratio (D/L)

Figure 5.7 shows the effect of D/L on the extraction kinetics. As mentioned in Section 5.2.2, three extraction baskets having the same diameter but different lengths were utilized. To maintain constant the bed porosity ($\varepsilon=0.41$) in all the three extractors, 65, 130 and 325 g of solid matrix were charged, respectively, in the basket of 0.1, 0.2 and 0.5 L volume. To preserve a constant solvent residence time, the ratio of mass of substrate to CO₂ flow rate was kept constant roughly at 10 g seeds/g CO₂/min. This approach is often selected as scale-up criterion in SC-CO₂ extraction process development [161]. The values of solvent flow rate are reported in Table 5.6: correspondingly, the superficial SC-CO₂ velocity increased from 0.084 mm/s for the 0.1 L basket to 0.45 mm/s for the 0.5 L basket. The other extraction conditions were as follows: pressure of 350 bar, temperature of 40 °C, particle diameter of 0.42 ± 0.04 mm.

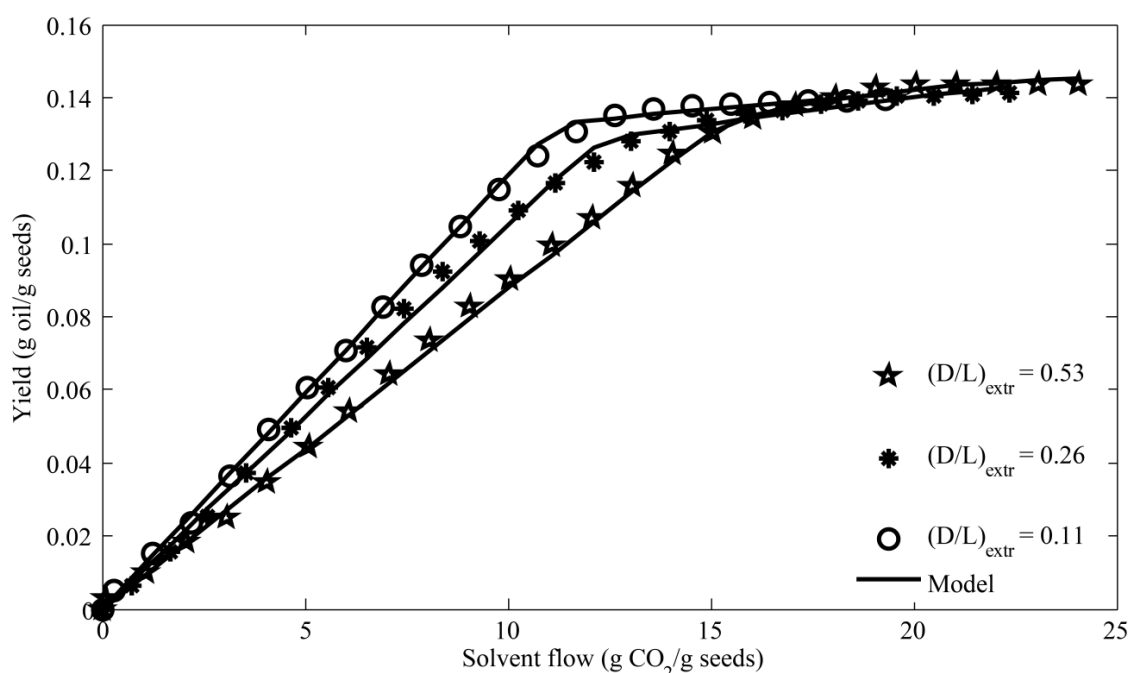


Figure 5.7: Extraction curves at different extractor diameter to length ratios: oil yield versus solvent consumption. The operating conditions are reported in Table 5.6.

The extraction rate increased when D/L decreased, i.e. the longer was the extractor basket, the lower the specific solvent consumption: Figure 5.7. Importantly, in these experimental runs it is believed that the solvent was not fully saturated by the

solute. According to the results of Section 5.4.3, for grape seeds the saturation occurred at values of about 14 g seeds/g CO₂/min. The differences in extraction rate when varying D/L are reflected in the values of the external mass transfer parameter: the lower was D/L, the higher $k_f a_0$ (Table 5.6). This result is clearly consistent with the dependence of k_f on solvent flow rate. The values of the grinding efficiency G are consistent with the small differences in the particle diameters. No specific trend can be observed for $k_s a_0$.

5.4.7 Extractor free volume

The extractor free volume v is different from the extractor bed porosity ε discussed in Section 5.4.5. In this case, there can be an empty space above the solid matrix in the extractor basket. The extractor free volume accounts also for this empty space. The extractor free volume was thus computed as the percentage of empty space in the extractor:

$$v = 100 (V_{extr} - V_{seeds})/V_{extr} \quad (5.1)$$

The same mass of grape seeds (100 g) was utilized inside the three different extraction baskets. In the case of the smallest extractor, the test is actually the same already utilized in the discussion of Section 5.4.5 concerning bed porosity; i.e. for $V_{extr}=0.1$ L, the indication of a free volume $v=10\%$ (Figure 5.8) coincides with $\varepsilon=0.10$ (Figures 5.6a and b). In that case the matrix completely filled the basket. Conversely, the extractor basket of 0.2 L was roughly half full, and that of 0.5 L was empty for more than three quarters.

In the case of the 0.2 L ($v=0.55$) and 0.5 L ($v=0.82$) extractors, the extraction curves mostly overlap (Figure 5.8). But, when analyzing Table 5.7, the corresponding values of the external and internal mass transfer parameters are unexpectedly different. One possible explanation is that the model was utilized outside its validity range. In other words, reasonably is not physically consistent to let the value of the bed porosity (model variable) equal to the extractor free volume calculated according to Eq. (5.1). This is most likely the case considering, in addition, that it is not known what is happening inside the extractor basket under these conditions. Grape seed particles have a mean density greater (but not so dissimilar) than that of SC-CO₂ and the extractor is operated in the down-flow mode. This would suggest that the bed of particles stays stable at the bottom of the basket. Nevertheless, it cannot be *a priori* excluded that the bed of particles (or a portion

of it) spreads along the entire volume of the extractor basket. In addition, it is not known if the plug flow assumption is still applicable. To get a clearer picture, further investigation is required. At this stage, the (quite random) values of the model adjustable parameters of Table 5.7 should be considered with caution, while the experimental trends of Figure 5.8 maintain their scientific interest.

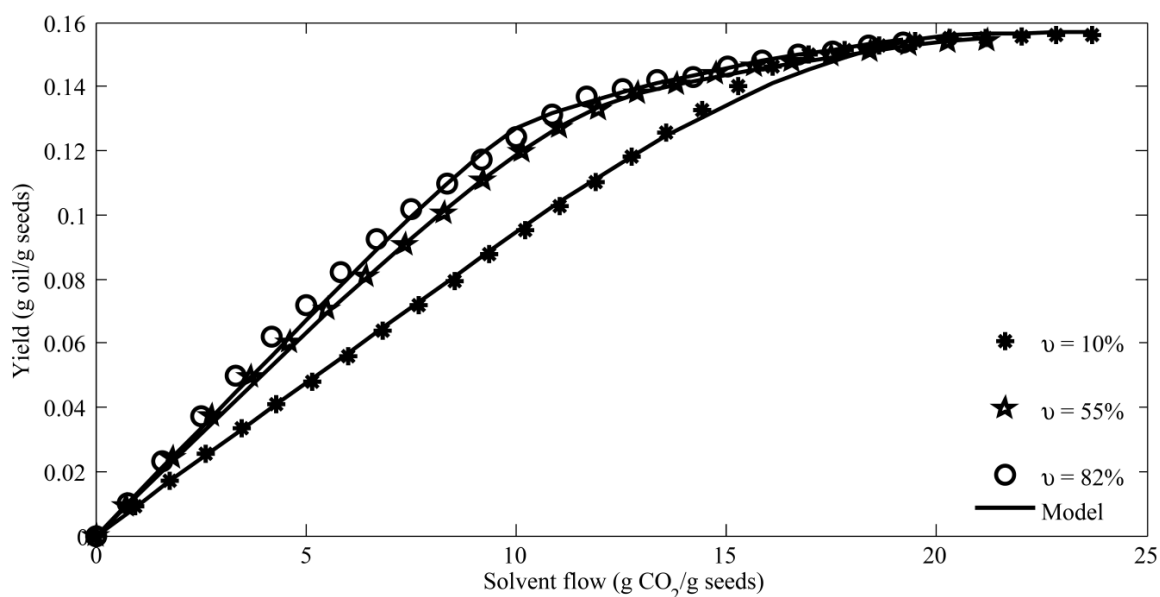


Figure 5.8: Extraction curves at different extractor free volume: oil yield versus solvent consumption. The operating conditions are reported in Table 5.7.

5.4.8 Effect of grape cultivars

Figure 5.9 shows a selection of extraction kinetic curves for all the six cultivars: the yield, expressed as gram of extracted oil per gram of seeds, is reported *versus* the extraction time. The experiment in this case is conducted at pressure 500 bar and temperature of 50 °C. The curves show the typical linear trend at the beginning, due to free oil extraction, followed by a decrease in the extraction rate due to the slower tied oil extraction. The extraction curves almost overlap in linear part for all the cultivars, and the small differences could be due to a slightly different solvent flow rate (manually controlled) in the various tests. Table 5.8 reports, for a selection of experimental tests, the operating conditions and the key parameters affecting mass transfer: internal and external mass transfer parameters and grinding efficiency. Each curve was modeled separately. The dimension of the milled seed particles was expressed in terms of the Sauter mean diameter (Smd), calculated after accurate measurement of the granulometric distribution of the

particle populations. A narrow range was observed for all the samples, with Smd values in the range 0.23-0.49 mm. The $k_f a_p$ resulted in the range $1-5 \cdot 10^{-2} \text{ s}^{-1}$, due to variations in flow rate and Smd , the external mass transfer parameter, $k_s a_p$, resulted in the range $0.4-6 \cdot 10^{-4} \text{ s}^{-1}$, and most of the values were around 10^{-4} s^{-1} . Values of $0.7-1.5 \cdot 10^{-5} \text{ s}^{-1}$ were obtained by Sovová et al. [14] for grape seeds of a un-specified cultivar. Actually, the authors [14] specified that the values they obtained were one or two orders of magnitude lower than other values from literature.

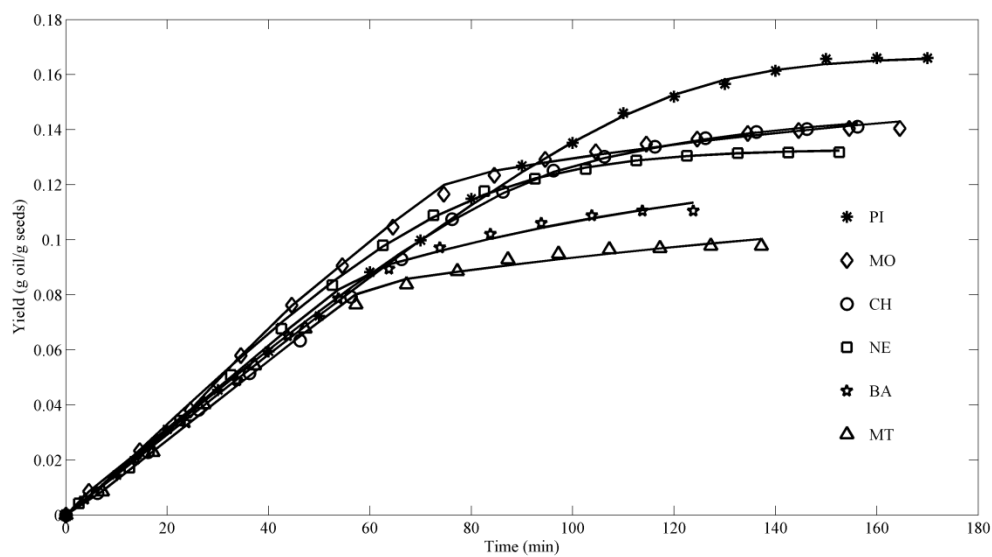


Figure 5.9: *Extraction curves at different grape cultivars: oil yield versus extraction time. The operating conditions are reported in Table 5.8.*

At this stage, it is not possible to state that the scatter of the $k_s a_p$ values - one order of magnitude - was due to the different vegetable structure (permeability to the oil) of the different grape seeds. In fact, the values obtained here allowed to state that for all grape cultivars (or at least for the six here analyzed) $k_s a_p$ can be assumed equal to 10^{-4} s^{-1} (or, to be conservative, equal to $1 \times 10^{-5} \text{ s}^{-1}$ the lowest value in all the experiment when addressing process scale up by using the Sovová model). Values in the range 0.43-0.75 were identified for the grinding efficiency G , with most of the values in the narrow range 0.60-0.70. As expected, the lower the Smd , the higher the value of G , and vice versa (Table 5.8).

Table 5.8 also reports the values of the indicators chosen to evaluate the capability of the model in fitting the experimental data. AARD values from 0.39 to 3.61% and RMSE from $3.7 \cdot 10^{-3}$ - $2.95 \cdot 10^{-2}$ were obtained, demonstrating an extremely good fitting of the model to the experimental data, as it is also self-evident from Figure 5.9.

Table 5.8: Operating conditions, mass transfer parameters and grinding efficiency ($k_s a_p$ and G from best fitting), and modeling errors for SC- CO_2 extractions - cultivar (Cv) 2012.

Cv	T (°C)	P (bar)	Smd (mm)	Flow (g CO ₂ /min)	$k_f a_p$ (sec ⁻¹) x10 ²	$k_s a_p$ (sec ⁻¹) x10 ⁴	G	RMSEx10 ²	AARD (%)
BA	50	500	0.40	7.58	2.25	1.67	0.54	0.74	1.48
			0.36	7.67	2.66	1.13	0.64	0.73	1.25
CH	50	500	0.27	7.56	4.06	2.80	0.67	0.82	1.62
			0.27	9.89	4.64	2.95	0.69	2.76	3.59
MO	50	500	0.28	7.11	3.73	0.96	0.67	0.56	0.39
			0.24	8.87	5.25	0.62	0.70	1.87	2.63
NE	50	500	0.49	7.26	1.63	3.66	0.43	0.63	2.17
			0.39	7.27	2.29	1.21	0.62	1.26	2.04
PI	50	500	0.36	7.99	2.71	5.98	0.63	0.54	0.67
			0.25	9.40	3.79	1.24	0.69	1.38	1.70
MT	50	500	0.34	7.27	2.78	0.83	0.63	0.70	2.38
			0.23	8.70	5.47	1.13	0.68	0.62	2.28

5.4.9 Critical evaluation of the key-parameters affecting extraction kinetics

This section addresses the modeling output from best fitting of experimental data, i.e. the values already presented in Tables 5.1 to 5.7 which have been here appropriately rearranged: namely, the amount of free oil and the external and internal mass transfer coefficients.

The mass fraction of free oil (g free oil/g seeds) is given by Gx_0 [110]. Gx_0 can be compared to the volume fraction of free oil ϕ_f (cm^3 free oil/ cm^3 seed particle) as proposed by Reverchon and Marrone [112,162]: Refer to equations in chapter 3

$$\phi_f = 3 d_c / d_p \quad (5.2)$$

and to the value of such variable as later modified by Fiori and Costa [113] by introducing a free oil correction factor α which takes into account the amount of oil characteristic of the vegetable species ($\alpha=0.472$ for grape seeds [113]): The discussion of this concept is made in Chapter 3, and Eq.s (3.11 and 3.12) is reproduced here for clarity.

$$\phi_f^* = 3 \alpha d_c / d_p \quad (3.12)$$

where d_c is the diameter of the oil bearing cell ($d_c=20 \mu\text{m}$ for grape seeds [104,112]).

Figure 5.10 reports the values of Gx_0 , ϕ_f and ϕ_f^* as a function of the mean particle diameter. Gx_0 values (represented as circles in Figure 5.10) were calculated from the values of Tables 5.1 to 5.7.

The questionable results of Table 5.7 were represented as empty circles in Figure 5.10. Gx_0 values show the expected decreasing trend as d_p increases. Even if they exhibit not negligible scattering, it is worth noticing that they locate between curves ϕ_f and ϕ_f^* , testifying that the free oil content by the BIC model of Sovovà [4] is comparable to the free oil by the BIC model by Reverchon and Marrone [112,162] and its modification by Fiori and Costa [40]. Importantly, similar amount of free oil results also from the BIC-SC models by Fiori when adopting the double shell hypothesis [104,155], as it was previously discussed [113].

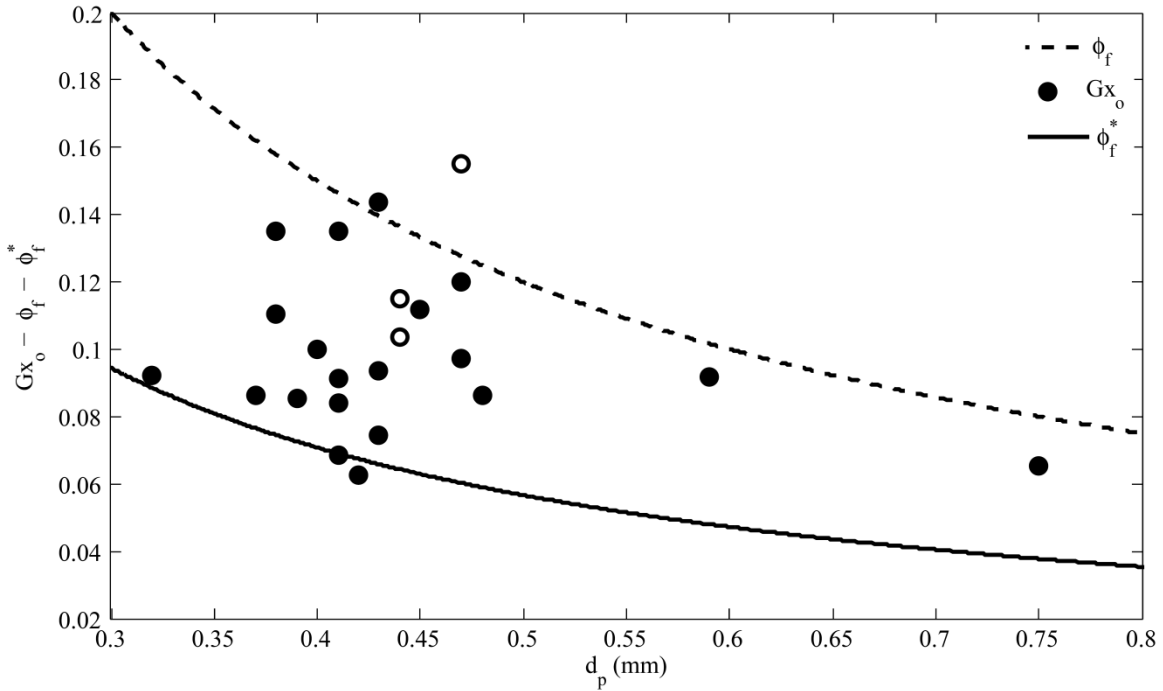


Figure 5.10: Free oil amount versus particle diameter. Gx_0 : g free oil/g seeds; ϕ_f and ϕ_f^* : cm^3 free oil/ cm^3 seed particle. Filled circles: significant data. Empty circles: questionable data from Table 5.7.

The values of the external and internal mass transfer coefficients can be computed from the values reported in Tables 5.1 to 5.7 and resorting to Eq. (3.11) to estimate a_0 :

$$a_0 = 6 \frac{1 - \varepsilon}{d_p} \quad (3.11)$$

The k_f values can be compared with the values predicted using various literature correlations valid for packed beds operating with supercritical fluids. Figure 5.11 shows, on a parity plot, the k_f values here obtained ($k_{f \text{ Mod}}$) and the k_f values obtained using the correlation proposed by Mongkholkhajornsilp et al.[163] ($k_{f \text{ MDDETP}}$). Such a correlation was chosen considering that it applies to low Reynolds number (Re) like those characterizing the tests performed ($0.25 \leq Re \leq 0.66$ for all the tests but one where $Re=1.59$). To calculate $k_{f \text{ MDDETP}}$, the density and viscosity of the supercritical fluid were assumed as those of pure CO_2 as available in the NIST database [164]. The value of the binary diffusion coefficient D_m of oil in SC- CO_2 was estimated using the correlation by Catchpole and King [165], simplifying the oil as consisting of triolein.

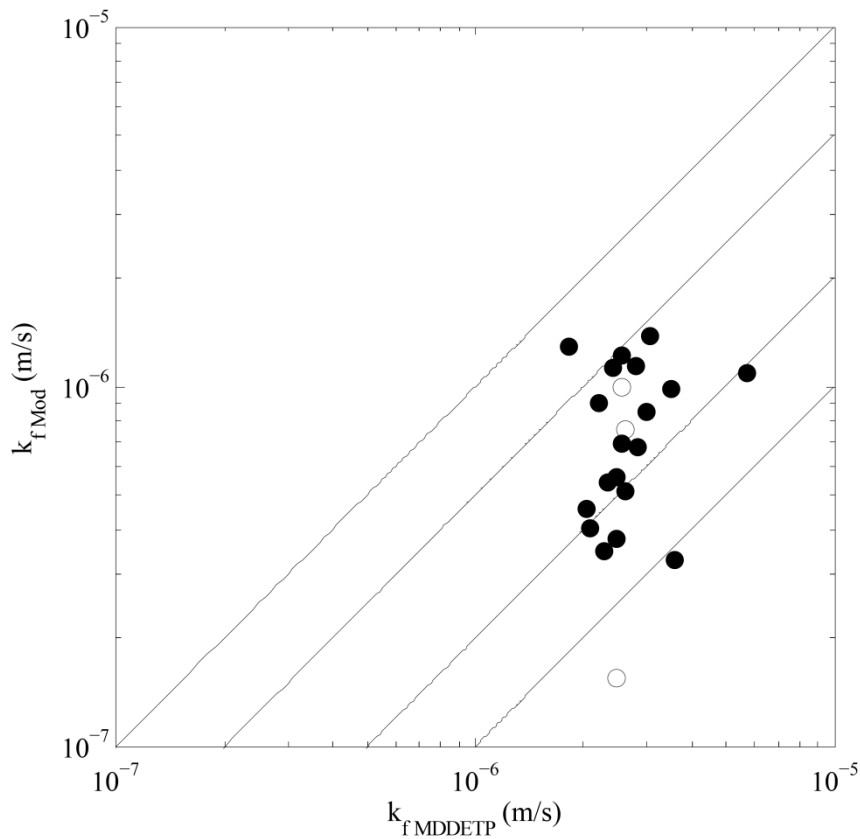


Figure 5.11: Comparison between the external mass transfer coefficient by this work ($k_{f\text{Mod}}$) and the external mass transfer coefficient by the correlation proposed by Mongkholkhajornsilp et al. [163] ($k_{f\text{MDDETP}}$). Filled circles: significant data. Empty circles: questionable data from Table 5.7.

Figure 5.11 testifies that the k_f values here obtained are up to an order of magnitude lower than the theoretical values: in most cases $0.2k_{f\text{MDDETP}} < k_{f\text{Mod}} < 0.5k_{f\text{MDDETP}}$. For further comparison, theoretical values of the external mass transfer coefficient were calculated using the correlation of Puiggene et al. [166] ($k_{f\text{PLR}}$), which is actually valid for higher Re ($10 < Re < 100$). Similar results were also obtained in this case: $0.1k_{f\text{PLR}} < k_{f\text{Mod}} < 0.5k_{f\text{PLR}}$. To summarize, it is possible to affirm that the k_f values computed in the present investigation, even if a little smaller, are in reasonably agreement with theoretical values.

Theoretically, the internal mass transfer coefficient should not depend on SC-CO₂ flow rate and bed porosity, while it should depend (to a small extent) on pressure and temperature and (to a large extent) on particle diameter. In an attempt to take account of these dependencies, del Valle et al. [167] proposed the utilization of the dimensionless

number referred as microstructural correction factor F_M which, after simple rearrangements, can be written as:

$$F_M = k_s d_p / D_m \quad (5.3)$$

Figure 5.12 reports F_M calculated according to Eq. (5.3) versus the particle diameter. Values range between $2 \cdot 10^{-4}$ and $1.5 \cdot 10^{-3}$, varying by almost one order of magnitude. Referring to the data obtained when studying the effect of the particle size (i.e. those deducted from Table 5.4 and indicated in Figure 5.12 with the symbol “star”) the scatter reduces significantly. On the one hand, this indicates that Eq. (5.3) manages to handle quite satisfactorily the dependence of k_s on d_p ; on the other hand, it is self-evident that the k_s data here obtained suffer from an intrinsic scatter which goes beyond the theoretical dependence of k_s on the operating variables.

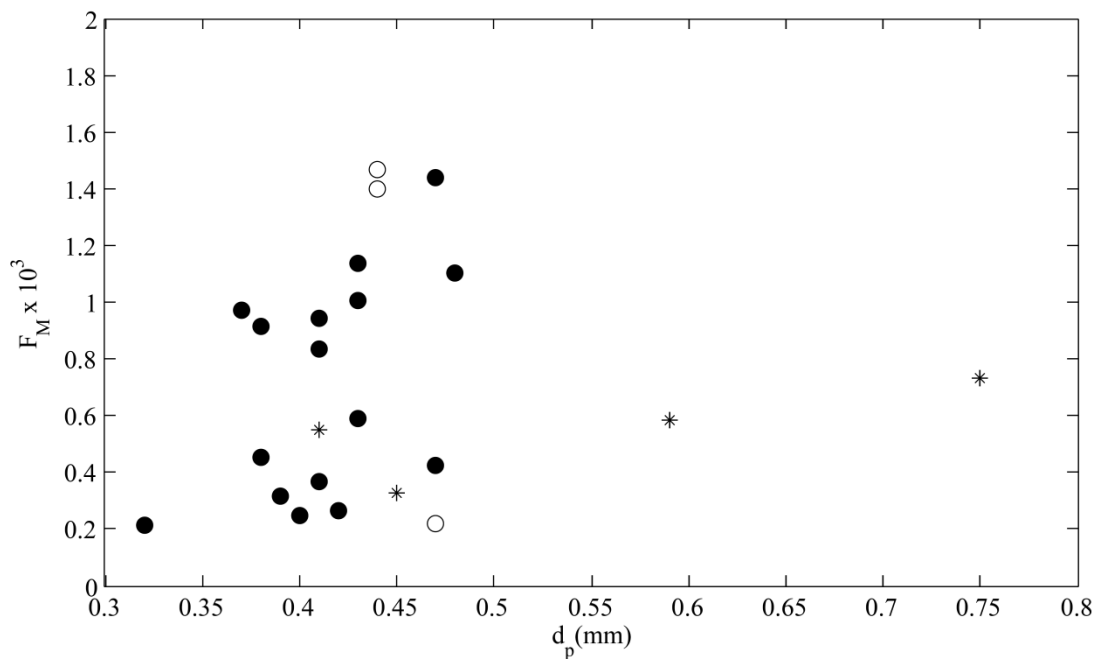


Figure 5.12: $F_M = k_s d_p / D_m$ versus particle diameter. Filled circles: significant data. Empty circles: questionable data from Table 5.7. “Star” symbols: data relevant to Table 5.4.

5.5 Conclusions

The effect of the main process variables affecting the supercritical CO₂ (SC-CO₂) extraction of oil from seeds (namely grape seeds) was investigated, both experimentally and through modeling. The extraction rate increased with an increase in pressure, temperature and solvent flow rate (but in this case the CO₂ specific consumption also increased). At a fixed ratio of mass of seeds to solvent flow rate, decreasing the extractor diameter to length ratio allowed to reduce the CO₂ specific consumption. An extractor bed porosity in the range of 0.23-0.41 had no effect on the extraction kinetics, but a further decrease in bed porosity resulted detrimental, probably due to the occurring of channeling. The particle size had no effect on the initial extraction rate, but reflected on the final asymptotic extraction yield, the smaller were the particles, the higher the final yield.

The experimental extraction data were modeled through the BIC model by Sovová [4]. Through best fitting procedures, the internal and external mass transfer parameters as well as the free oil content were calculated: in most cases their dependence on the process variables was as expected. The best fitted values of the model parameters were discussed based on literature correlations and other extraction models available in the literature. This allowed a critical comparison showing that the values of the external mass transfer coefficient here obtained are comparable but slightly lower than those theoretically predicted, while the amount of free oil is in very good agreement with that foreseen by other extraction models. Finally, the values of the internal mass transfer coefficient (rearranged in a dimensionless form) resulted scattered by almost one order of magnitude. The BIC model allowed for a very good fitting of the experimental data, with maximum root mean square error of $1.20 \cdot 10^{-2}$ and percent average absolute relative deviation of 6.1% considering all the investigated conditions.

6. Subcritical water Extraction of polyphenols from grape skins and defatted grape seeds

In this Chapter, the attention is moved to the utilization of grape skins and defatted grape seeds. Polyphenols were extracted from grape skins and defatted grape seeds (cultivar: *Pinot Nero*) by using subcritical water in a semi-continuous mode. The extraction kinetics was simulated by a simple model from literature. The present research outlines the potentialities of using subcritical water for extracting valuable polyphenols from food processing by-products, and the effect of the operating conditions on extraction kinetics.

6.1 Introduction

The uses of subcritical water (SW) as an extraction solvent for natural products were recently presented by several authors; interesting literature reviews on the topic are also available [41,54–56]. It has been widely reported that the solubility of organic compounds in SW depends on several factors like chain length, type and position of side groups, molecular weight, position of hydrogen bonding etc. of the solute being solubilized [41]. An increase in temperature results in reduction of hydrogen bonding strength in water, which makes the water a solvent of less polarity which in turn increases the solubility of some organic compounds. As polyphenols contain a wide range of compounds, the optimum solubility within SW depends on the proper selection of the operating conditions.

Some works used SW for the extraction of high added valued compounds from

* Part of the present Chapter has been published as: Kurabachew Simon Duba, Alessandro Alberto Casazza, Hatem Ben Mohamed, Patrizia Perego, Luca Fiori. Extraction of Total Polyphenols from Grape Skins and Defatted Grape Seeds using Subcritical Water: Experiment and Modeling. *Food and Bioproducts Processing* 94 (2015) 29–38

wine-making by-product; to point out some: Aliakbarian et al. [58] studied SW extraction of phenolic compounds from grape pomace. Bucić-Kojić et al. [168] investigated the effect of the temperature on the extraction kinetics of phenolic compounds from grape seeds utilizing a water-ethanol mixture, operating in the batch mode. Monrad et al. [60] extracted anthocyanins and flavan-3-ols from red grape pomace using SW in a modified oilseed expeller operating in the continuous mode. Prado et al. [72] hydrolyzed in SW defatted grape seeds in order to obtain sugars. Vergara-Salinas et al. [61] extracted grape pomace with SW in order to evaluate the variation in the chemical and biological antioxidant activity of the extracts when using different extraction temperatures.

In this work, SW extraction of polyphenols from *Pinot Nero* grape skins and defatted seeds was investigated at constant pressure of 10 MPa and flow rate of 2-5 mL/min, under three operating temperatures, namely 80, 100 and 120 °C. The extraction kinetics was modeled and discussed.

6.2 Material and Methods

6.2.1 Defatting of grape seeds

The defatting pre-treatment was done with a supercritical CO₂ (SC-CO₂) equipment (Proras, Rome, Italy) whose design was previously described in Chapter 2 and detailed in [13]. Also the procedure utilized was exactly the same as that detailed in Chapter 2. The extractor basket utilized in this study had an internal volume of 100 mL and was charged with 65 g of milled grape seeds. Pressure, temperature, and CO₂ flow rate were kept constant during the extraction process at 50 MPa, 50 °C, and 8 g/min – CO₂, respectively. The extraction process was stopped when no more oil was extracted from the matrix, which was assumed to be completely defatted. The resulting oil yield resulted equal to 15.5 ± 0.5 g_{oil}/g_{seeds}.

6.2.2 Subcritical water extraction

In order to perform the SW extractions, the same equipment (Proras, Rome, Italy) previously utilized for defatting the grape seeds was utilized with minor plant modifications as shown in Figure 6.1. A nitrogen line was connected to the extractor to purge the system before extraction and to de-oxygenate the deionized water utilized as

solvent. During the entire SW extraction process, the CO₂ feed line remained closed. The extractor (100 mL volume) was half filled with glass beads, then further with the substrate to be extracted (2 g), finally with other glass beads till it was completely filled. The extractor was then closed.

In order to remove O₂ from the deionized water used as solvent, N₂ was bubbled into the water tank for 15 min while the tank remained open. The oxygen inside the extractor and in the pipe lines was removed by letting N₂ pass through the system for 5 min. During this phase, the back-pressure valve at the extractor outlet was maintained open. After N₂ purging, the back-pressure valve was closed and the extractor temperature control loop was put in auto mode letting the system reaching the desired set point extraction temperature. Then the water was pumped to the extractor by means of a HPLC pump (Gilson, Middleton, USA) – water pump in Figure 6.1. As a result of this, the desired pressure was attained. The set point extraction pressure was maintained setting its value as the maximum pressure value of the HPLC pump.

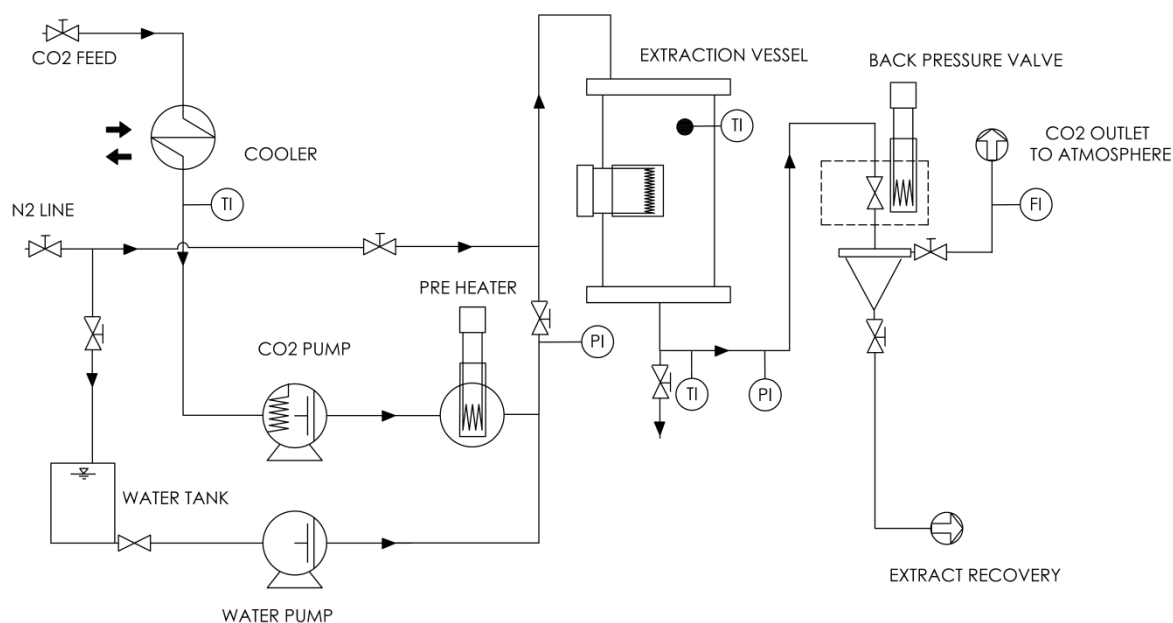


Figure 6.1: P&ID of the extraction equipment

The process was kept in static extraction mode for 20 min before back pressure valve was partially opened and dynamic extraction started. The solvent flow rate resulted from the set point value given to the HPLC pump and the back pressure valve. The

water/polyphenols extract was collected every 20 min during the 2 h extraction time. At the end of the extraction time, the water pump was stopped and the solvent inside the extractor was drained out by opening a drain valve placed in a “tee” on the outlet pipe of the extractor (Figure 6.1). As a result of this procedure, samples were collected after 20, 40, 60, 80, 100, and 120 min. Moreover, in order to quantify all the extracted polyphenols, one more sample was collected after the final drainage of the extractor. The extracts were brought to a final volume of 13 mL using a rotary evaporator (Heidolph, Schwabach, Germany). The concentrates were stored at -20 °C before analysis.

6.2.3 Determination of total polyphenol

The total polyphenol (TP) content was determined by a colorimetric method using the Folin-Ciocalteu assay resorting to the same procedure as previously reported [169]. Measures were carried out at 725 nm using a UV-Vis spectrophotometer, model Lambda 25 (Perkin Elmer, Wellesley, MA) and the calibration curve was made with standard solutions of gallic acid in the range 0.01-1.00 mg/mL. All analyses were performed in triplicate. TP yield was expressed as milligrams of equivalent gallic acid per gram of dried substrate (mg_{GAE}/g). The method response was described by the linear equation:

$$ABS_{725} = 0.0017TP \quad (6.1)$$

with $R^2 = 0.9940$.

6.3 Modeling

The SW extraction kinetics of TP was modeled by the so-called “two-site kinetic model”. The literature reports that this model was applied to the SW extraction of essential oil from savory [170] and *Z. Multiflora* [171], an anti-cancer compound (*damnacanthol*) from roots of *Morinda* [172], and polycyclic aromatic hydrocarbons from contaminated soils [173]. The model is an extension of the “one-site kinetic model”, mostly referred as Crank’s [98] hot ball diffusion model, which is based on Fick’s second law of diffusion and exploits the similarities with the diffusion of heat in a spherical hot ball cooling down in a uniform medium. It assumes that initially the solute is uniformly distributed in the solid matrix, which contains small quantities of extractable materials so that the extraction is not limited by solubility, i.e. the solute never saturates the solvent.

The two-site kinetic model considers a fast and a slow extraction period relevant to two different solute fractions. The desorption rate of fast extracted fraction of polyphenols, F , is given by first-order rate constant k_1 , and that of slowly released fraction $(1 - F)$ is given by first-order rate constant k_2 [170]. Thus, the extraction profile is given by Eq. (2).

$$C/C_0 = 1 - [Fe^{-k_1t}] - [(1-F)e^{-k_2t}] \quad (6.2)$$

Where, C is the mass of TP extracted per mass of substrate, C_0 is the initial mass of TP per mass of substrate, and t is time.

A more explicit form of Eq. (6.2) is given by Sovová [97] for the extraction of solutes under the assumption of mixed flow conditions and with the existence of solute-matrix interactions. According to Sovová [97], the first-order rate constants, represented as lumped parameters k_1 and k_2 , are expressed by Eq.s (6.3) and (6.4).

$$k_1 = \frac{QK_m}{(1 + \varepsilon Q/\gamma k_f a_0)} \quad (6.3)$$

$$k_2 = \frac{1}{[\lambda R/5D_e + \varepsilon/K_m \gamma k_f a_0]} \quad (6.3)$$

Where Q is specific solvent flow rate, K_m is mass partition coefficient, ε is bed void fraction, γ is solvent-to-solid mass ratio in the extractor, k_f is mass transfer coefficient in the fluid, a_0 is specific surface area, λ is characteristic particle dimension (volume-to-surface ratio), R is particle radius, and D_e is effective diffusion coefficient.

In order to reduce the number of model adjustable parameters, reference was done to the well-known representation referred as “broken and intact cells model” [4] which is largely used in the extraction of solutes from solid substrates (also see Chapter 3). Under this assumption, the solutes are contained in cells of the plant matrix and, as a result of mechanical milling pretreatment, some cells in the solids are broken and the remaining cells in the core of the particles are intact. The solute in the broken cell is directly exposed to the particle surface and can be easily extracted (fast desorption): this solute is referred as “free solute” and the extraction rate depends on first-order rate constant k_1 . Conversely, the solute in the intact cells is much more difficult to extract due to the high mass transfer resistance inside the particle itself: in this case the solute is referred as “tied solute” and the

extraction rate depends on k_2 . Such a schematization thus establishes a link between the two extraction rate constants and two solute fractions, referred as “free” and “tied” on the basis of their availability due to their location inside the substrate. It is worth underlining that, in an alternative description, k_1 and k_2 can be related to two solute fractions or classes having different solubility: actually, polyphenols consist in a mixture of substances of very different solubility in SW.

The value of F was determined following the approach of Reverchon and Marrone [112], who assumed that the particle surface is completely covered with free solute and the thickness of this layer is equal to the radius of solute bearing cell. For grape seed oil supercritical CO₂ extraction, Fiori et al. [104] found a better agreement between experimental data and model predictions by doubling the thickness of this layer under what was called “double shell hypothesis”. Combining the two approaches F is given by Eq. (6.5).

$$F = 6d_c/d_p \quad (6.5)$$

Where d_p is the mean diameter of the particle (0.5 mm) and d_c is the solute bearing cell diameter. The solute bearing cell diameter was set equal to 20 μm , value previously measured for grape seeds using scanning electron microscope [104].

Accordingly, the value of $F=0.24$ was taken for all the investigated conditions. It is worth underlining that such a value of F derives from a schematization of the physical and geometrical characteristics of milled grape seed particles. Considering the good modeling results (see Section 6.5.4), $F=0.24$ was utilized also for slab-like milled grape skin particles, even if in this case there was no direct correlation with the morphological characteristics of the substrate.

The model, written as a MATLAB™ code, was utilized in best-fitting the experimental data according to the least square minimization technique by using k_1 and k_2 as the model adjustable parameters. The goodness of the model fitting to experimental data was assessed considering two statistical criteria, the percent average absolute relative deviation (AARD (%)), calculated according to Eq. (3.13), and the root mean square error (RMSE), given by Eq.(3.14) of Chapter 3.

6.4 Statistical analysis

Influences of the TP yields were assessed by analysis of variance (ANOVA) and Tukey's post hoc test [174]. Multiple comparison of the means was made by the least significant difference test at $p = 0.05$. The Statistica v. 6.0 software (StatSoft, Tulsa, OK, USA) was used for the analysis.

6.5 Results and Discussion

6.5.1 Total Polyphenol Yields

The TP extraction yield for both grape skins and defatted seeds at different temperatures is presented in Table 6.1. All the data points represent the average of at least two repeated extractions, each analyzed for TP in triplicate.

Table 6.1: Extraction yield of TP for Pinot Nero grape skins and defatted seeds

Temp.(°C)	Skins TP (mg _{GAE} /g)		Defatted seeds TP (mg _{GAE} /g)
	2 mL/min	5 mL/min	2 mL/min
80	44.3±0.4 ^a	41±2 ^a	44±2 ^a
100	66±4 ^b	55±1 ^b	102±2 ^b
120	77±3 ^c	58±3 ^b	124±1 ^c

Different letters (a-c) within columns show significant differences at $p < 0.05$

The TP yield increased with temperature for both skins and defatted seeds, while it decreased when the flow rate increased from 2 to 5 ml/min. In principle, it could be expected that, for a fixed extraction duration, a higher solvent flow rate would reflect in higher extraction yield. This behavior, quite common in the literature addressing standard extraction processes, was observed for SW extraction by Khajenoori et al. [171]. These authors experienced an increase in yield at increasing solvent flow rate during the SW extraction of essential oil from *Zataria multiflora* [171].

Conversely, the present work shows an opposite behavior, also confirmed by some other works in the literature. Rangsiwong et al. [175] observed a decrease in corilagin extraction yield from *Terminalia chebula* Retz when increasing the SW flow rate. According to the authors, this was probably due to the action of the higher amount of hydronium and hydroxide ions which passed through the substrate, reacting to some extent

with the solute being extracted [175].

Pinelo et al. [176] also observed a decrement in polyphenol extraction yield when studying the mass transfer during continuous solid–liquid extraction of grape pomace. The authors hypothesized that, although higher flow rates favor higher concentration gradients between the sample and the solvent, the residence time had a major weight than the concentration gradient in the mass transfer mechanisms ascribed to the process [176]. In their work, when the flow rate was changed from 3 to 2 mL/min, the polyphenol yield increased from 17.0 to 38.1 mg_{GAE}/g, indicating a higher quantity of phenols passing from grape pomace to solvent in the second case [176].

Another effect can be the cause of the trend here observed. We experienced a compaction of the substrate (grape skins) due to the SW extraction process. In the experiments, as reported in Section 6.2.3, the milled particles to be extracted were loaded in the middle of the extractor, with bottom and top layers filled with glass beads. At the end of the extraction operations, the particles resulted in a compact cake and did not dispersed through the voids of the glass beads bed. Hence, it is possible to hypothesize that, during continuous SW extraction, the compaction degree of the substrate was directly proportional to the flow rate, thereby affecting the extraction of solute from this layer either by creating local flow inhomogeneity (channeling) or by increasing the internal mass transfer resistance. This possible explanation needs further investigation. Given these results and considerations, the defatted seeds were extracted only with a flow rate of 2 mL/min.

6.5.2 Grape skins SW extraction kinetics

The TP extraction kinetics curves relevant to grape skins at the flow rate of 2 and 5 mL/min for three operating temperatures of 80, 100 and 120 °C and constant pressure of 10 MPa are presented in Figures 6.2a and b.

For both solvent flow rates, the TP yield increased with the increase in temperature. At a fixed temperature, the initial rate of extraction was higher at the higher solvent flow rate while, conversely, the final yield was higher at the lower solvent flow rate, as discussed in Section 6.5.1. Because of these opposing trends, the extraction curves at different solvent flow rates crossed each other (see also Figure 6.4 in section 6.5.4). The cross over points shifted in time to the left with the increase in temperature. At 80 °C, the

two extraction kinetics curves (2 and 5 mL/min) overlapped at the end of the test (120 min); at 100 °C, they crossed at about 60 min; at 120 °C, they crossed at about 20 min.

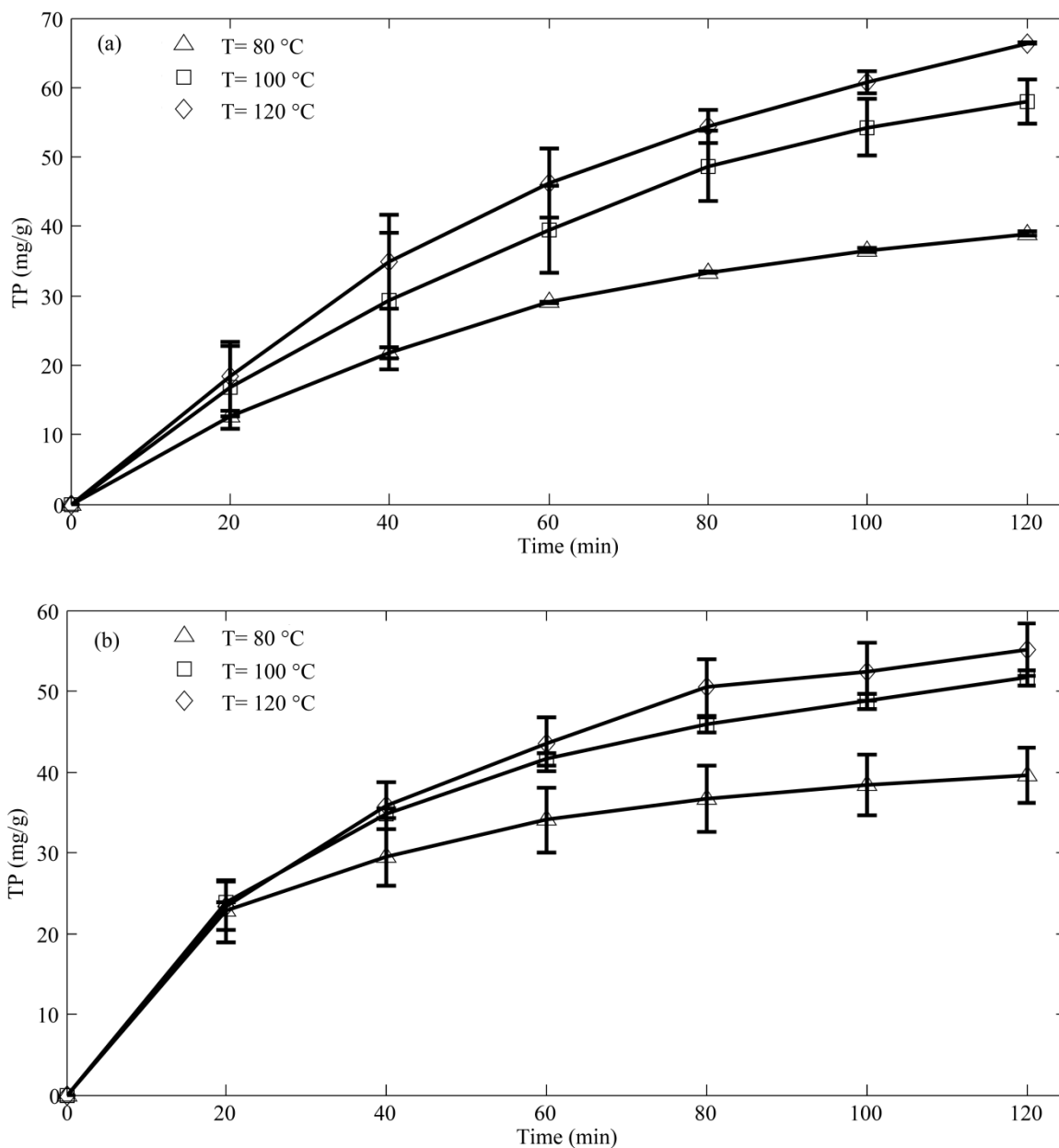


Figure 6.2: TP yield (mg_{GAE}/g) relevant to SW extraction from grape skins at different temperatures. (a) solvent flow rate equal to 2 mL/min; (b) solvent flow rate equal to 5 mL/min. Experimental data.

6.5.3 Defatted grape seeds SW extraction kinetics

For defatted seeds, the experiments were conducted at a flow rate of 2 mL/min. In

this case, the TP yields resulted higher than those of skins (see Table 6.1, Figures 6. 2 and 6.3). It must be stated that the TP yields reported in Table 6.1 are greater than the final yields presented in Figures 6.2 and 6.3, because the values of Table 6.1 also accounts for the amount of polyphenols in the water drained out from the extractor after the end of the two hours extraction period, while in Figures 6.2 and 6.3 only the kinetics data were plotted. Even though there is not direct comparison of TP yield from defatted grape seeds and skins in the literature relevant to SW extraction (to the best of our knowledge), some studies present interesting data which have close links with the results reported in this study. It is worth underlining that during the CO₂ defatting process the amount of polyphenols in the seeds remain unvaried as pure CO₂ is incapable of extracting such polar compounds, as demonstrated by Fiori et al. [169].

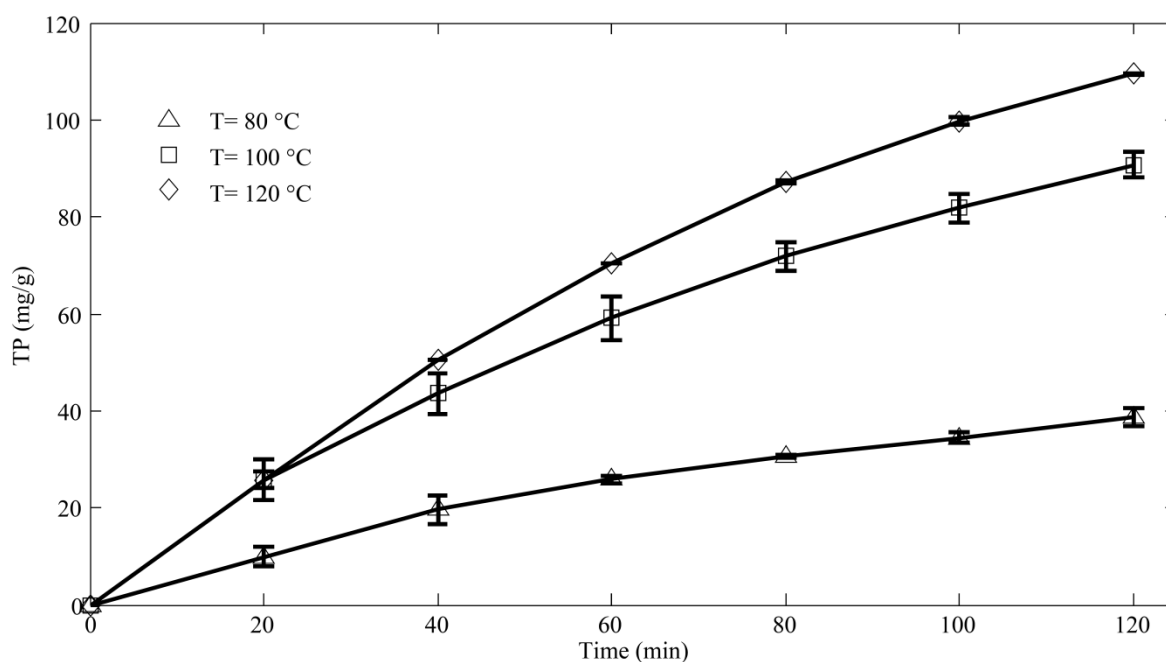


Figure 6.3: TP yield (mg_{GAE}/g) relevant to SW extraction from defatted grape seeds at different temperatures and at a solvent flow rate equal to 2 mL/min. Experimental data.

Casazza et al. [53] reported a comparison between un-defatted grape seeds and skins of *Pinot Nero* extracted by different non-conventional techniques. They found out that TP in seeds is one order of magnitude higher than that in skins, and the yields of TP can vary up to 390% simply by changing the extraction technique. Aliakbarian et al. [58] performed SW extraction of grape pomace and found a yield of 31 ± 3 mg_{GAE}/g at operation conditions of 140 °C and 11.6 MPa when the flow rate was 1-2 mL/min. Bucic-

Kojić et al. [168] reported a TP yield from grape seeds of 130 mg_{GAE}/g when extracting at a temperature of 80 °C using an ethanol-water solution in a batch reactor. Sólyom et al. (2014) studied the thermal degradation of grape marc polyphenols; they found a TP yield of 83 ± 3 mg_{GAE}/g and hinted that grape marc may preserve at least 90% of the active compounds up to 150 °C (in their case the yield at 100 °C was higher than that at 150 °C). In fact, wide ranges of TP yields from wine industry by-products are reported in the literature due to the several factors which influence the total yield, such as the extraction temperature, time, technique, solvent type, cultivars and type of pretreatment.

6.5.4 Extraction kinetics: modeling results

The extraction kinetics of both grape skins and defatted seeds was modeled with the two-site kinetic model described in Section 6.3. When modeling, the value of C_o was set equal to the maximum extraction yield achieved for the two substrates, i.e. 77 and 124 mg_{GAE}/g for, respectively, grape skins and defatted seeds (Table 6.1).

The model curves are reported together with the experimental data in Figures 6.4 and 6.5. The model adjustable parameters from best fitting are presented in Table 6.2 along with the deviation of model predictions from experimental data. There are clear trends for both fast and slow desorption rate constants k_1 and k_2 , for both skins and defatted seeds. The desorption rate of fast extracted fraction of polyphenols, expressed as first order rate constant k_1 , increases both with temperature and flow rate. Generally, an increase in temperature enhances the solvent power of water for little polar organic solutes, while an increase in flow rate increases the concentration gradient. As the characteristic particle dimensions are similar for both skins and seeds, the increase in k_1 with temperature can be explained in terms of the mass partition coefficient of the solute (which is defined as the ratio of equilibrium concentration of the solute in the fluid phase at the particle surface to the solute concentration in the solid phase). Looking at Eq. (6.3), the first order rate constant k_1 is directly proportional to the partition coefficient. So, with the increase in temperature the solute partition coefficient will increase, and hence the desorption rate constant k_1 will also increase. This can be also observed from Figure 6.4 where the initial rate of extraction increases with both temperature and flow, while in the following the flow makes an inversion of the trends (see the discussion on crosses over at Section 6.5.2).

For grape skins, except at the lowest temperature of 80 °C, the desorption rate

constant of slowly released fraction k_2 decreases when flow rate increases. Consequently, the decrease in the TP yield when the flow rate increases incurred in second part of the extraction (Figure 6.4) k_2 reflects the characteristics of the matrix and should largely depend on effective diffusivity, Eq. (6.4). Accordingly, the structure of the bulk material must have changed with flow rate as hypothesized in Section 6.5.1.

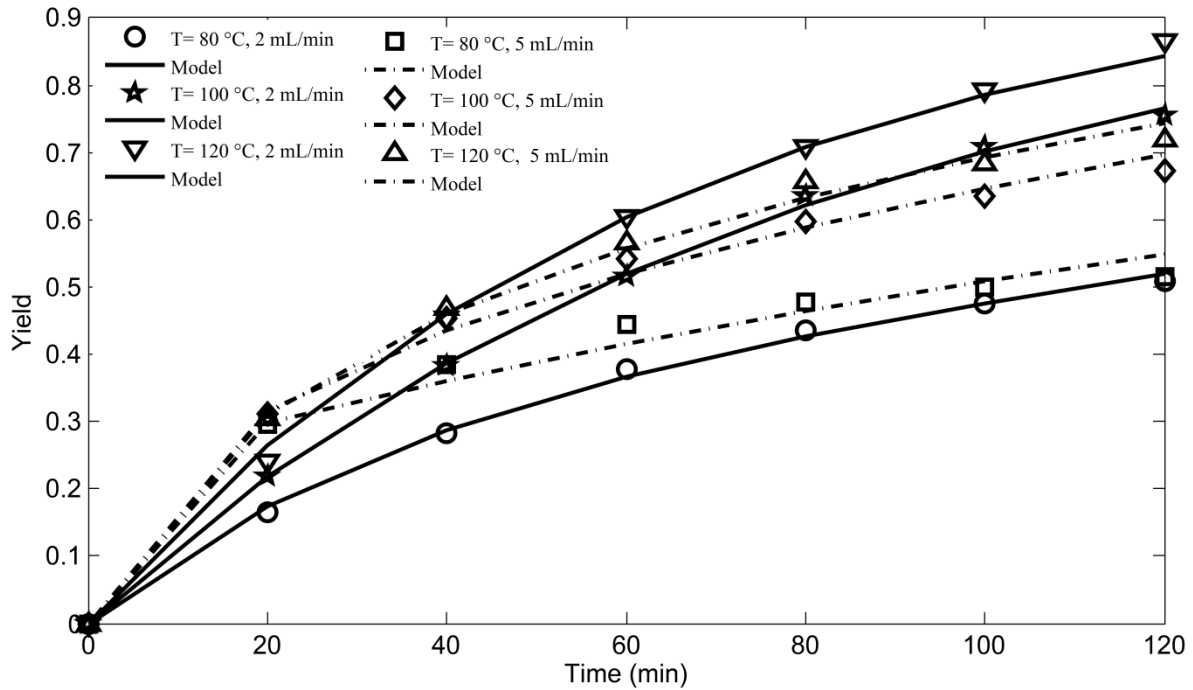


Figure 6.4: TP yield (dimensionless) relevant to SW extraction from grape skins at different temperatures and solvent flow rates. Experimental data and model curves

When we compare the model parameters for skins and defatted seeds at 2 mL/min, since in both cases the experiments were conducted at constant specific flow rate and bed void volume, the external mass transfer coefficients k_f are largely expected to be similar. This is confirmed by the values of k_1 - Table 6.2 - which strongly depend on k_f through Eq. (6.3), with small variations which can be attributed to the structural difference between skins and defatted seeds.

Table 6.2: Model adjustable parameters for SW extraction of grape skins and defatted seeds

<i>T</i> (°C)	Skins								Defatted seeds			
	2 mL/min				5 mL/min				2 mL/min			
	k_1 (min^{-1})	k_2 (min^{-1})	<i>RMSE</i> * 10 ²	<i>AARD</i> (%)	k_1 (min^{-1})	k_2 (min^{-1})	<i>RMSE</i> * 10 ²	<i>AARD</i> (%)	k_1 (min^{-1})	k_2 (min^{-1})	<i>RMSE</i> * 10 ²	<i>AARD</i> (%)
80	0.0154	0.0039	2.16	1.19	0.0739	0.0044	5.20	1.99	0.0146	0.0012	0.99	1.27
100	0.0163	0.0111	1.84	0.57	0.1019	0.0077	3.98	1.38	0.0148	0.0099	1.28	0.66
120	0.0334	0.0155	3.42	1.22	0.1865	0.0091	4.04	1.21	0.0168	0.0148	9.11	3.78

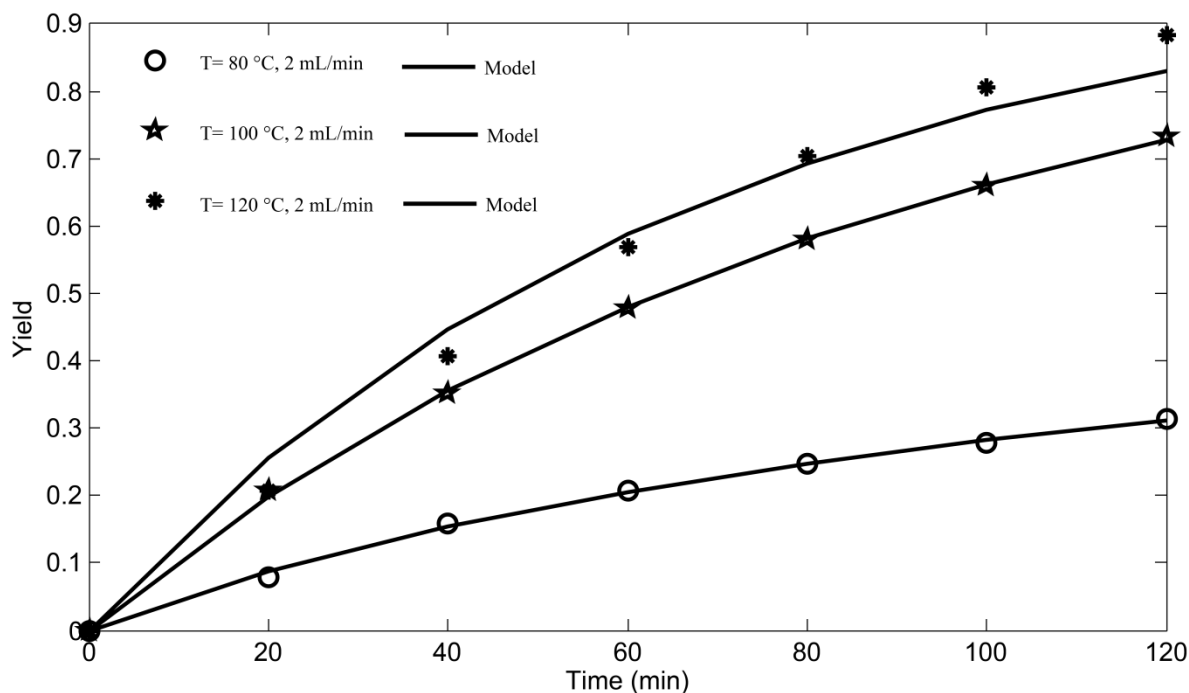


Figure 6.5: TP yield (dimensionless) relevant to SW extraction from defatted grape seeds at different temperatures and at a solvent flow rate equal to 2 mL/min. Experimental data and model curves

The deviation between model predictions and experimental data are quantified and compared using RMSE and AARD (%), as shown in Table 6.2. Remarkable good agreement between model predictions and experimental data was found. Interestingly, the values of model adjustable parameters are consistent with the values reported elsewhere in the literature and relevant to different substrates and extractable compounds [170–172]. Thus, the present results testify that the conventional two-site kinetic model can be successfully applied also to the SW extraction of polyphenols from wine-making by-products. Moreover the model, when supplemented with Eqs. (6.3) and (6.4) for the definition of fast and slow extracted fractions rate constant k_1 and k_2 , describes the underlining physical phenomena of the SW extraction process, i.e. its dependence on mass transfer and partition coefficients. The model is reasonably simple and information generated thereof has a vast practical importance especially in scale up and process design.

6.6 Conclusions

Subcritical water extractions of polyphenols from grape skins and defatted grape seeds were conducted in semi-continuous extractor. Relatively high yields of total polyphenols were obtained for both skins and seeds. Increasing the extraction temperature, the total polyphenols yields increased. Increasing the solvent flow rate resulted beneficial only in the initial extraction phase, while in the following the extraction rate decreased substantially: the final total polyphenols yields were higher for the lower solvent flow rate. This aspect can find explanation in degradation phenomena as previously reported in the literature or in fluid-dynamic aspects as here inferred considering the matrix which compacted due to extraction.

The kinetics of extraction was modeled by the two-site kinetic model, a simple model from literature; remarkable good agreement between model predictions and experimental data was observed with root mean square error in the range of 10^{-2} - 10^{-1} and percent average absolute relative deviation of 0.5-4%. The model can be thus utilized for predicting the extraction of polyphenols from grape residues and similar substrates and as a preliminary tool for designing subcritical water extraction processes.

7. Scale-up and Economic Analysis of Supercritical CO₂ extraction process

In this Chapter, a preliminary feasibility study for the establishment of supercritical CO₂ (SC-CO₂) extraction plant of capacity 3000 ton/yr. grape seeds was envisaged. For the proposed production capacity, the total investment requirement was estimated at US\$13,330,900 out of which US\$ 4,775,413 was the purchased equipment cost. The cost of production was estimated at a value of US\$ 10/kg-oil. The SC-CO₂ extraction plant is economically viable with rate of return on investment estimated at 8.25% and payback period of 5 year at the current minimum retail selling price rate of grape seed oil in the market. The project has an attractive socio-economic and environmental benefit and generates substantial revenue for the local government in the form of tax. Besides it will provide an opportunity for the wine-makers to sustainably sell wet grape marc at a price of up to US\$ 10/ton.

7.1 Introduction

Vegetable oils have historically been a valued commodity for food use and to a lesser extent for non-edible applications such as pharmaceutical, detergents, cosmetics, biodiesel and lubricants [178]. According to the Global Agricultural Information Network (GAIN) 2014 annual report on Oilseeds and Products in EU-28, the European Union is highly dependent on imports of oilseeds and oilseeds products to meet the demand for food, feed and industrial uses, including biofuel production [179]. Market survey published by the Centre for the Promotion of Imports (Dutch acronym CBI) indicates that

* Under preparation (To be submitted to *Journal of Chemical Engineering Research and Design*) as: Kurabachew Simon Daba, Luca Fiori, *Economic Analysis and Scale-up of Supercritical CO₂ extraction process*

the total EU imports of vegetable oils and fat in 2007 was € 8.9 billion and it is estimated that this figure increase by around 1% per year. Italy is the largest importer, accounting for 20% of total EU imports followed by Germany (15%) and The Netherlands (14%) [180].

Grape seeds, which is one of the by-products of wine-making process, contain substantial percentage of oil [114] (see Chapter 2). The European Union is the world leader in wine production, with almost half of the global vine-growing area and about 60% of production by volume with France, Italy and Spain being the leading producers [181]. Therefore, the importance of the feasibility study for the establishment of grape seeds oil extraction plant in the region is a matter of great concern.

Generally, vegetable oil extraction plants are either mechanical or solvent extraction process. The mechanical extraction can be accomplished by a batch hydraulic press or a continuous screw expeller [182]. When using hydraulic press, fresh ground materials are covered with a filter cloth and placed in a pressing cylindrical chamber made of perforated wall [182,183]. In order to assist the extractability of the oil, a heat source is supplied to the wall of the cylinder [184]. Under hydraulic press extraction process, the yield of extraction depends on the pressing time, applied pressure and wall temperature [183,184]. The biggest challenge of this technique is the removal of the pressed cake from the chamber. While in the screw expeller, the extractions are made in continuous mode. The unit consists of a tapered helical rotating shaft in a constant diameter cylindrical barrel which acts as a feeder in the narrow diameter section and compresses the material against the wall and squeezes the oil out of the seed as it drives the material through the barrel and discharge the cake at another end [182,185]. In general, mechanical extraction techniques are applied to solid materials with relatively high initial extractable solute concentration and are characterized by superior product quality and low yield.

Like the mechanical extraction techniques, the solvent extraction can be batch or continuous process [186]. The batch system are used for the extraction of less oily materials in a single or series of extractors where the solvent flow in counter current direction to a stationary bed of ground solids. While a continuous operation are used with material with high oil content through immersion or percolation method [186]. The organic solvent extraction processes are commonly operated at atmospheric pressure and

normal boiling point of the solvents. The solvents are separated from the product by distillation process and recycled for the subsequent extraction. The major advantage of organic solvent extraction is the high product yield [114] and the major drawback is the presence of residual solvent in the product stream.

The use of SC-CO₂ for the extraction of seeds oil is an alternative to the conventional organic solvent extraction process [83]. The extraction process occurs under elevated pressure and temperature to keep the extraction fluid at supercritical phase. The process has several advantage over conventional organic solvent and mechanical extraction techniques as discussed elsewhere [114,147] and detailed in Chapter 1-5.

Despite its advantages, the development of supercritical CO₂ technologies are struggling with the perception that high pressure process requires high initial investment cost with respect to the conventional counterparts. But, according to Perrut [6], a CEO of SEPAREX, one of a company specialized in the design and manufacturing of supercritical and high pressure equipment technologies in Europe, when dealing with very large volume of materials, the perception is far from true as the capital amortization sharply decreases as capacity increases.

Therefore, a through economic analysis of SC-CO₂ extraction process under industrial scale scenario is highly commendable to make an informed decision about the process. In this work, the data generated at lab scale unit (Chapter 4 and 5) are used for the scale-up operation and the economic analysis of the plant was conducted.

7.2 Scale-up operation

The majority of the literatures dealing with SC-CO₂ operation are based on lab scale units and recently substantial effort are being made to address the design and scale-up issues [187]. In general during SC-CO₂ extraction operation, the rate of extraction is governed by either solute solubility or internal diffusion and in some cases the combination of both [147]. A rule of thumb for scale-up operation of supercritical system were presented by Clavier & Perrut [188]. It was proposed that, it suffices to keep the ratio of solvent mass to solid mass (F/S) constant between the lab and pilot/large scale extractors when the solute solubility is the rate limiting step and the ratio of solvent flow rate to solid mass (Q/S) when the internal diffusion is the limiting step. In the case where both the external and internal mass transfer resistances are the rate governed steps, both

the ratios of F/S and Q/S can be kept constant.

Mezzomo et al [189] studied the effect of different scale-up scenario for the SC-CO₂ extraction of peach almond oil considering constant Reynolds number (Re), F/S, Q/S, and both F/S and Q/S between lab and large scale extractor and suggested that, for peach almond oil extraction, where the internal diffusion is the rate governing step, the best scale-up criteria is to maintain constant Q/S. Prado et al.[16,190] confirmed that maintaining constant F/S can be effectively employed for scale-up of SC-CO₂ extraction of clove flower, sugarcane residue and grape seeds oil while de Melo et al. [161] used constant Q/S for the scale-up of SC-CO₂ extraction of *Eucalyptus globulus* bark. Whereas Jokić et al [191] suggested the use of geometric similarity between lab and pilot scale extractor as an additional scale-up criteria when moving from lab to pilot scale operation during SC-CO₂ extraction of soybean oil in addition to Q/S.

In almost all the scale-up operation reported in the literatures, the so called ‘aspect ratio’ of extractor i.e. diameter to length (D/L) ratio between the small and large scale units are not constant. Núñez & del Valle [192] indicated that, the production cost depends on the aspect ratio of the extractor especially when specific solvent flow rate are kept constant and previous work by Duba & Fiori [147] (Chapter 5) confirm that the rate of SC-CO₂ extraction depends on extractor D/L ratio. Therefore, in this work a constant aspect ratio was maintained in addition to the ratio of F/S and Q/S when moving from lab to industrial scale unit.

7.3 Economic Analysis

The economic analysis of any new project starts with the estimation of the total capital investment which is the sum of fixed and working capital investments required for the erection and operation of the plant.

7.3.1 Fixed capital investment (FCI)

The FCI is the capital needed to purchase and erect the required manufacturing equipment and plant facilities. Generally, FCI has two components, the direct cost and indirect cost [193]. The direct cost includes the cost for purchasing, delivery, and installation of manufacturing equipment, instrumentation and control, piping and installation, electric system, building, yard improvement, service facilities and cost of land. The indirect component includes the engineering and supervision cost, legal

expenses, construction expenses, contractor's fee and contingency.

7.3.2 Working capital investment (WCI)

The WCI is the fund needed to conduct the day-to-day company business which is the sum of manufacturing cost and general expenses [146]. The manufacturing cost has three components, the variable production cost, also called the direct production cost, the fixed charges and the plant overhead cost [193]. The direct production cost includes, the cost of raw materials, operating labor, direct supervisory and clerical labor, utilities, operating supplies, maintenance and repairs and laboratory charges. The fixed charge components consists of depreciation cost, local taxes, insurance and financial interest. The plant overhead cost includes the cost for packaging, medical services, restaurants, recreational facilities and storage facilities among others. The second component of the working capital which is called general expenses includes the administrative cost, distribution and marketing cost and the research and development cost.

7.3.3 Feasibility studies of SC-CO₂ extraction process

The production cost of SC-CO₂ extraction process depends on operating conditions like temperature, pressure, matrix particle diameter, solvent flow rate, aspect ratio of extractors and the number of extractors in series [192,194]. In the past two decades considerable numbers of research works were published addressing the techno-economic analysis of SC-CO₂ extraction process at large/industrial scale units. Some of the notable example includes: (1) The work by Montero et al. [195] which estimated the investment cost of SC-CO₂ extraction for remediation of contaminated soil in two extractors of capacity 1950 L. (2) The work by Rosa et al [196] which estimated the manufacturing costs and technical–economical evaluation of clove bud oil and ginger oleoresin in SC-CO₂ for industrial scale unit in two 400 L extractors. (3) The work by Shariaty-Niassar et al. [197] which studied the economic analysis of rosemary extractions using SC-CO₂ in two extractors of 200 L. (4) The work by Fiori [83] which investigated the feasibility of industrial scale extraction of grape seed oil in three extractors of capacity 800 L. (5) The work of Mezzomo et al. [198] which presented the economic viability of SC-CO₂ extraction of peach almond, spearmint and marigold in two extractors of capacity 400 L. (6) The work of Prado et al. [16] which studied economic evaluation of SC-CO₂ of grape seed oil under two scenario of raw material cost using

extractors of capacity 5 L, 50 L and 500 L. (7) The work by Leitão et al. [199] which studied the economic evaluation of *anacardium occidentale* leaves extraction using SC-CO₂ and estimated the cost of manufacturing in extractors previously used by Prado et al. [16]. (8) The work of Prado et al. [200] which investigated the cost of manufacturing of mango leaves extracts using SC-CO₂ in an extractors of different capacity, the minimum cost was reported for two extractors of capacity 300 L and (10) the work by Rocha-Uribe et al.[201] which recently estimated the cost of manufacturing of habanero chili in extractors of volume from 5 to 400 L and proposed an equation to estimate the manufacturing costs of industrial size supercritical extraction systems. The authors do not claim the list is exhaustive but every effort is made to include the literature work in the past twenty years specifically dealing with techno-economic evaluation of SC-CO₂ extraction of solute from solid matrix.

The cost estimation approach and the degree to which the cost components were included in the determination of techno-economic viability of the SC-CO₂ extraction process in literatures are significantly different from one another. Some researches [196,198,202] used an empirical equation (Eqn.(7.1)) proposed by Turton et al. [203] to estimate the total cost of manufacturing (COM) of the supercritical extraction plant, others used commercial software [16,200] to estimate COM, while another groups [195,197] used a guideline of Peters and Timmerhaus [193] like approach to estimate the working capital, yet there are some other researches [83,194] which estimated part of the direct production cost (i.e. cost of raw material, operating labor and utility) based on the capacity and operating condition of the proposed plant and roughly estimated the remaining components. The researchers also differ in the level to which the components of fixed capital investment were estimated.

To the best of our knowledge there are only two research works i.e. Fiori [83] and Prado et al. [16] which directly addressed the economic analysis of SC-CO₂ extraction grape seeds oil. This two works serve as a starting point for any subsequent studies in the field, but they both either significant under estimated or completely not taken into account substantial amount of cost components either in the form of fixed capital or working capital investment. Therefore, the objective of the current study is to build on the previous work of Fiori [83] by taking into account as much as possible all the foreseeable cost components. The approach of Peters and Timmerhaus [193] was used to estimate the

total capital investment required to establish a SC-CO₂ extraction of grape seeds oil after main components of the direct production cost were estimated from the proposed operating conditions.

$$COM = 0.28FCI + 2.73C_{OL} + 1.23(C_{UT} + C_{RM}) \quad (7.1)$$

Where, FCI is the fixed capital investment, C_{OL} is cost of operating labor, C_{UT} is utility cost and C_{RM} is cost of raw material.

7.3.4 Profitability analysis

The profitability of the project was estimated in terms of rate of return on investment (*ROI*) and payback period (*PBP*) according to Eqn. (7.2) and Eqn. (7.3) respectively [193]. The return on investment is the ratio of net profit (*N_p*) to the total capital investment (*TCI*) [193] while the payback period is the time required to recover the fixed capital cost of the project after the start of production [203]. Even though the terms are subjective, it is obvious that, projects with higher return on investment and shorter payback periods are more attractive.

$$ROI = \frac{N_p}{TCI} \quad (7.2)$$

$$PBP = \frac{N_p}{(FCI + depreciation/year)} \quad (7.3)$$

7.4 Result and discussion

The value of F/S equal to 13 kg CO₂/kg-solids was used for scale-up operation, which was according to the amount of CO₂ needed to extract 90% of the grape seed oil using experimental lab scale equipment as presented by Duba and Fiori [147] (refer to Figure 5.7 of Chapter 5) under extraction condition mostly commonly used at industrial scale operation of 35 MPa and 313 K [194]. The corresponding amount of Q/S ratio similar to lab scale condition was 6 kg CO₂ · hr⁻¹/kg-solids. When dealing with scale-up of SC-CO₂ extraction of *Eucalyptus globulus* bark (where internal diffusion is the rate controlling step), de Melo et al. [161] used the value of Q/S to be equal to 10 kg CO₂ · hr⁻¹/kg-solids. The aspect ratio (D/L) equal to 0.26 was maintained constant which is closed to the recommended range of 0.125 < D/L < 0.250 [192] for industrial scale extractors.

In fact in the previous work by the Duba and Fiori [147] (Chapter 5) which also

investigated the effect of D/L ratio on the kinetics of extraction, a relatively large increase in the rate of extraction was observed when the D/L ratio was reduced from 0.53 to 0.26 than when moving from 0.26 to 0.11. Based on the prescribed condition, the dimension of the proposed industrial scale extractors which are required to handle 3000 ton of grape seed per year (based on 300 working day and 24 operation hour per day) is calculated as three extractors of volume 650 L with internal diameter of 0.6m and 2.3m height when bed porosity is maintained at 0.41 and particle diameter is 0.40mm. This dimension also takes into account an extra 1.5% increase in the total volume for safety purpose at industrial scale unit.

A schematic diagram of the proposed supercritical extraction plant is shown in Figure 7.1. The system consists of a make-up CO₂ cylinder (M-CO₂), CO₂ storage vessel (SV), heat exchangers (HX₁, HX₂, HX₃ and HX₄), a CO₂ pump (P), extractors (E₁, E₂ and E₃) and separators (S). A subcooled liquid CO₂ in SV is further cooled by HX₁ to guarantee a liquid phase at the pump suction head. Then, the liquid is compressed to the required pressure by the pump into the extractors which first passes through a pre-heater HX₂ to convert to supercritical phase. Heat sources are supplied into the extractors to bring and maintain the CO₂ at required temperature. After extraction, the CO₂ is converted to vapor phase by heat exchanger HX₃. At this point, the oil precipitates from the stream using flash separator (S). The CO₂ is then recycled back to the storage vessel after converted to saturated liquid by condenser HX₄ while the oil is sent to packaging unit.

To simulate a continuous countercurrent operation, two extractors are operated at a time according to the scenario depicted in Table 7.1. The operation of the extractors under third scenarios where E₃ is loaded with fresh ground seeds and E₂ contain a partially defatted material from the preceding scenario is shown in Figure 7.1. The solid lines indicate the active lines of operation (the open valves and the direction of CO₂ flow) while a dash lines indicate off or inactive routes. Under this condition, fresh CO₂ first enters extractor E₂ and move counter currently to extractor E₃ while extractor E₁ is in off mode to undergo depressurization, unloading of defatted matrix, reloading of fresh materials and finally enter into the system as a 2^o extractor under third scenario and the cycle goes on. During depressurization operation a fraction of CO₂ will be lost and an equivalent amount is supplied by the make-up CO₂ cylinder.

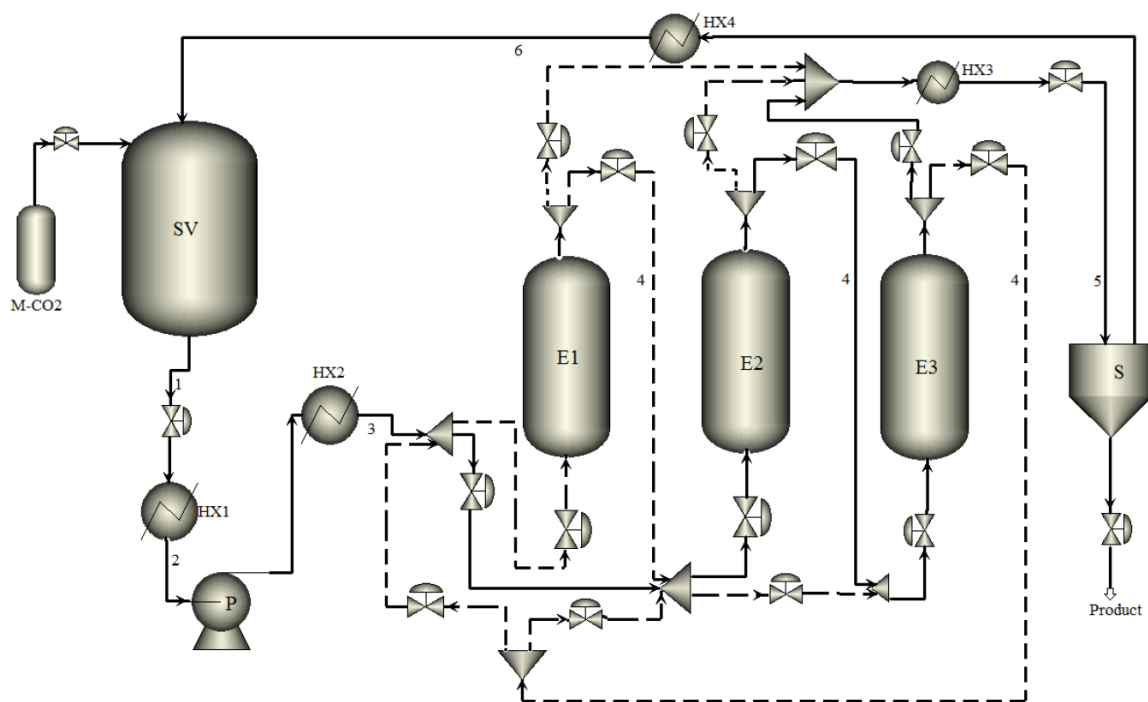


Figure 7.1: Schematic diagram of multi-unit SC-CO₂ extraction plant

Table 7.1: Operating scenario of the extraction process

Scenario	E_1	E_2	E_3
1	1° (partially defatted)	2° (fresh)	OFF
2	OFF	1° (partially defatted)	2° (fresh)
3	2° (fresh)	OFF	1° (partially defatted)

Grape marc generally contains moisture in the range of 60-65%, with roughly 45-55% skins, 42-50% seeds and 1-4% stalks [204] on dry basis. Therefore, before the extraction operation thermal and mechanical conditionings are necessary in order to remove most of the excess water from the substrate and skins and stalks from the seeds. Fiori [83] indicate that, an energy self-sufficient system can be achieved by using a rotary dryer to remove the water content of grape marc by burning whole of stalks and fraction of the skins in a combustor to generate the amount of hot air necessary for the dryer. Specifically, to dry 15000 ton of grape marc of 60% moisture content and of composition 51% skins, 47% seeds and 2% stalks on dry basis, it suffice to burn 1200 ton skin and 130 ton of stalks. The harvest season of grape fruit occur in two month time (In Italy between mid-August and mid-October). Therefore, to get high quality product, the grape marc should be collected, dried and stored in a reasonable time after it is produced in the winery. To achieve that, the dryer capacity must be in such a way that it can handle solid

mass flow rate equal to a yearly production accumulated over three month period (a one month safety allowance after harvest for the wineries to crush the fruits was foreseen) which is approximately 1.67×10^5 kg/day.

During the design of rotary dryer with direct air to solid contact, the maximum allowable solid velocity and aspect ratio are 0.1m/s and 6 respectively [193]. Assuming 12.5% of dryer cross sectional area are covered by solid (optimum range is between 10-15%) [193] and the bulk density of grape marc as 200 kg/m^3 [205], the dimension of the dryer can be effectively specified as a diameter of (0.99m) approximated as 1m and length of (5.95m) approximated as 6m. The furnace capacity which burns the skins and stalks to supply required hot air to the rotary dryer is estimated based on the caloric value of dry grape skins and stalks presented by Vattente et al [206] as an average of 19MJ/kg for both skins and stalks.

The seeds, stalks and skins separator proposed in this work was a grain cleaner which consists of three layer of vibrating sieve and cyclone separator [207] in which light impurity are sucked in to the cyclone using air blower while the stacks and skins are collected on the top, small particles at the bottom and good seeds are retained on the middle sieve. The cleaner capacity is proportional to the throughput of the rotary dryer. To mill the seeds, a ball mill with capacity of 500 kg/hr was proposed to supply a fresh ground matrix to the extractors on hourly bases.

The fixed capital investment was estimated after the purchased cost of the plant equipment was determined. The cost of the main equipment, the SC-CO₂ extraction plant was estimated from the literature data of such plant at industrial scale. The cost was estimated as an average of the value based on the data reported by: Shariaty-Niassar et al. [197] in 2009 for SC-CO₂ extraction plant using two extractors of volume 400 L, Rosa et al. [196] for two extractors of volume 800 L in 2005 and Rocha-uribe et al. [201] for extractor of volume 200 L in 2014 (cost quotation dated 2008).

Since the cost data's are for different time line and different extractors volume, the costs were first brought to the current time line (2013) using Chemical Engineering Plant Cost Index (CEPCI) [208–210] and then corrected for the equipment size according to the six-tenth rule [193]. The main reason why the year 2013 was chosen as the current time line is the fact that it corresponds to the last year on which the CEPCI is updated. Hence, the cost of the proposed extraction plant was estimated at a value of US\$

4,300,237. In a similar fashion, the cost of the rotary dryer, furnace and ball mill were estimated from the purchased equipment's cost figures from year 2000 data presented in Peters and Timmerhaus [193] at a value of US\$ 42,967, US\$ 358,063 and US\$ 28,645 respectively. Whereas, the cost for seeds cleaner was quoted by SYNMEC [207] at a value of US\$ 5,500 while the cost of the skid-steer loader is estimated at USD 40,000[83]. Accordingly, the total fixed capital investments for complete plant was estimated from purchased equipment cost and presented in Table 7.2.

Table 7.2: *Estimated fixed capital investment of the complete SC-CO₂ extraction plant*

Item	Cost components	Cost in \$US
Direct cost	Purchased Equipment (PEC)	4,775,413
	• Extraction plant	4,300,237
	• Rotary dryer	42,967
	• Ball miller	28,645
	• Seeds cleaner	5,500
	• Furnace	358,063
	• Skid-steer loader	40,000
	Installation, insulation & painting (25% of PEC)	1,193,853
	Instrumentation & control, installed (8% of PEC)	382,033
	Piping, installed (10% of PEC)	477,541
	Electrical, installed (10% of PEC)	477,541
Indirect cost	Buildings and auxiliary (10% of PEC)	477,541
	Land (5% of PEC)	238,770
	(15% of FCI)	1,415,769
	• Engineering and supervision (5% of FCI)	471,923
	• Legal expenses (1% of FCI)	94,384
	• Construction expenses & contractor's fee (4% of FCI)	377,538
	• Contingency (5% of FCI)	471,923
Total FCI		9,438,464

The manufacturing costs was estimated from the direct production cost and fixed capital investment. The main components of the direct production cost considered are, the cost of grape marc, the electric energy required to run the dryer, the cleaner and the miller, the cost of operating labors, the cost of make-up CO₂, the cost of energy to drive SC-CO₂ through the system and other components shown in Table 7.4 which were determined as a function of other costs. It must be noted that, the energy cost for the dryer considered here is not the amount of energy to dry the grape marc but rather the direct energy to rotate the dryer.

When estimating the production cost, Fiori [83] reported that, the cost of grape marc as US\$ 1/ton (in 2010) arguing the substance is the waste product of distillation process and citing personal communication with some of the CEO of the wineries in the Northern region of Italy. Prado et al [16] considered two scenarios of grape marc cost as 0 and US\$ 2.70/ton. Our recent communication with some of the management of the wineries indicate that the cost of grape marc is around US\$ 10/ton so to be conservative the current work assumes the cost of grape marc at this new value.

The power requirement to run the cleaner was supplied by the manufacturer while that of the rotary dryer and miller were estimated according to their specification [193]. The cost of electric power for Italy was estimated at US\$ 0.14/kw [20], and the operating labor cost for the operators at a value of US\$ 48,000/year-person. It was envisaged that there are two operators per shift and three shifts per-day and an additional of two operators to compensate for holydays and weekends plus two operators working on the dryer for three months.

It was foreseen that after each extraction process approximately 2% of the CO₂ in the extractor will be lost [83,192,200]. The cost of CO₂ was estimated at a value of US\$ 0.24/kg [20]. The cost required to drive the CO₂ through the system were estimated according to the operation presented in Table 7.3 which includes (1) the energy required by pre-cooler to further cool the liquid CO₂ in the storage vessel before the pump, (2) the energy required by the pump at the given CO₂ flow rate, (3) the energy required to pre-heat the sub-cooled CO₂ to supercritical phase before the extractor, (4) the heater required to rise and maintain the CO₂ inside the extractor at the required temperature, (5) the heat required to superheat the CO₂ exit from the extractor to vapor to separate the product and (6) the heat required to condense and sub-cool the CO₂ to storage vessel condition for recycling. A similar approach was previously used by Fiori [83] and del Valle and Núñez [194]. The value of fluid enthalpy at a given pressure and temperature were taken from NIST database [164] and the cost of energy was estimated according to the procedure presented by del Valle et al [194] through Eqn.(4-6).

$$e_c = (H_2 - H_1) + (H_6 - H_5) \quad (7.4)$$

$$e_h = (H_3 - H_2) + (H_4 - H_3) + (H_5 - H_4) \quad (7.5)$$

$$e_p = \frac{(H_3 - H_2)}{\eta_e \eta_i} \quad (7.6)$$

e_c , e_h , e_p , are the energy required for cooling, heating and pumping the CO₂ respectively, H_i ($i = 1 - 6$) is the enthalpy of the CO₂ at position (1-6) as shown in Figure 7.1 and Table 7.3, η_e and η_i are electric efficiency of the pump motor (= 85%) and isentropic efficiency of the pump (= 90%).

Table 7.3: Specific enthalpy at position of the supercritical extraction plant at a given condition

Position	CO ₂ state	T (°C)	P(bar)	H(KJ/kg)
1	Subcooled liquid	15	60	237,13
2	Subcooled liquid	10	60	222,79
3	Supercritical	35	350	259,41
4	Supercritical	40	350	268,80
5	vapor	25	60	416.21
6	Saturated liquid	20	60	254.28

Table 7.4 shows the total working capital investments required to run the plant per year. The fixed charge cost component were estimated by assuming a straight line depression of depreciable asset over ten years, 1% property tax and 4% insurance charges over fixed capital investment [193] and an average loan interest rate of the European Union area of 5% [211] on total capital investment. The plant overhead cost was estimated as a function of total operating labor cost, maintenance and repair cost and the direct supervision and clerical labor cost whereas the general expenses was estimated at a value of 15% of total product cost [193].

The cost of production was estimated at the value of US\$ 10/kg-oil which is comparable to the amount previously estimated by Fiori [83] in 2010 at a value of € 5.9/kg-oil (a price which was equal to US\$ 8.26/kg-oil at that time). Taking into account the inclusion of several cost components and considering that the price of grape marc was assumed at a value of US\$ 10/ton against US\$ 1/ton in Fiori [83], a slight increase in the cost of production per mass of oil is understandable. Prado et al [16] estimated the cost of grape seeds oil at a price of US\$ 12/kg-oil where a commercial simulator SuperPro Designer v6.0 was used to estimate the manufacturing cost.

The cost of manufacturing (COM) was also estimated according to the Turton et al. [203] using Eqn. (7.1) for purpose of comparison. It must be highlighted that, from the definitions, the COM predicted by Turton et al. [203] corresponds to the working capital investment (WCI) according to Peters and Timmerhaus [193] as discussed in Section

7.3.2. The difference between the two methods stands at 9% with Turton et al. [203] empirical approach estimating the higher value.

Table 7.4: Estimated total working capital investment per year

Item	Cost components	Cost in \$US/yr.
Manufacturing Cost	Direct Production cost	1,022,522
	• Raw material	150,000
	• Operating labor (OL)	456,000
	• Utilities	157,403
	• Make-up CO ₂	14,433
	• Maintenance and repair (MRC) (2% FCI)	188,769
	• Operating supplies (10% MRC)	18,876
	• Laboratory charges (10% of OL)	45,600
	• Direct Supervision & Clerical labor (DSC) (10% of OL)	45,600
	Fixed charges	1,940,862
	• Depreciation	802,269
	• Local taxes (4% of FCI)	377,538
	• Insurance (1% of FCI)	94,384
	• Interest (5% of TCI)	666,670
General Expenses	Plant overhead costs (50% of OL, MRC & DSC)	345,184
	(15% of TPC)	583,865
	• Administrative cost (5% of TPC)	194,621
	• Distribution and marketing (5% of TPC)	194,621
	• Research and development (5% of TPC)	194,621
Total Product Cost (TPC)		3,892,435

Figure 7.2 show the cumulative cash position over the proposed project life considering a retailing selling price of grape seeds oil of US\$ 14/kg which corresponds to the minimum amount available on the market i.e. US\$ 14-42/kg-oil [83] in Italy and US\$ 40/kg-oil in Brazil [16]. It was envisaged that the construction and commissioning of the plant takes two year and the plant will start working at full scale operation at first year of operation. Under the proposed condition, SC-CO₂ extraction of grape seeds oil is economically viable with the rate of return on investment estimated at 8.25% and payback period of 5 year.

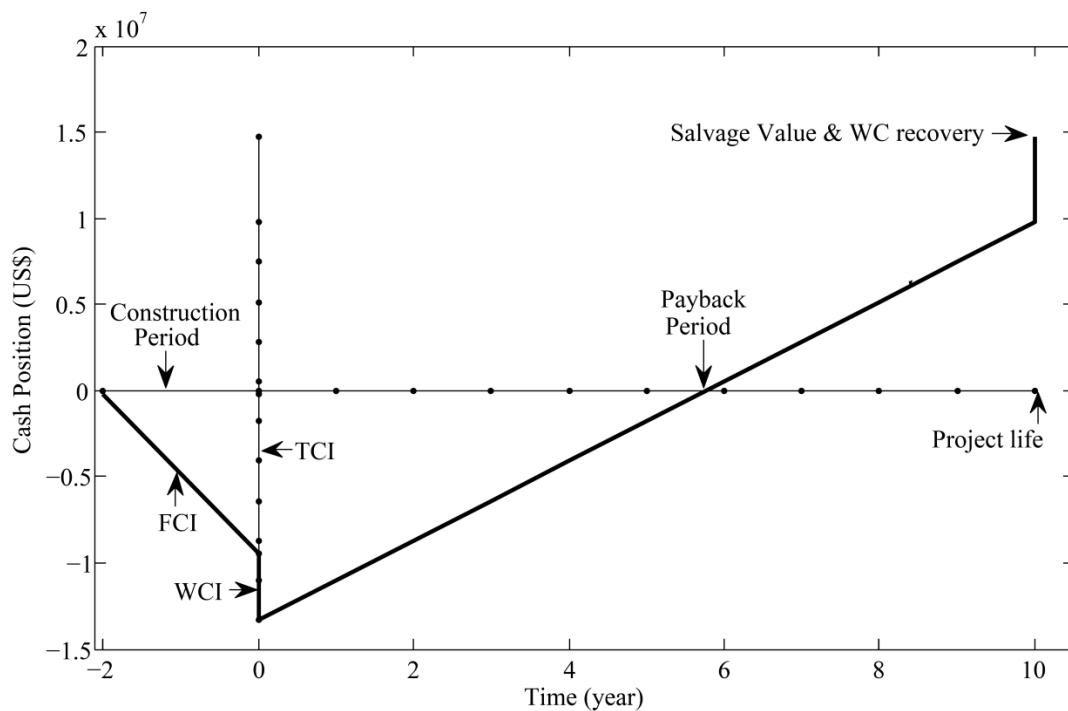


Figure 7.2: Cumulative cash position at minimum retail price

7.5 Conclusions

This preliminary study on the establishment of supercritical CO₂ (SC-CO₂) plant for the extraction of grape seeds oil indicates that, the process is technically and economically feasible. The estimated total capital investment required to establishment such plant with capacity of 3000 ton/year is US\$ 13,330,899 out of which US\$ 9,438,464 is the fixed capital investment and the amount required to run the plant is US\$ 3,892,435 per year.

At current minimum retail selling price rate of grape seeds oil in the market, the proposed project can completely recover the fixed capital investment in five years. Besides, the project enables the development of valorization strategies for wine-making wastes and reduces their environmental impact and provides wine-makers with the possibility of selling by-products at reasonable price.

The project has a socio-economic benefit by creating a job opportunity and generating revenue for the local government in the form of tax. The establishment of such plant will also help toward an effort to meet the demand and supply of vegetable oil by producing high quality product from locally available material. Therefore, the authors

strongly believe that, it is in the region and stakeholders interest to invest further for a detailed analysis and technical and economic evaluation for the establishment of SC-CO₂ extraction plant for the extraction of grape seeds oil.

8. Final Remark

In this work, supercritical CO₂ (SC-CO₂) extraction of grape seed oils and subcritical water (SW) extractions of polyphenols from grape skins and defatted grape seeds were conducted in semi-continuous extractor. The oil yields depend on grape cultivar and, for some cultivars, on harvesting years. The oils extracted by SC-CO₂ have similar quality as those obtained by mechanical extraction and the yield is comparable to that of conventional *n*-hexane extraction. In addition, both the skins and defatted grape seeds are rich source of polyphenols and SW is a potential green solvent for the extraction of these valuable compounds.

The effect of process variables on the kinetics of SC-CO₂ extraction of oil from seeds and SW extraction of polyphenols from grape skins and defatted grape seeds were studied both experimentally and through modeling. For SC-CO₂ extraction, the extraction rate increased with an increase in pressure, temperature and solvent flow rate (but in this case the specific CO₂ consumption also increased). At a fixed ratio of mass of seeds to solvent flow rate, decreasing the extractor diameter to length ratio allowed to reduce the specific CO₂ consumption. The optimum extractor bed porosity was found to be between 0.23-0.41. The particle size of milled solid matrix had no effect on the initial extraction rate, but reflected on the final asymptotic extraction yield; the smaller were the particles, the higher the final yield in a given extraction time. With regard to polyphenols, the yield increase with increase in extraction temperature. Increasing the solvent flow rate resulted beneficial only in the initial extraction phase, while in the following the extraction rate decreased substantially.

The kinetics of SC-CO₂ extraction of seed oil can be effectively modeled by broken and intact cells (BIC), the shrinking core (SC), and the bridge (combined BIC-SC) models. The BIC model allowed achieving the minimum deviation between model predictions and experimental data followed by SC and BIC-SC model. These results reflect the number of model adjustable parameters of the different models: 3, 2 and 1 for BIC, SC and BIC-SC respectively. The kinetics of extraction of polyphenols can be effectively modeled by a simple model; the two-site kinetic model, which allowed achieving a remarkable agreement between model predictions and experimental data. The model can be thus utilized for predicting the extraction of polyphenols from grape residues and similar substrates and as a preliminary tool for designing subcritical water extraction processes.

In general, the work shows the establishment of SC-CO₂ plant for the extraction of grape seeds oil is technically viable and economically feasible. The project enables the

development of valorization strategies for wine-making wastes and reduces their environmental impact and provides wine-makers with the possibility of selling by-products at reasonable price. The project has substantial socio-economic benefits and establishment of such plant will also help toward an effort to meet the demand of vegetable oil by producing high quality product from locally available material.

9. References

- [1] ChemicalLogic Corporation, Phase Diagram Data and Equations, (<http://www.chemicallogic.com/> (accessed 31.12.14)).
- [2] Ž. Knez, E. Markočič, M. Leitgeb, M. Primožič, M. Knez Hrnčič, M. Škerget, Industrial applications of supercritical fluids: A review, *Energy*. (2014) 1–9. doi:10.1016/j.energy.2014.07.044.
- [3] E. Reverchon, C. Marrone, Supercritical extraction of clove bud essential oil: isolation and mathematical modeling, *Chem. Eng. Sci.* 52 (1997) 3421–3428.
- [4] H. Sovová, Rate of the vegetable oil extraction with supercritical CO₂-I. Modeling of Extraction curves, *Chem. Eng. Sci.* 49 (1994) 409–414.
- [5] I. Goodarznia, M.H. Eikani, Supercritical carbon dioxide extraction of essential oils: Modeling and simulation, *Chem. Eng. Sci.* 53 (1998) 1387–1395.
- [6] M. Perrut, Supercritical fluid applications: industrial developments and economic issues, *Ind. Eng. Chem. Res.* 39 (2000) 4531–4535. doi:10.1021/ie000211c.
- [7] E. Reverchon, I. De Marco, Supercritical fluid extraction and fractionation of natural matter, *J. Supercrit. Fluids.* 38 (2006) 146–166. doi:10.1016/j.supflu.2006.03.020.
- [8] E. Schütz, Supercritical Fluids and Applications – A Patent Review, *Chem. Eng. Technol.* 30 (2007) 685–688. doi:10.1002/ceat.200600297.
- [9] J.M. del Valle, J.C. de la Fuente, Supercritical CO₂ extraction of oilseeds: review of kinetic and equilibrium models, *Crit. Rev. Food Sci. Nutr.* 46 (2006) 131–160. doi:10.1080/10408390500526514.
- [10] F. Sahena, I.S.M. Zaidul, S. Jinap, A. A. Karim, K. A. Abbas, N. A. N. Norulaini, et al., Application of supercritical CO₂ in lipid extraction – A review, *J. Food Eng.* 95 (2009) 240–253. doi:10.1016/j.jfoodeng.2009.06.026.
- [11] M.M.R. de Melo, A. J.D. Silvestre, C.M. Silva, Supercritical fluid extraction of vegetable matrices: Applications, trends and future perspectives of a convincing

- green technology, *J. Supercrit. Fluids*. 92 (2014) 115–176.
doi:10.1016/j.supflu.2014.04.007.
- [12] J.W. King, Modern supercritical fluid technology for food applications., *Annu. Rev. Food Sci. Technol.* 5 (2014) 215–38. doi:10.1146/annurev-food-030713-092447.
- [13] L. Fiori, Grape seed oil supercritical extraction kinetic and solubility data: Critical approach and modeling, *J. Supercrit. Fluids*. 43 (2007) 43–54.
doi:10.1016/j.supflu.2007.04.009.
- [14] H. Sovová, J. Kučera, J. Jež, Rate of the vegetable oil extraction with supercritical CO₂-II. Extraction of grape oil, *Chem. Eng. Sci.* 49 (1994) 415–420.
- [15] M. Bravi, F. Spinoglio, N. Verdone, M. Adami, A. Aliboni, A. D'Andrea, et al., Improving the extraction of α -tocopherol-enriched oil from grape seeds by supercritical CO₂. Optimisation of the extraction conditions, *J. Food Eng.* 78 (2007) 488–493. doi:10.1016/j.jfoodeng.2005.10.017.
- [16] J.M. Prado, I. Dalmolin, N.D.D. Carareto, R.C. Basso, A.J.A Meirelles, J. Vladimir Oliveira, et al., Supercritical fluid extraction of grape seed: Process scale-up, extract chemical composition and economic evaluation, *J. Food Eng.* 109 (2012) 249–257. doi:10.1016/j.jfoodeng.2011.10.007.
- [17] F. Temelli, Perspectives on supercritical fluid processing of fats and oils, *J. Supercrit. Fluids*. 47 (2009) 583–590. doi:10.1016/j.supflu.2008.10.014.
- [18] I.S.M. Zaidul, N. A N. Norulaini, A. K. Mohd Omar, R.L. Smith, Supercritical carbon dioxide (SC-CO₂) extraction and fractionation of palm kernel oil from palm kernel as cocoa butter replacers blend, *J. Food Eng.* 73 (2006) 210–216.
doi:10.1016/j.jfoodeng.2005.01.022.
- [19] E. Reverchon, G. Delta Porta, Rose concrete fractionation by supercritical CO₂, *J. Supercrit. Fluids*. 9 (1996) 199–204. doi:10.1016/S0896-8446(96)90033-9.
- [20] L. Fiori, M. Manfrini, D. Castello, Supercritical CO₂ fractionation of omega-3 lipids from fish by-products: Plant and process design, modeling, economic feasibility, *Food Bioprod. Process.* 92 (2014) 120–132.
doi:10.1016/j.fbp.2014.01.001.

- [21] G. Brunner, N.T. MacHado, Process design methodology for fractionation of fatty acids from palm fatty acid distillates in countercurrent packed columns with supercritical CO₂, *J. Supercrit. Fluids*. 66 (2012) 96–110. doi:10.1016/j.supflu.2012.02.012.
- [22] J. Jung, M. Perrut, Particle design using supercritical fluids: Literature and patent survey, *J. Supercrit. Fluids*. 20 (2001) 179–219. doi:10.1016/S0896-8446(01)00064-X.
- [23] M.T.M.S. Gomes, D.T. Santos, M.A. A Meireles, Trends in Particle Formation of Bioactive Compounds Using Supercritical Fluids and Nanoemulsions, *Food Public Heal*. 2 (2012) 142–152. doi:10.5923/j.fph.20120205.05.
- [24] Z. Knez, E. Weidner, Particles formation and particle design using supercritical fluids, *Curr. Opin. Solid State Mater. Sci*. 7 (2003) 353–361. doi:10.1016/j.cossms.2003.11.002.
- [25] M. Henczka, J. Bałdyga, B.Y. Shekunov, Particle formation by turbulent mixing with supercritical antisolvent, *Chem. Eng. Sci*. 60 (2005) 2193–2201. doi:10.1016/j.ces.2004.11.015.
- [26] S.-D. Yeo, E. Kiran, Formation of polymer particles with supercritical fluids: A review, *J. Supercrit. Fluids*. 34 (2005) 287–308. doi:10.1016/j.supflu.2004.10.006.
- [27] T.K. Fahim, I.S.M. Zaidul, M.R. Abu Bakar, U.M. Salim, M.B. Awang, F. Sahena, et al., Particle formation and micronization using non-conventional techniques-review, *Chem. Eng. Process. Process Intensif*. 86 (2014) 47–52. doi:10.1016/j.cep.2014.10.009.
- [28] A. Tabernero, E.M. Martín del Valle, M. A. Galán, Supercritical fluids for pharmaceutical particle engineering: Methods, basic fundamentals and modelling, *Chem. Eng. Process. Process Intensif*. 60 (2012) 9–25. doi:10.1016/j.cep.2012.06.004.
- [29] M. Perrut, Sterilization and virus inactivation by supercritical fluids (a review), *J. Supercrit. Fluids*. 66 (2012) 359–371. doi:10.1016/j.supflu.2011.07.007.

- [30] S. Spilimbergo, D. Komes, A. Vojvodic, B. Levaj, G. Ferrentino, High pressure carbon dioxide pasteurization of fresh-cut carrot, *J. Supercrit. Fluids*. 79 (2013) 92–100. doi:10.1016/j.supflu.2012.12.002.
- [31] T. Parton, A. Bertucco, N. Elvassore, L. Grimolizzi, A continuous plant for food preservation by high pressure CO₂, *J. Food Eng.* 79 (2007) 1410–1417. doi:10.1016/j.jfoodeng.2006.04.023.
- [32] S. Spilimbergo, A. Bertucco, F.M. Lauro, G. Bertoloni, Inactivation of *Bacillus subtilis* spores by supercritical CO₂ treatment, *Innov. Food Sci. Emerg. Technol.* 4 (2003) 161–165. doi:10.1016/S1466-8564(02)00089-9.
- [33] L. Garcia-Gonzalez, A. H. Geeraerd, S. Spilimbergo, K. Elst, L. Van Ginneken, J. Debevere, et al., High pressure carbon dioxide inactivation of microorganisms in foods: The past, the present and the future, *Int. J. Food Microbiol.* 117 (2007) 1–28. doi:10.1016/j.ijfoodmicro.2007.02.018.
- [34] F. Galvanin, R. De Luca, G. Ferrentino, M. Barolo, S. Spilimbergo, F. Bezzo, Bacterial inactivation on solid food matrices through supercritical CO₂: A correlative study, *J. Food Eng.* 120 (2014) 146–157. doi:10.1016/j.jfoodeng.2013.07.027.
- [35] L. Calvo, E. Torres, Microbial inactivation of paprika using high-pressure CO₂, *J. Supercrit. Fluids*. 52 (2010) 134–141. doi:10.1016/j.supflu.2009.11.002.
- [36] L. Garcia-Gonzalez, A. H. Geeraerd, K. Elst, L. Van Ginneken, J.F. Van Impe, F. Devlieghere, Inactivation of naturally occurring microorganisms in liquid whole egg using high pressure carbon dioxide processing as an alternative to heat pasteurization, *J. Supercrit. Fluids*. 51 (2009) 74–82. doi:10.1016/j.supflu.2009.06.020.
- [37] G. Bertoloni, A. Bertucco, M. Rassa, K. Vezzù, Medical device disinfection by dense carbon dioxide, *J. Hosp. Infect.* 77 (2011) 42–46. doi:10.1016/j.jhin.2010.09.020.
- [38] M. Herrero, M. Castro-Puyana, L. Rocamora-Reverte, J. A. Ferragut, A. Cifuentes, E. Ibáñez, Formation and relevance of 5-hydroxymethylfurfural in bioactive subcritical water extracts from olive leaves, *Food Res. Int.* 47 (2012) 31–37. doi:10.1016/j.foodres.2012.01.008.

- [39] C.-I. Cheigh, E.-Y. Chung, M.-S. Chung, Enhanced extraction of flavanones hesperidin and narirutin from Citrus unshiu peel using subcritical water, *J. Food Eng.* 110 (2012) 472–477. doi:10.1016/j.jfoodeng.2011.12.019.
- [40] M. Herrero, M. Castro-Puyana, J. A. Mendiola, E. Ibañez, Compressed fluids for the extraction of bioactive compounds, *TrAC - Trends Anal. Chem.* 43 (2013) 67–83. doi:10.1016/j.trac.2012.12.008.
- [41] A.G. Carr, R. Mammucari, N.R. Foster, A review of subcritical water as a solvent and its utilisation for the processing of hydrophobic organic compounds, *Chem. Eng. J.* 172 (2011) 1–17. doi:10.1016/j.cej.2011.06.007.
- [42] P. Wataniyakul, P. Pavasant, M. Goto, A. Shotipruk, Microwave pretreatment of defatted rice bran for enhanced recovery of total phenolic compounds extracted by subcritical water., *Bioresour. Technol.* 124 (2012) 18–22. doi:10.1016/j.biortech.2012.08.053.
- [43] P.P. Singh, M.D. A. Saldaña, Subcritical water extraction of phenolic compounds from potato peel, *Food Res. Int.* 44 (2011) 2452–2458. doi:10.1016/j.foodres.2011.02.006.
- [44] M. Uematsu, E.U. Franck, Static Dielectric Constant of Water and Steam, *J. Phys. Chem. Ref. Data.* 9 (1980) 1291–1306.
- [45] A.A. Maryett, E. R.E. Smith, *Table of Dielectric Constants of Pure Liquids*, Washington, D.C., 1951.
- [46] A. Cvetanović, J. Švarc-Gajić, P. Mašković, S. Savić, L. Nikolić, Antioxidant and biological activity of chamomile extracts obtained by different techniques: perspective of using superheated water for isolation of biologically active compounds, *Ind. Crops Prod.* xxxx (2014) xxxx–xxxx. doi:10.1016/j.indcrop.2014.09.044.
- [47] M.-J. Ko, C.-I. Cheigh, S.-W. Cho, M.-S. Chung, Subcritical water extraction of flavonol quercetin from onion skin, *J. Food Eng.* 102 (2011) 327–333. doi:10.1016/j.jfoodeng.2010.09.008.
- [48] A. Paula, D. Fonseca, J.L. Pasquel-reátegui, G. Fernández, J. Martínez, Pressurized liquid extraction of bioactive compounds from blackberry (*Rubus*

- fruticosus L.*) residues : A comparison with conventional methods, *Frin.* (2014). doi:10.1016/j.foodres.2014.12.042.
- [49] M. Tanaka, A. Takamizu, M. Hoshino, M. Sasaki, M. Goto, Extraction of dietary fiber from Citrus junos peel with subcritical water, *Food Bioprod. Process.* 90 (2012) 180–186. doi:10.1016/j.fbp.2011.03.005.
- [50] M. Latoui, B. Aliakbarian, A. A. Casazza, M. Seffen, A. Converti, P. Perego, Extraction of phenolic compounds from *Vitex agnus-castus L.*, *Food Bioprod. Process.* 90 (2012) 748–754. doi:10.1016/j.fbp.2012.01.003.
- [51] H. Bagherian, F. Zokae Ashtiani, A. Fouladitajar, M. Mohtashamy, Comparisons between conventional, microwave- and ultrasound-assisted methods for extraction of pectin from grapefruit, *Chem. Eng. Process. Process Intensif.* 50 (2011) 1237–1243. doi:10.1016/j.cep.2011.08.002.
- [52] M.F. Barrera Vázquez, L.R. Comini, R.E. Martini, S.C. Núñez Montoya, S. Bottini, J.L. Cabrera, Comparisons between conventional, ultrasound-assisted and microwave-assisted methods for extraction of anthraquinones from *Heterophyllaea pustulata* Hook f. (*Rubiaceae*)., *Ultrason. Sonochem.* 21 (2014) 478–84. doi:10.1016/j.ultsonch.2013.08.023.
- [53] A. A. Casazza, B. Aliakbarian, S. Mantegna, G. Cravotto, P. Perego, Extraction of phenolics from *Vitis vinifera* wastes using non-conventional techniques, *J. Food Eng.* 100 (2010) 50–55. doi:10.1016/j.jfoodeng.2010.03.026.
- [54] L. Ramos, E.M. Kristenson, U. A. T. Brinkman, Current use of pressurised liquid extraction and subcritical water extraction in environmental analysis., *J. Chromatogr. A.* 975 (2002) 3–29.
- [55] E.S. Ong, J.S.H. Cheong, D. Goh, Pressurized hot water extraction of bioactive or marker compounds in botanicals and medicinal plant materials., *J. Chromatogr. A.* 1112 (2006) 92–102. doi:10.1016/j.chroma.2005.12.052.
- [56] M. Herrero, A Cifuentes, E. Ibanez, Sub- and supercritical fluid extraction of functional ingredients from different natural sources: Plants, food-by-products, algae and microalgaeA review, *Food Chem.* 98 (2006) 136–148. doi:10.1016/j.foodchem.2005.05.058.

- [57] X. Wang, Q. Chen, X. Lü, Pectin extracted from apple pomace and citrus peel by subcritical water, *Food Hydrocoll.* 38 (2014) 129–137.
doi:10.1016/j.foodhyd.2013.12.003.
- [58] B. Aliakbarian, A. Fathi, P. Perego, F. Dehghani, Extraction of antioxidants from winery wastes using subcritical water, *J. Supercrit. Fluids.* 65 (2012) 18–24.
doi:10.1016/j.supflu.2012.02.022.
- [59] K. S. Duba, A. A. Casazza, H. B. Mohammed, P. Perego, L. Fiori, Food and Bioproducts Processing Extraction of polyphenols from grape skins and defatted grape seeds using subcritical water : Experiments and modeling, *Food Bioprod. Process.* 94 (2015) 29–38. doi:10.1016/j.fbp.2015.01.001.
- [60] J.K. Monrad, M. Suárez, M.J. Motilva, J.W. King, K. Srinivas, L.R. Howard, Extraction of anthocyanins and flavan-3-ols from red grape pomace continuously by coupling hot water extraction with a modified expeller, *Food Res. Int.* 65 (2014) 77–87. doi:10.1016/j.foodres.2014.04.020.
- [61] J.R. Vergara-salinas, M. Vergara, C. Altamirano, Á. Gonzalez, J.R. Pérez-correa, Characterization of pressurized hot water extracts of grape pomace : Chemical and biological antioxidant activity, *Food Chem.* 171 (2015) 62–69.
doi:10.1016/j.foodchem.2014.08.094.
- [62] V.H. Alvarez, J. Cahyadi, D. Xu, M.D. A. Saldaña, Optimization of phytochemicals production from potato peel using subcritical water: Experimental and dynamic modeling, *J. Supercrit. Fluids.* 90 (2014) 8–17.
doi:10.1016/j.supflu.2014.02.013.
- [63] H.M. Chen, X. Fu, Z.G. Luo, Properties and extraction of pectin-enriched materials from sugar beet pulp by ultrasonic-assisted treatment combined with subcritical water, *Food Chem.* 168 (2015) 302–310.
doi:10.1016/j.foodchem.2014.07.078.
- [64] M.T. Fernández-Ponce, L. Casas, C. Mantell, M. Rodríguez, E. Martínez de la Ossa, Extraction of antioxidant compounds from different varieties of *Mangifera indica* leaves using green technologies, *J. Supercrit. Fluids.* 72 (2012) 168–175.
doi:10.1016/j.supflu.2012.07.016.

References

- [65] M. Herrero, T.N. Temirzoda, A. Segura-Carretero, R. Quirantes, M. Plaza, E. Ibañez, New possibilities for the valorization of olive oil by-products, *J. Chromatogr. A.* 1218 (2011) 7511–7520. doi:10.1016/j.chroma.2011.04.053.
- [66] Y. Narita, K. Inouye, High antioxidant activity of coffee silverskin extracts obtained by the treatment of coffee silverskin with subcritical water., *Food Chem.* 135 (2012) 943–9. doi:10.1016/j.foodchem.2012.05.078.
- [67] X. Wang, X. Lü, Characterization of pectic polysaccharides extracted from apple pomace by hot-compressed water, *Carbohydr. Polym.* 102 (2014) 174–184. doi:10.1016/j.carbpol.2013.11.012.
- [68] N. Simsek Kus, Organic reactions in subcritical and supercritical water, *Tetrahedron.* 68 (2012) 949–958. doi:10.1016/j.tet.2011.10.070.
- [69] Y. Yang, F. Hildebrand, Phenanthrene degradation in subcritical water, *Anal. Chim. Acta.* 555 (2006) 364–369. doi:10.1016/j.aca.2005.08.078.
- [70] M.N. Islam, M.-S. Shin, Y.-T. Jo, J.-H. Park, TNT and RDX degradation and extraction from contaminated soil using subcritical water, *Chemosphere.* 119 (2015) 1148–1152. doi:10.1016/j.chemosphere.2014.09.101.
- [71] B. Kayan, B. Gözmen, Degradation of Acid Red 274 using H₂O₂ in subcritical water: application of response surface methodology., *J. Hazard. Mater.* 201-202 (2012) 100–6. doi:10.1016/j.jhazmat.2011.11.045.
- [72] J.M. Prado, L. A. Follegatti-Romero, T. Forster-Carneiro, M. A. Rostagno, F. Maugeri Filho, M.A. A. Meireles, Hydrolysis of sugarcane bagasse in subcritical water, *J. Supercrit. Fluids.* 86 (2014) 15–22. doi:10.1016/j.supflu.2013.11.018.
- [73] W. Abdelmoez, S.M. Nage, A. Bastawess, A. Ihab, H. Yoshida, Subcritical water technology for wheat straw hydrolysis to produce value added products, *J. Clean. Prod.* 70 (2014) 68–77. doi:10.1016/j.jclepro.2014.02.011.
- [74] R.L. Holliday, B.Y.M. Jong, J.W. Kolis, Organic synthesis in subcritical water Oxidation of alkyl aromatics, *J. Supercrit. Fluids.* 12 (1998) 255–260.
- [75] S.D. Allmon, J.G. Dorsey, Retention mechanisms in subcritical water reversed-phase chromatography, *J. Chromatogr. A.* 1216 (2009) 5106–5111. doi:10.1016/j.chroma.2009.04.068.

- [76] S.D. Allmon, J.G. Dorsey, Properties of subcritical water as an eluent for reversed-phase liquid chromatography-Disruption of the hydrogen-bond network at elevated temperature and its consequences, *J. Chromatogr. A.* 1217 (2010) 5769–5775. doi:10.1016/j.chroma.2010.07.030.
- [77] F. Yu, S. Rui-Juan, Y. Na, L. Yuan-De, H. Tian-Bao, Separations of Some Alcohols, Phenols, and Carboxylic Acids by Coupling of Subcritical Water Chromatography and Flame Ionization Detection with Postcolumn Splitting, *Chinese J. Anal. Chem.* 35 (2007) 1335–1338. doi:10.1016/S1872-2040(07)60083-8.
- [78] Y. Yang, Subcritical water chromatography: A green approach to high-temperature liquid chromatography, *J. Sep. Sci.* 30 (2007) 1131–1140. doi:10.1002/jssc.200700008.
- [79] P. He, Y. Yang, Studies on the long-term thermal stability of stationary phases in subcritical water chromatography, *J. Chromatogr. A.* 989 (2003) 55–63. doi:10.1016/S0021-9673(02)01656-4.
- [80] M.O. Fogwill, K.B. Thurber, Rapid column heating method for subcritical water chromatography, *J. Chromatogr. A.* 1139 (2007) 199–205. doi:10.1016/j.chroma.2006.11.016.
- [81] F. Saura-Calixto, Dietary fiber as a carrier of dietary antioxidants: an essential physiological function, *J. Agric. Food Chem.* 59 (2011) 43–49. doi:10.1021/jf1036596.
- [82] P.S.C. Sri Harsha, C. Gardana, P. Simonetti, G. Spigno, V. Lavelli, Characterization of phenolics, in vitro reducing capacity and anti-glycation activity of red grape skins recovered from winemaking by-products, *Bioresour. Technol.* 140 (2013) 263–268. doi:10.1016/j.biortech.2013.04.092.
- [83] L. Fiori, Supercritical extraction of grape seed oil at industrial-scale: Plant and process design, modeling, economic feasibility, *Chem. Eng. Process.* 49 (2010) 866–872. doi:10.1016/j.cep.2010.06.001.
- [84] C. Crews, P. Hough, P. Brereton, J. Godward, M. Lees, S. Guiet, et al., Quantitation of the main constituents of some authentic sesame seed oils of

- different origin, *J. Agric. Food Chem.* 54 (2006) 6261–6265.
doi:10.1021/jf0603578.
- [85] C.G. Pereira, M.A.A. Meireles, Supercritical fluid extraction of bioactive compounds: fundamentals, applications and economic perspectives, *Food Bioprocess Technol.* 3 (2010) 340–372. doi:10.1007/s11947-009-0263-2.
- [86] L.D. Kagliwal, A.S. Pol, S.C. Patil, R.S. Singhal, V.B. Patravale, Antioxidant-rich extract from dehydrated seabuckthorn berries by supercritical carbon dioxide extraction, *Food Bioprocess Technol.* 5 (2011) 2768–2776. doi:10.1007/s11947-011-0613-8.
- [87] P.P. Constantinides, J. Han, S.S. Davis, Advances in the use of tocopherols as drug delivery vehicles, *Pharm. Res.* 23 (2006) 243–255. doi:10.1007/s11095-005-9262-9.
- [88] Y. Choi, J. Lee, Antioxidant and antiproliferative properties of a tocotrienol-rich fraction from grape seeds, *Food Chem.* 114 (2009) 1386–1390.
doi:10.1016/j.foodchem.2008.11.018.
- [89] G. Panfili, A. Fratianni, M. Irano, Normal phase high-performance liquid chromatography method for the determination of tocopherols and tocotrienols in cereals, *J. Agric. Food Chem.* 51 (2003) 3940–3944. doi:10.1021/jf030009v.
- [90] L. Fernandes, S. Casal, R. Cruz, J.A. Pereira, E. Ramalhosa, Seed oils of ten traditional Portuguese grape varieties with interesting chemical and antioxidant properties, *Food Res. Int.* 50 (2013) 161–166. doi:10.1016/j.foodres.2012.09.039.
- [91] C.P. Passos, R.M. Silva, F.A. Da Silva, M.A. Coimbra, C.M. Silva, Enhancement of the supercritical fluid extraction of grape seed oil by using enzymatically pre-treated seed, *J. Supercrit. Fluids.* 48 (2009) 225–229.
doi:10.1016/j.supflu.2008.11.001.
- [92] C. Da Porto, E. Porretto, D. Decorti, Comparison of ultrasound-assisted extraction with conventional extraction methods of oil and polyphenols from grape (*Vitis vinifera* L.) seeds, *Ultrason. Sonochem.* 20 (2013) 1076–1080.
doi:10.1016/j.ultsonch.2012.12.002.

- [93] F. Agostini, R. A. Bertussi, G. Agostini, A. C. Atti Dos Santos, M. Rossato, R. Vanderlinde, Supercritical extraction from vinification residues: fatty acids, α -tocopherol, and phenolic compounds in the oil seeds from different varieties of grape, *ScientificWorldJournal*. 2012 (2012) 1–9. doi:10.1100/2012/790486.
- [94] T.H.J. Beveridge, B. Girard, T. Kopp, J.C.G. Drover, Yield and composition of grape seed oils extracted by supercritical carbon dioxide and petroleum ether: varietal effects, *J. Agric. Food Chem.* 53 (2005) 1799–1804. doi:10.1021/jf040295q.
- [95] O. Döker, U. Salgın, İ. Şanal, Ü. Mehmetoğlu, A. Çalimli, Modeling of extraction of β -carotene from apricot bagasse using supercritical CO₂ in packed bed extractor, *J. Supercrit. Fluids.* 28 (2004) 11–19. doi:10.1016/S0896-8446(03)00006-8.
- [96] S. Machmudah, A. Sulaswaty, M. Sasaki, M. Goto, T. Hirose, Supercritical CO₂ extraction of nutmeg oil: Experiments and modeling, *J. Supercrit. Fluids.* 39 (2006) 30–39. doi:10.1016/j.supflu.2006.01.007.
- [97] H. Sovová, Steps of supercritical fluid extraction of natural products and their characteristic times, *J. Supercrit. Fluids.* 66 (2012) 73–79. doi:10.1016/j.supflu.2011.11.004.
- [98] J. Crank, *The Mathematics of Diffusion*, 2nd ed., Clarendon Press, Oxford, 1975.
- [99] S.N. Naik, H. Lentz, R.C. Maheshwari, Extraction of perfumes and flavours from plant materials with liquid carbon dioxide under liquid-vapor equilibrium conditions, *Fluid Phase Equilib.* 49 (1989) 115–126.
- [100] C.S. Tan, D.C. Liou, Modeling of desorption at super critical conditions, *AIChE J.* 35 (1989) 1029–1031.
- [101] A.R. Monteiro, P.T. V Rosa, P. Cx, Multicomponent Model To Describe Extraction of Ginger Oleoresin with Supercritical Carbon Dioxide, *Ind. Eng. Chem. Res.* 42 (2003) 1057–1063.
- [102] T. Veress, Sample preparation by supercritical fluid extraction for quantification A model based on the diffusion-layer theory for determination of extraction time, *J. Chromatogr. A.* 668 (1994) 285–291.

- [103] M. Goto, B.C. Roy, T. Hirose, Shrinking-core leaching model for supercritical-fluid extraction, *J. Supercrit. Fluids*. 9 (1996) 128–133. doi:10.1016/S0896-8446(96)90009-1.
- [104] L. Fiori, D. Basso, P. Costa, Supercritical extraction kinetics of seed oil: A new model bridging the “broken and intact cells” and the “shrinking-core” models, *J. Supercrit. Fluids*. 48 (2009) 131–138. doi:10.1016/j.supflu.2008.09.019.
- [105] M.G. Bernardo-gil, M.B. King, M.M. Esqui, Mathematical models for supercritical extraction of olive husk oil, *J. Supercrit. Fluids*. 16 (1999) 43–58.
- [106] L.M. A. S. Campos, E.M.Z. Michielin, L. Danielski, S.R.S. Ferreira, Experimental data and modeling the supercritical fluid extraction of marigold (*Calendula officinalis*) oleoresin, *J. Supercrit. Fluids*. 34 (2005) 163–170. doi:10.1016/j.supflu.2004.11.010.
- [107] R.M. A. Domingues, M.M.R. de Melo, C.P. Neto, A.J.D. Silvestre, C.M. Silva, Measurement and modeling of supercritical fluid extraction curves of *Eucalyptus globulus* bark: Influence of the operating conditions upon yields and extract composition, *J. Supercrit. Fluids*. 72 (2012) 176–185. doi:10.1016/j.supflu.2012.08.010.
- [108] M. Goto, T. Hirose, Extraction of peppermint oil by supercritical carbon dioxide, *J. Chem. Eng. Jpn.* 26 (1993) 401–407.
- [109] K.S. Duba, L. Fiori, Comparison of different kinetics models for supercritical CO₂ extraction of seed oil, in: Reverchon (Eds.) *Proceedings of the 10th Conference on Supercritical Fluids and Their Applications*, Naples, Italy, (2013) 45–50.
- [110] J. Šťastová, J. Jež, M. Bártlová, H. Sovová, Rate of the vegetable oil extraction with supercritical CO₂-III. Extraction from sea buckthorn, *Chem. Eng. Sci.* 51 (1996) 4347–4352.
- [111] H. Sovová, Mathematical model for supercritical fluid extraction of natural products and extraction curve evaluation, *J. Supercrit. Fluids*. 33 (2005) 35–52. doi:10.1016/j.supflu.2004.03.005.
- [112] E. Reverchon, C. Marrone, Modeling and simulation of the supercritical CO₂ extraction of vegetable oils, *J. Supercrit. Fluids*. 19 (2001) 161–175.

- [113] L. Fiori, P. Costa, Supercritical Extraction of seed oil: Analysis and comparison of up-to-date models, in: M. Belinsky R (Ed.), *Supercrit. Fluids*, Nova Science Publishers, Inc., New York, 2011: pp. 705–722.
- [114] L. Fiori, V. Lavelli, K.S. Duba, P.S.C. Sri Harsha, H. Ben Mohamed, G. Guella, Supercritical CO₂ extraction of oil from seeds of six grape cultivars: Modeling of mass transfer kinetics and evaluation of lipid profiles and tocol contents, *J. Supercrit. Fluids*. 94 (2014) 71–80. doi:10.1016/j.supflu.2014.06.021.
- [115] F. Meyer, M. Stamenic, I. Zizovic, R. Eggers, Fixed bed property changes during scCO₂ extraction of natural materials – Experiments and modeling, *J. Supercrit. Fluids*. 72 (2012) 140–149. doi:10.1016/j.supflu.2012.08.022.
- [116] L. Fiori, D. Basso, P. Costa, Seed oil supercritical extraction: Particle size distribution of the milled seeds and modeling, *J. Supercrit. Fluids*. 47 (2008) 174–181. doi:10.1016/j.supflu.2008.08.003.
- [117] H. Sovovà, M. Zarevu, M. Vacek, K. Stra, Solubility of two vegetable oils in supercritical CO₂, *J. Supercrit. Fluids*. 20 (2001) 15–28.
- [118] M. Hojjati, Y. Yamini, M. Khajeh, A. Vatanara, Solubility of some statin drugs in supercritical carbon dioxide and representing the solute solubility data with several density-based correlations, *J. Supercrit. Fluids*. 41 (2007) 187–194. doi:10.1016/j.supflu.2006.10.006.
- [119] H. Li, D. Jia, S. Li, R. Liu, Correlating and predicting the solubilities of structurally similar organic solid compounds in supercritical CO₂ using the compressed gas model and the reference solubilities, *Fluid Phase Equilib.* 350 (2013) 13–26. doi:10.1016/j.fluid.2013.04.010.
- [120] Y. Yamini, M. Moradi, Measurement and correlation of antifungal drugs solubility in pure supercritical CO₂ using semiempirical models, *J. Chem. Thermodyn.* 43 (2011) 1091–1096. doi:10.1016/j.jct.2011.02.020.
- [121] A. Galia, A. Argentino, O. Scialdone, G. Filardo, A new simple static method for the determination of solubilities of condensed compounds in supercritical fluids, *J. Supercrit. Fluids*. 24 (2002) 7–17.

- [122] M. Hosseini Anvari, G. Pazuki, A study on the predictive capability of the SAFT-VR equation of state for solubility of solids in supercritical CO₂, *J. Supercrit. Fluids*. 90 (2014) 73–83. doi:10.1016/j.supflu.2014.03.005.
- [123] M. Khamda, M.H. Hosseini, M. Rezaee, Measurement and correlation solubility of cefixime trihydrate and oxymetholone in supercritical carbon dioxide (CO₂), *J. Supercrit. Fluids*. 73 (2013) 130–137. doi:10.1016/j.supflu.2012.09.006.
- [124] S. Zhao, D. Zhang, An experimental investigation into the solubility of Moringa oleifera oil in supercritical carbon dioxide, *J. Food Eng.* 138 (2014) 1–10. doi:10.1016/j.jfoodeng.2014.03.031.
- [125] J.M. del Valle, J.C. de la Fuente, E. Uquiche, A refined equation for predicting the solubility of vegetable oils in high-pressure CO₂, *J. Supercrit. Fluids*. 67 (2012) 60–70. doi:10.1016/j.supflu.2012.02.004.
- [126] C. Garlapati, G. Madras, Solubilities of palmitic and stearic fatty acids in supercritical carbon dioxide, *J. Chem. Thermodyn.* 42 (2010) 193–197. doi:10.1016/j.jct.2009.08.001.
- [127] S.N. Reddy, G. Madras, An association and Wilson activity coefficient model for solubilities of aromatic solid pollutants in supercritical carbon dioxide, *Thermochim. Acta*. 541 (2012) 49–56. doi:10.1016/j.tca.2012.04.025.
- [128] V.F. Cabral, W.L.F. Santos, E.C. Muniz, A. F. Rubira, L. Cardozo-Filho, Correlation of dye solubility in supercritical carbon dioxide, *J. Supercrit. Fluids*. 40 (2007) 163–169. doi:10.1016/j.supflu.2006.05.004.
- [129] P. Coimbra, M.H. Gil, C.M.M. Duarte, B.M. Heron, H.C. de Sousa, Solubility of a spiroindolinonaphthoxazine photochromic dye in supercritical carbon dioxide: Experimental determination and correlation, *Fluid Phase Equilib.* 238 (2005) 120–128. doi:10.1016/j.fluid.2005.09.024.
- [130] R.S. Alwi, T. Tanaka, K. Tamura, Measurement and correlation of solubility of anthraquinone dyestuffs in supercritical carbon dioxide, *J. Chem. Thermodyn.* 74 (2014) 119–125. doi:10.1016/j.jct.2014.01.015.

-
- [131] K. A. Araus, J.M. del Valle, P.S. Robert, J.C. de la Fuente, Effect of triolein addition on the solubility of capsanthin in supercritical carbon dioxide, *J. Chem. Thermodyn.* 51 (2012) 190–194. doi:10.1016/j.jct.2012.02.030.
- [132] G. Brunner, *Gas extraction: an introduction to fundamentals of supercritical fluids and the application to separation processes*, Darmstadt : Steinkopff: Springer, New York, 1994.
- [133] J. Chrastil, Solubility of Solids and Liquids in Supercritical Gases, *J. Phys. Chem.* 86 (1982) 3016–3021.
- [134] Y. Adachi, B.C.Y. Lu, Supercritical Fluid Extraction with Carbon Dioxide and Ethylene, *Fluid Phase Equilib.* 14 (1983) 147–156.
- [135] J.M. del Valle, J.M. Aguilera, An Improved Equation for Predicting the Solubility of Vegetable Oils in, *Ind. Eng. Chem. Res.* 27 (1988) 1551–1553.
- [136] D.L. Sparks, R. Hernandez, L.A. Estévez, Evaluation of density-based models for the solubility of solids in supercritical carbon dioxide and formulation of a new model, *Chem. Eng. Sci.* 63 (2008) 4292–4301. doi:10.1016/j.ces.2008.05.031.
- [137] S.K. Kumar, P. Johnston, Modelling the Solubility of Solids in Supercritical Fluids with Density as the Independent Variable, *J. Supercrit. Fluids.* 1 (1988) 15–22.
- [138] K.D. Bartle, A.A. Clifford, S.A. Jafar, G.F. Shilstone, Solubilities of Solids and Liquids of Low Volatility in Supercritical Carbon Dioxide, *J. Phys. Chem. Ref. Data.* 20 (1990) 1–45.
- [139] J. Mendez-santiago, A.S. Teja, The solubility of solids in supercritical fluids, *Fluid Phase Equilib.* 158-160 (1999) 501–510.
- [140] Z. Yu, S.S.H. Rizvi, J.A. Zollweg, Solubilities of Fatty Acids, Fatty Acid Esters, Triglycerides, and Fats and Oils in Supercritical Carbon Dioxide, *J. Supercrit. Fluids.* 7 (1994) 51–59.
- [141] M.D. Gordillo, M.A. Blanco, A. Molero, E.M. De Ossa, Solubility of the antibiotic Penicillin G in supercritical carbon dioxide, *J. Supercrit. Fluids.* 15 (1999) 183–190.

- [142] A. Jouyban, H. Chan, N.R. Foster, Mathematical representation of solute solubility in supercritical carbon dioxide using empirical expressions, *J. Supercrit. Fluids*. 24 (2006) 19–35.
- [143] C.I. Park, M.S. Shin, H. Kim, Solubility of climbazole and triclocarban in supercritical carbon dioxide: Measurement and correlation, *J. Chem. Thermodyn.* 41 (2009) 30–34. doi:10.1016/j.jct.2008.08.009.
- [144] M. Mukhopadhyay, *Natural Extracts Using Supercritical Carbon Dioxide*, 1st ed., CRC Press LLC, Filorida, 2000.
- [145] D. Peng, D.B. Robinson, A New Two-Constant Equation of State, *Ind. Eng. Chem. Fundamentals*. 15 (1976) 59–64.
- [146] D.W. Green, R.H. Perry, *Perry's Chemical Engineering Handbook*, 8th ed., McGraw-Hill, New York, 2007.
- [147] K.S. Duba, L. Fiori, Supercritical CO₂ extraction of grape seed oil: Effect of process parameters on the extraction kinetics, *J. Supercrit. Fluids*. 98 (2015) 33–43. doi:10.1016/j.seizure.2014.02.015.
- [148] Z. Huang, S. Kawi, Y.. Chiew, Solubility of cholesterol and its esters in supercritical carbon dioxide with and without cosolvents, *J. Supercrit. Fluids*. 30 (2004) 25–39. doi:10.1016/S0896-8446(03)00116-5.
- [149] U. Salgın, S. Salgın, Effect of main process parameters on extraction of pine kernel lipid using supercritical green solvents: Solubility models and lipid profiles, *J. Supercrit. Fluids*. 73 (2013) 18–27. doi:10.1016/j.supflu.2012.11.002.
- [150] H. Mhemdi, E. Rodier, N. Kechaou, J. Fages, A supercritical tuneable process for the selective extraction of fats and essential oil from coriander seeds, *J. Food Eng.* 105 (2011) 609–616. doi:10.1016/j.jfoodeng.2011.03.030.
- [151] S.G. Özkal, M.E. Yener, L. Bayındırlı, Mass transfer modeling of apricot kernel oil extraction with supercritical carbon dioxide, *J. Supercrit. Fluids*. 35 (2005) 119–127. doi:10.1016/j.supflu.2004.12.011.
- [152] C. M. Fernández, L. Fiori, M. Jesús, Á. Pérez, J. Francisco, *The Journal of Supercritical Fluids* Supercritical extraction and fractionation of *Jatropha curcas*

- L . oil for biodiesel production, *J. Supercrit. Fluids*. 97 (2015) 100–106.
doi:10.1016/j.supflu.2014.11.010.
- [153] E.L.G. Oliveira, A.J.D. Silvestre, C.M. Silva, Review of kinetic models for supercritical fluid extraction, *Chem. Eng. Res. Des.* 89 (2011) 1104–1117.
doi:10.1016/j.cherd.2010.10.025.
- [154] Z. Huang, X.-H. Shi, W.-J. Jiang, Theoretical models for supercritical fluid extraction, *J. Chromatogr. A*. 1250 (2012) 2–26.
doi:10.1016/j.chroma.2012.04.032.
- [155] L. Fiori, Supercritical extraction of sunflower seed oil: Experimental data and model validation, *J. Supercrit. Fluids*. 50 (2009) 218–224.
doi:10.1016/j.supflu.2009.06.011.
- [156] L. Fiori, D. Calcagno, P. Costa, Sensitivity analysis and operative conditions of a supercritical fluid extractor, *J. Supercrit. Fluids*. 41 (2007) 31–42.
doi:10.1016/j.supflu.2006.09.005.
- [157] S. A. B. Vieira de Melo, G.M.N. Costa, A. C.C. Viana, F.L.P. Pessoa, Solid pure component property effects on modeling upper crossover pressure for supercritical fluid process synthesis: A case study for the separation of Annatto pigments using SC-CO₂, *J. Supercrit. Fluids*. 49 (2009) 1–8. doi:10.1016/j.supflu.2008.12.006.
- [158] S.G. Özkal, U. Salgın, M.E. Yener, Supercritical carbon dioxide extraction of hazelnut oil, *J. Food Eng.* 69 (2005) 217–223. doi:10.1016/j.jfoodeng.2004.07.020.
- [159] G. Anitescu, L.L. Tavlarides, Solubility of individual polychlorinated biphenyl (PCB) congeners in supercritical fluids: CO₂, CO₂/MeOH and CO₂/n-C₄H₁₀, *J. Supercrit. Fluids*. 14 (1999) 197–211. doi:10.1016/S0896-8446(98)00109-0.
- [160] C. Grosso, J.P.P. Coelho, F.L.P.L.P. Pessoa, J.M.N. a. M.N. a Fareleira, J.G.G. Barroso, J.S.S. Urieta, et al., Mathematical modelling of supercritical CO₂ extraction of volatile oils from aromatic plants, *Chem. Eng. Sci.* 65 (2010) 3579–3590. doi:10.1016/j.ces.2010.02.046.
- [161] M.M.R. de Melo, R.M. A. Domingues, M. Sova, E. Lack, H. Seidlitz, F. Lang Jr., et al., Scale-up studies of the supercritical fluid extraction of triterpenic acids from

- Eucalyptus globulus bark, *J. Supercrit. Fluids*. 95 (2014) 44–50.
doi:10.1016/j.supflu.2014.07.030.
- [162] C. Marrone, M. Poletto, E. Reverchon, A. Stassi, V.P. Don, I.-F. Sa, Almond oil extraction by supercritical CO₂ : experiments and modelling, 53 (1998).
- [163] D. Mongkholkhajornsilp, S. Douglas, P.L. Douglas, A. Elkamel, W. Teppaitoon, S. Pongamphai, Supercritical CO₂ extraction of nimbin from neem seeds—A modelling study, *J. Food Eng.* 71 (2005) 331–340.
doi:10.1016/j.jfoodeng.2004.08.007.
- [164] NIST, Fluid Thermodynamic and Transport Properties, Version 5.0 (<http://www.nist.gov/srd/nist23.htm>).
- [165] O.J. Catchpole, M.B. King, Measurement and correlation of binary diffusion coefficients in near critical fluids, *Ind. Eng. Chem. Res.* 33 (1994) 1828–1837.
doi:10.1021/ie00031a024.
- [166] J. Puiggené, M. A. Larrayoz, F. Recasens, Free liquid-to-supercritical fluid mass transfer in packed beds, *Chem. Eng. Sci.* 52 (1997) 195–212. doi:10.1016/S0009-2509(96)00379-X.
- [167] J.M. del Valle, J.C. Germain, E. Uquiche, C. Zetzi, G. Brunner, Microstructural effects on internal mass transfer of lipids in prepressed and flaked vegetable substrates, *J. Supercrit. Fluids*. 37 (2006) 178–190.
doi:10.1016/j.supflu.2005.09.002.
- [168] A. Bucić-Kojić, H. Sovová, M. Planinić, S. Tomas, Temperature-dependent kinetics of grape seed phenolic compounds extraction: experiment and model., *Food Chem.* 136 (2013) 1136–40. doi:10.1016/j.foodchem.2012.09.087.
- [169] L. Fiori, D. de Faveri, A. A. Casazza, P. Perego, Grape by-products: extraction of polyphenolic compounds using supercritical CO₂ and liquid organic solvent – a preliminary investigation, *CyTA - J. Food.* 7 (2009) 163–171.
doi:10.1080/11358120902989715.
- [170] A. Kubátová, B. Jansen, J.-F. Vaudoisot, S.B. Hawthorne, Thermodynamic and kinetic models for the extraction of essential oil from savory and polycyclic

- aromatic hydrocarbons from soil with hot (subcritical) water and supercritical CO₂, *J. Chromatogr. A.* 975 (2002) 175–88.
- [171] M. Khajenoori, A. H. Asl, F. Hormozi, Proposed Models for Subcritical Water Extraction of Essential Oils, *Chinese J. Chem. Eng.* 17 (2009) 359–365.
doi:10.1016/S1004-9541(08)60217-7.
- [172] T. Anekpankul, M. Goto, M. Sasaki, P. Pavasant, A. Shotipruk, Extraction of anti-cancer damnacanthol from roots of *Morinda citrifolia* by subcritical water, *Sep. Purif. Technol.* 55 (2007) 343–349. doi:10.1016/j.seppur.2007.01.004.
- [173] M.N. Islam, Y.-T. Jo, S.-K. Jung, J.-H. Park, Thermodynamic and kinetic study for subcritical water extraction of PAHs, *J. Ind. Eng. Chem.* 19 (2013) 129–136.
doi:10.1016/j.jiec.2012.07.014.
- [174] D. Granato, V.M. de Araújo Calado, B. Jarvis, Observations on the use of statistical methods in Food Science and Technology, *Food Res. Int.* 55 (2014) 137–149. doi:10.1016/j.foodres.2013.10.024.
- [175] P. Rangswong, N. Rangkadilok, J. Satayavivad, M. Goto, A. Shotipruk, Subcritical water extraction of polyphenolic compounds from *Terminalia chebula* Retz. fruits, *Sep. Purif. Technol.* 66 (2009) 51–56.
doi:10.1016/j.seppur.2008.11.023.
- [176] M. Pinelo, J. Sineiro, M.J. Núñez, Mass transfer during continuous solid–liquid extraction of antioxidants from grape byproducts, *J. Food Eng.* 77 (2006) 57–63.
doi:10.1016/j.jfoodeng.2005.06.021.
- [177] K. Sólyom, R. Solá, M.J. Cocero, R.B. Mato, Thermal degradation of grape marc polyphenols., *Food Chem.* 159 (2014) 361–6.
doi:10.1016/j.foodchem.2014.03.021.
- [178] C. Lu, J. A. Napier, T.E. Clemente, E.B. Cahoon, New frontiers in oilseed biotechnology: Meeting the global demand for vegetable oils for food, feed, biofuel, and industrial applications, *Curr. Opin. Biotechnol.* 22 (2011) 252–259.
doi:10.1016/j.copbio.2010.11.006.
- [179] P. Spencer, R. Krautgartner, X. Audran, L.E. Rehder, M. Boshnakova, M. Dobrescu, et al., *EU-28 Oilseeds and Products Annual*, Vienna, 2014.

- [180] ProFound, CBI market survey: The vegetable oils and fats (including oil seeds) market in the EU, 2009.
- [181] C. Sloop, O. Bettini, EU-27 Wine Annual Report and Statistics, Washington, D.C., 2013.
- [182] A. Leticia, M.T. Pighinelli, R. Gambetta, E. Agroenergy, Oil Presses, in: G.A. Uduak (Ed.), Oilseeds, 1st ed., In Tech, Rijeka, Croatia, 2012: pp. 33–52.
- [183] E. Subroto, R. Manurung, H. Jan, A. Augustinus, Optimization of mechanical oil extraction from *Jatropha curcas* L . kernel using response surface method, Ind. Crop. Prod. 63 (2015) 294–302. doi:10.1016/j.indcrop.2014.08.050.
- [184] E. Subroto, R. Manurung, H. Jan, A. Augustinus, Mechanical extraction of oil from *Jatropha curcas* L . kernel : Effect of processing parameters, Ind. Crop. Prod. 63 (2015) 303–310. doi:10.1016/j.indcrop.2014.06.018.
- [185] A. Chapuis, J. Blin, P. Carré, D. Lecomte, Separation efficiency and energy consumption of oil expression using a screw-press: The case of *Jatropha curcas* L. seeds, Ind. Crops Prod. 52 (2014) 752–761. doi:10.1016/j.indcrop.2013.11.046.
- [186] E. Bernardini, Batch and continuous solvent extraction, J. Am. Oil Chem. Soc. 53 (1976) 275–278. doi:10.1007/BF02605700.
- [187] C. Pronyk, G. Mazza, Design and scale-up of pressurized fluid extractors for food and bioproducts, J. Food Eng. 95 (2009) 215–226. doi:10.1016/j.jfoodeng.2009.06.002.
- [188] C. Jean-Yves, M. Perrut, Scale-Up Issues for Supercritical Fluid Processing in Compliance with GMP, in: P. York, U.B. Kompella, B.Y. Shekunov (Eds.), Supercrit. Fluid Technol. Drug Prod. Dev., 1st ed., Marcel Dekker, Inc., New York, 2005: pp. 565–596.
- [189] N. Mezzomo, J. Martínez, S.R.S.S. Ferreira, Supercritical fluid extraction of peach (*Prunus persica*) almond oil: Kinetics, mathematical modeling and scale-up, J. Supercrit. Fluids. 51 (2009) 10–16. doi:10.1016/j.supflu.2009.07.008.
- [190] J.M. Prado, G.H.C.C. Prado, M.A. A. Meireles, Scale-up study of supercritical fluid extraction process for clove and sugarcane residue, J. Supercrit. Fluids. 56 (2011) 231–237. doi:10.1016/j.supflu.2010.10.036.

- [191] S. Jokić, B. Nagy, Z. Zeković, S. Vidović, M. Bilić, D. Velić, et al., Effects of supercritical CO₂ extraction parameters on soybean oil yield, *Food Bioprod. Process.* 90 (2012) 693–699. doi:10.1016/j.fbp.2012.03.003.
- [192] G. A. Núñez, J.M. del Valle, Supercritical CO₂ oilseed extraction in multi-vessel plants. 2. Effect of number and geometry of extractors on production cost, *J. Supercrit. Fluids.* 92 (2014) 324–334. doi:10.1016/j.supflu.2014.05.017.
- [193] M.S. Peters, K.D. Timmerhaus, *Plant Design and Economics for Chemical Engineers*, 5th ed., McGraw-Hill, New York, 2003.
- [194] J.M. del Valle, G. A. Núñez, R.I. Aravena, Supercritical CO₂ oilseed extraction in multi-vessel plants. 1. Minimization of operational cost, *J. Supercrit. Fluids.* 92 (2014) 197–207. doi:10.1016/j.supflu.2014.05.018.
- [195] G. A. Montero, T.D. Giorgio, K.B. Schnelle, Scale-up and economic analysis for the design of supercritical fluid extraction equipment for remediation of soil, *Environ. Prog.* 15 (1996) 112–121. doi:10.1002/ep.670150214.
- [196] P.T. V Rosa, M.A. A. Meireles, Rapid estimation of the manufacturing cost of extracts obtained by supercritical fluid extraction, *J. Food Eng.* 67 (2005) 235–240. doi:10.1016/j.jfoodeng.2004.05.064.
- [197] M. Shariaty-Niassar, B. Aminzadeh, P. Azadi, S. Soltanali, Economic evaluation of herb extraction using supercritical fluid, *Chem. Ind. Chem. Eng. Q.* 15 (2009) 143–148. doi:10.2298/CICEQ0903143S.
- [198] N. Mezzomo, J. Martínez, S.R.S. Ferreira, Economical viability of SFE from peach almond, spearmint and marigold, *J. Food Eng.* 103 (2011) 473–479. doi:10.1016/j.jfoodeng.2010.10.032.
- [199] N.C.M.C.S. Leitão, G.H.C. Prado, P.C. Veggi, M. A.A. Meireles, C.G. Pereira, *Anacardium occidentale* L. leaves extraction via SFE: Global yields, extraction kinetics, mathematical modeling and economic evaluation, *J. Supercrit. Fluids.* 78 (2013) 114–123. doi:10.1016/j.supflu.2013.03.024.
- [200] I.M. Prado, G.H.C. Prado, J.M. Prado, M.A. A. Meireles, Supercritical CO₂ and low-pressure solvent extraction of mango (*Mangifera indica*) leaves: Global yield,

- extraction kinetics, chemical composition and cost of manufacturing, *Food Bioprod. Process.* 91 (2013) 656–664. doi:10.1016/j.fbp.2013.05.007.
- [201] J.A. Rocha-uribe, J.I. Novelo-pérez, C.A. Ruiz-mercado, Cost estimation for CO₂ supercritical extraction systems and manufacturing cost for habanero chili, *J. Supercrit. Fluids.* (2014) 2–5. doi:10.1016/j.supflu.2014.03.014.
- [202] P. Lisboa, A.R. Rodrigues, J.L. Martín, P. Simões, S. Barreiros, A. Paiva, Economic analysis of a plant for biodiesel production from waste cooking oil via enzymatic transesterification using supercritical carbon dioxide, *J. Supercrit. Fluids.* 85 (2014) 31–40. doi:10.1016/j.supflu.2013.10.018.
- [203] W.B.W. Richard Turton, Richard C. Baile, *Analysis, Synthesis, and Design of Chemical Processes*, 3rd ed., Pearson Education, Inc., Boston, 2009.
- [204] L. Fiori, L. Florio, Gasification and combustion of grape marc: Comparison among different scenarios, *Waste and Biomass Valorization.* 1 (2010) 191–200. doi:10.1007/s12649-010-9025-7.
- [205] E. Carmona, M.T. Moreno, M. Avilés, J. Ordovás, Use of grape marc compost as substrate for vegetable seedlings, *Sci. Hortic.* 137 (2012) 69–74. doi:10.1016/j.scienta.2012.01.023.
- [206] M. Valente, A. Brillard, C. Schönnenbeck, J.-F. Brilhac, Investigation of grape marc combustion using thermogravimetric analysis. Kinetic modeling using an extended independent parallel reaction (EIPR), *Fuel Process. Technol.* 131 (2015) 297–303. doi:10.1016/j.fuproc.2014.10.034.
- [207] SYNMEC, (<http://www.synmec.com/html/en/index.html>)
- [208] Chemical Engineering Cost Indices (CEPCI) March 2014, *Access Intell.* 121 (2014) 72.
- [209] W.M. Vatauvuk, Updating the CE Plants Cost Index, *Chem. Eng.* (2002) 62–70.
- [210] Chemical Engineering Cost Indices (CEPCI) January 2008, (2008).
- [211] EU Commission, 2013. *Access to Finance: Loans*, (http://ec.europa.eu/enterprise/publications/index_en.htm, (accessed 17.06.13)).

10. Appendix

About the author

EDUCATION AND QUALIFICATIONS

- 01/2012 – Present **University of Trento, Italy**
PhD student, Doctoral School of Civil and Environmental Engineering
- 07/2007 – 07/2009 **Indian Institute of Technology (IIT)-Roorkee, India**
Master of Technology in Civil (Environmental) Engineering
- 09/2000 – 07/2005 **Bahir Dar University, Ethiopia**
Bachelor of Science in Chemical Engineering

WORK EXPERIENCE

- 07/2009 – 12/2011 **Lecturer, Department of Chemical Engineering, Bahir Dar University (Ethiopia)**
Responsible for undergraduate courses: *Process Plant Design and Economics, Thermal Unit Operations, Mass Transfer Unit Operations, Air Pollution Control and Management, and Environmental Biotechnology*
- 07/2006 – 07/2007 **Assistant lecturer, Department of Chemical Engineering, Bahir Dar University (Ethiopia)**
Assisted in undergraduate courses: *Reactor design and Fluid Mechanics for Process Engineers.*
- 07/2005 – 07/2006 **Graduate Assistant, Department of Chemical Engineering, Bahir Dar University (Ethiopia)**
Graduate assistant for undergraduate lab courses: *Mechanical Unit lab, Thermal Unit Operation (Tutorial) and Process Control and Instrumentation lab.*

LANGUAGE SKILLS

English, Afan Oromo, Amharic, Basic Italian

COMPUTING SKILLS

Programming: C++, MATLAB and Statistical Analysis System (SAS), AutoCAD, Aspen Plus

AWARDS & HONORS

- 01/2012 – present 27th cycle Doctoral Grant, Doctoral School of Civil and Environmental Engineering, University of Trento, Italy
- 07/2007 – 07/2009 Master of Science Scholarship Grant, Ethiopian Ministry of Education
- 10/03/2006 Award (second place) from the Ethiopian Society of Chemical Engineers (ESChE) for the best three undergraduate projects in 2004/2005
- 16/06/2005 Award from the Ethiopian Society of Chemical Engineers (ESChE) for outstanding achievement as fourth year Chemical Engineering student of Bahir Dar University in 2003/2004

PUBLICATIONS

Peer reviewed Journals

1. **Kurabachew Simon Duba**, Luca Fiori, Economic Analysis and Scale-up of Supercritical CO₂ extraction process, *Chemical Engineering Research and Design (To be submitted)*
2. **Kurabachew Simon Duba**, Luca Fiori, Solubility of grape seed oil in supercritical CO₂: Experiment and Modeling, *The Journal of Chemical Thermodynamics (To be submitted)*.
3. **Kurabachew Simon Duba**, Luca Fiori, Supercritical Fluid Extraction of Vegetable Oils: Different Approach to Modeling the Mass Transfer Kinetics, *Chemical Engineering Transactions, Volume 43, 2015. In press*
4. **Kurabachew Simon Duba**, Alessandro Alberto Casazza, Hatem Ben Mohamed, Patrizia Perego, Luca Fiori. Extraction of Total Polyphenols from Grape Skins and Defatted Grape Seeds using Subcritical Water: Experiment and Modeling. *Food and Bioproducts Processing 94 (2015) 29–38*
5. **Kurabachew Simon Duba**, Luca Fiori. Supercritical CO₂ Extraction of Grape Seed Oil: Effect of Process Parameters on Extraction Kinetics. *J. of Supercritical Fluids 98 (2015) 33–43*.
6. Luca Fiori, Vera Lavelli, **Kurabachew Simon Duba**, Pedapati Siva Charan Sri Harsha, Hatem Ben Mohamed, Graziano Guella. Supercritical CO₂ extraction of oil from seeds of six grape cultivars: modeling of mass transfer kinetics and evaluation of lipid profiles and tocol contents. *J. of Supercritical Fluids 94 (2014) 71–80*
7. M. Ali, **K. S. Duba**, A.S. Kalamdhad, A. Bhatia, A. Khursheed, A.A. Kazmi, N. Ahmed. High rate composting of herbal pharmaceutical industry solid waste. *Water Science and Technology, 65 (2012) 1817-25*

Conference Proceeding

- 1 **K. S. Duba**, A. Casazza, P. Perego, H. Mohamed, L. Fiori. Subcritical Water Extraction Kinetics of Polyphenols from Grape Skins and Defatted Grape Seeds: Experiment and Modeling, Proceedings of 14th European Meeting on Supercritical Fluids, 18-21 May 2014, Marseille, France.
- 2 **K. S. Duba**, L. Fiori. Effect of Process Parameters on Supercritical CO₂ Extraction of Grape Seed Oil: Experiment and Modeling, Proceedings of 14th European Meeting on Supercritical Fluids, 18-21 May 2014 Marseille, France.
- 3 **K. S. Duba**, L. Fiori. Comparison of different kinetic models for supercritical CO₂ extraction of seed oil, Proceedings of the 10th Conference on Supercritical Fluids and Their Applications, Naples, Italy, April 29-May 06 2013, p. 45-50.
- 4 L. Fiori, **K. S. Duba**, R. Berti, L. Torri. Supercritical CO₂ extraction, fatty acid and aroma profile of grape seed oil from different grape cultivars, Proceedings of the 10th Conference on Supercritical Fluids and Their Applications, Naples, Italy, April 29-May 06 2013, p. 163-168
- 5 M. Ali, **K. S. Duba**, A. S. Kalamdhad, A. Bhatia, A. Khursheed, A. A. Kazmi, N. Ahmed. High Rate Composting of Herbal Pharmaceutical Industry Solid Waste, 8th IWA International Symposium on Waste Management Problems in Agro-Industries, 21-24 June 2011 Çeşme, Turkey.

Extended Abstract

- 1 G. Spigno, L. Maggi, D. Amendola, L. Fiori, **K. S. Duba**, V. Lavelli, M. Marietti, G. Zeppa, R. Marchiani, L. Torri, M. Fiochi. VALORVITIS - Valorization of the wine industry by-products for the production of high-added value compounds. 6th IWA specialized conference, 'Winery 2013' "Viticulture and Winery wastes: environmental impact and management", 26-30 May 2013, Narbonne, France.

INVITED TALK

- 1 On 'Supercritical CO₂ for valorization of industrial by-products', Presentation on Jan 3, 2014 to academic staff and postgraduate students of the School of Chemical and Food Engineering, Bahir Dar University, Ethiopia.

OTHER ACTIVITIES

- ✓ Organizing committee-National Conference on Science, Technology and Innovation for Prosperous Ethiopia (NCSTI), 16th -18th May, 2012 at the Institute of Technology, Bahir Dar University (Resigned in December 2011 to move to Italy for PhD study)
- ✓ Member of Chemical Engineering Department Academic Council (AC) (09/2010-12/2011)
- ✓ Academic Advisor for undergraduate Chemical Engineering students (09/2009-12/2011)
- ✓ Sub portal coordinator (08/2010- 12/2011)- School of Chemical and Food Engineering, Bahir Dar University

CONSULTING

- 1 Prepared a feasibility study for the establishment of edible oil refinery plant for the United Nations Industrial Development Organization (UNIDO) Cluster Development program, Bahir Dar Edible Oil Cluster, 09/2010-05/2011

AFFILIATION

International Society for the Advancement of supercritical fluids (I.S.A.S.F)